CONSTRUCTION AND TESTING OF BROADBAND HIGH IMPEDANCE GROUND PLANES (HIGPS) FOR SURFACE MOUNT ANTENNAS

THESIS

Bora Cakiroglu, First Lieutenant, TUAF

AFIT/GE/ENG/08-02

DEPARTMENT OF THE AIR FORCE
AIR UNIVERSITY

AIR FORCE INSTITUTE OF TECHNOLOGY

Wright-Patterson Air Force Base, Ohio

The views expressed in this thesis are those of the author and do not reflect the official policy or position of the United States Air Force, Department of Defense, or the United States Government.

AFIT/GE/ENG/08-02

CONSTRUCTION AND TESTING OF BROADBAND HIGH IMPEDANCE GROUND PLANES (HIGPS) FOR SURFACE MOUNT ANTENNAS

THESIS

Presented to the Faculty

Department of Electrical and Computer Engineering

Graduate School of Engineering and Management

Air Force Institute of Technology

Air University

Air Education and Training Command

In Partial Fulfillment of the Requirements for the

Degree of Master of Science in Electrical Engineering

Bora Cakiroglu, BS

First Lieutenant, TUAF

March 2008

AFIT/GE/ENG/08-02

CONSTRUCTION AND TESTING OF BROADBAND HIGH IMPEDANCE GROUND PLANES (HIGPS) FOR SURFACE MOUNT ANTENNAS

Bora Cakiroglu, BS
First Lieutenant, USAF

Approved:

/ /signed//	04 MAR 2008
Dr Andrew Terzuoli (Chairman)	date
//signed//	04 MAR2008
Dr Peter Collins (Member)	date
/ /signed//	04 MAR 2008
Dr Michael Havrilla (Member)	date

AFIT/GE/ENG/08-02

Abstract

The purpose of this research was to design and build appropriate broadband high impedance ground planes for surface mount antennas. Broadband, low-profile antennas, such as spirals, log-periodics, and bow-ties, suffer substantially in gain and bandwidth performance when they are brought close to a conducting surface. Thus, when standard broadband antenna designs are conformally placed on vehicle bodies, they can no longer achieve the high data rates required by modern communication. A simple remedy for this has been to place an absorber lined cavity behind the antenna to preserve some bandwidth, at the expense of reduced gain. However, recently introduced high impedance ground planes have novel electromagnetic features that have been shown to improve conformal antenna performance without the detrimental effects of absorber losses.

In this research, first, square patch ground planes for narrowband antennas were built and analyzed. Second, a log-periodic broadband antenna was analyzed with square and circular patch ground planes. Finally, two novel triangular-patch high impedance ground plane designs as a meta-substrate for a broadband bow-tie antenna were presented. Consequently, the high impedance ground plane provided a suitable platform for the bow-tie with removing the undesired effects of a regular metallic ground plane. Results indicated that the novel designs have better gain than the bow-tie in free space, and the bow-tie over a metallic surface.

Acknowledgments

First and foremost, I would like to thank my wife, Ahu Cakiroglu for her constant support and understanding during the time here in the United States. Thank you to my parents for their support and for providing me with great opportunities while growing up, and for making me the person who I am today.

I'd like to express my sincere appreciation to my thesis committee, Dr. Andrew Terzuoli, Dr. Peter Collins, and Dr. Michael Havrilla, for their guidance and support throughout the course of this thesis effort.

I also sincerely appreciate the guidance and support of Dr. Kubilay Sertel. His insight and experience has kept me on the right track. I would also like thank to Mr. Charlie McNeeley, who patiently helped me in fabricating the structures, and graciously shared his experience and techniques. If he would not have helped me, I'd still be fabricating and testing antennas. Thank you to my fellow classmate, Murat Dogrul, for his support during our time here at AFIT. Finally, thanks to the Turkish Air Force who provided me with this great opportunity.

Bora Cakiroglu

Table of Contents

Page

Page

List of Figures

Figure Page

Figure Page

Figure Page

List of Tables

List of Abbreviations and Acronyms

dB: Decibel

DNG: Double Negative

DPS: Double Positive

EBG: Electromagnetic Band Gap

ENG: Epsilon (ε) Negative

GPS: Global Positioning System

HIGP: High Impedance Ground Plane

LH: Left-handed

MNG: Mu (μ) Negative

MTM: Metamaterial

NIM: Negative-Index Material

NRI: Negative Refractive Index

PEC: Perfect Electric Conductor

PMC: Perfect Magnetic Conductor

RF: Radio Frequency

RH: Right-handed

SNG: Single Negative

TACAN: Tactical Air Navigation

UAV: Unmanned Aerial Vehicle

UHF : Ultra High Frequency

VHF: Very High Frequency

CONSTRUCTION AND TESTING OF BROADBAND HIGH IMPEDANCE GROUND PLANES (HIGPS) FOR SURFACE MOUNT ANTENNAS

1. Introduction

The idea of using an artificial material for electromagnetic application is not new, but dates back to Jadagis Chunder Bose in 1898. His experiments on constructed twisted elements, recently known as chiral media, may be the first studies on metamaterials. Artificial dielectrics were explored for lightweight microwave antennas in the 1950s and 1960s (Alu and others, 2006:5).

These artificial materials, such as high impedance ground planes and electromagnetic band-gap structures, can be used to provide several advantages for antenna applications, due to their unusual electromagnetic features, such as suppression of surface waves and reflection of electromagnetic waves in phase (Munk, 2000; Joannopoulos and others, 1995; Rahmat-Samii and Mosallaei, 2001:506-564; Sievenpiper and others, 1999b:1245-1248; Yablonovitch, 1987:2059). This breakthrough brought considerable attention for many antenna applications.

Today, antennas are used in many applications, such as wireless internet, wireless communication, air traffic control, global positioning systems, and military weapon guidance and control systems.

Antennas are also vital for modern military forces to control the entire electromagnetic spectrum as desired. Broadband antennas, which provide more

operational frequency band, are more useful for military applications in controlling the emissions over the electromagnetic spectrum. Moreover, broadband antennas are more difficult to electronically attack by enemies. Therefore, antennas which operate on wider frequency bands are of greater interest to the military.

Broadband, low-profile antennas, such as spirals log-periodics, leaky-waves, and bow-ties have well known. These antennas provide wider operative frequency bands, than basic antennas (Balanis, 2005). But these antennas cannot maintain their broadband properties when brought near conductive surfaces, such as the metallic surface of an air plane or an Unmanned Aerial Vehicle (UAV).

Aircraft have several different antennas for communication, such as navigation, radar, and threat warning. Tactical Air Navigation (TACAN), Global Positioning System (GPS), Very High Frequency (VHF), and Ultra High Frequency (UHF) antennas are some of the examples. All of these antennas operate in different frequency bands. If a low profile broadband antenna could be developed to work without losing its broadband properties on a conductive surface, this broadband antenna could replace antennas on aircraft. One antenna, instead of three or more antennas, reduces the weight of the air vehicle, which is much more important for UAVs. One broadband antenna also can reduce the negative aerodynamic effects of antennas mounted on the vehicle. Therefore, broadband antennas are of primary interest to the designers of these types of systems.

The purpose of this chapter is to outline the research which focused on developing high impedance ground planes for surface mount antennas, and address the background, problem statement, research questions,objectives, and methodology applied.

1.1. Background

A high impedance ground plane (HIGP) is a metallic ground plane that has the potential to improve the performance of many antennas. This novel ground plane suppresses electromagnetic surface waves, and also reflects electromagnetic waves in phase. For these unusual features, HIGPs function as perfect magnetic conductor-like (PMC-like) structures which do not truly exist in nature. HIGPs have special electromagnetic features, such as reflecting incident waves in phase, and absorbing surface waves. These man-made structures are made of well known perfect electric conductor (PEC) materials, but they behave as PMC materials. Potential advantages of the HIGPs include improved antenna patterns, doubled antenna gain, and cheaper fabrication of conformal antennas (Sievenpiper and others, 1999a:2059, Yang and Rahmat-Samii, 2003a:2691).

1.2. Problem Statement

So far, metals have been used as electric ground planes. The use of a metal as an electric ground plane has some operative difficulties. Metals are nearly PECs. The main feature of a PEC surface is reflecting electromagnetic waves completely, but with a 180-degree phase change in the E-field.

PEC ground planes are also not suitable for surface-mounted antennas. When an antenna is mounted on a conductive surface of an air vehicle, opposite-directioned image currents occurred in the metallic surface of the air vehicle cancelling the currents on the

antenna. Moreover, reflections from such conductive skins severely deteriorate the operation bandwidth, matching, and gain. The standard remedy for this problem was to place the antenna on an absorber cavity, which is too thick to be mounted on a surface of air vehicles (Sievenpiper and others, 1999b:1245-1248).

Another remedy for this problem is using a thin metamaterial ground plane. The HIGP as a thin metamaterial ground plane design can be a suitable replacement for the absorber cavity while maintaining broadband characteristics of the antenna. An antenna which is located directly above a HIGP has no current cancellation problem, but has higher gain, better directivity and performance than usual antennas.

1.3. Research Questions and Objectives

Is it possible to build a low profile surface-mounted broadband antenna for an air vehicle? This research attempts to develop a high impedance ground plane with a low profile conformal broadband antenna. After the discovery of PMC-like HIGPs, it is possible to build a low profile surface-mounted antenna. The primary goal of this research is to develop an operative HIGP and a surface mounted broadband antenna.

How can an optimum HIGP design be developed for the low profile broadband antenna? The first step is to develop an HIGP which has a larger band gap and bandwidth. Certain design parameters for the optimum HIGP design are used to build the most efficient HIGP-antenna system.

This research intends to develop a more efficient antenna and ground plane system which is useful for many electromagnetic applications, especially for air vehicles.

Optimization and improvement studies are objectives. The performance improvement of the final design when conformed to the fuselage of a real air vehicle can be a further objective.

1.4. Methodology

HIGP designs are built in the microwave laboratory of the Air Force Institute of Technology (AFIT). The milling machine is used for the construction. After building the first HIGP samples, characteristics of every design are analyzed by via electromagnetic measurements.

What measurements should be done for the designed HIGP? The band gap and the bandwidth of the HIGP should be measured to determine the features of the HIGP design. The determination of band gap and the bandwidth of HIGP lead us to the determination of the appropriate broadband antenna. One of the purposes of this research is to be able to find the widest band gap. The reflection phase of the HIGP design is measured by using a focus beam system or a network analyzer. An anechoic chamber is also used for the determination of the surface currents.

What kind of a broadband antenna should be used for the designed HIGP? The second step is to build a broadband antenna with operative frequencies similar to the band gap of HIGP. Therefore some broadband antennas such as spiral, bow-tie, and log-periodic antennas, are used for the optimum HIGP-antenna system. Finally, by mounting the broadband antenna on the ground plane, the first overall system is developed. After

the first system design, different geometric-shape HIGPs are built to develop more efficient antenna and ground plane systems.

How can the HIGP-antenna system be measured? A network analyzer is used for return loss measurements and an anechoic chamber is used for radiation pattern of the HIGP-antenna system. Measurement techniques are detailed in chapter III–Methodology and the measurement results are analyzed in chapter IV–Results and Analysis.

1.5. Thesis Overview

Chapter 2–Literature Review presents the background theory for this research. A review of the metamaterials, HIGPs and also some basic electromagnetic background for understanding the features of the HIGPs are provided.

Chapter 3–Methodology identifies the methods developed in this research. It indicates how HIGP designs are built for certain frequencies, and also provides detailed measurement techniques for surface wave measurements and phase measurements.

Chapter 4–Results analyzes the results of the measurements and gives an overall comparison of HIGP designs to PEC and PMC. The results are also indicated in figures so as to be able to determine limitations of the HIGP and antenna system.

Chapter 5–Conclusion summarizes the results and also provides recommendations for future studies.

2. Literature Review

2.1 Chapter Overview

The purpose of this chapter is to present the basic electromagnetic background for understanding the features of the HIGP in the research, and to cover what researchers have achieved up to this point. A review of the metamaterials and HIGPs is also provided.

2.2 Historical Perspective

From narrowband to broadband, many different kinds of antennas are used daily. Scientists continue to develop more efficient, useful, smaller and less expensive broadband antennas (Mosallaei and Sarabandi, 2004; Bell and Iskander 2004; Broas and others 2005). The standard broadband antennas, which have been designed so far, such as spiral, log periodic, sinuous, and leaky wave antennas, rapidly lose their broadband properties when brought in close proximity to a conducting surface. The standard remedy has been to cut into the ground plane to create an absorber lined cavity behind the broadband element in an effort to preserve some bandwidth. If a novel metamaterial is used to develop a smaller surface-mounted broadband antenna, thin metamaterial designs can be suitable replacements for the absorber cavity, while maintaining broadband characteristics of the antenna element.

There have been many studies in the high impedance ground plane area. The term "High Impedance Ground Plane" was first used in 1999 by Sievenpiper. Sievenpiper developed a metallic structure that behaves like a perfect magnetic conductor (Sievenpiper 1999). Before Sievenpiper's HIGP, there were many studies on metamaterials in the literature (Brown and others, 1993; Kominami and others, 1985; Veselago, 1968; Yablonovitch 1987).

2.3 Metamaterials (MTMs)

The term "metamaterials" consists of two words, "meta" which means "beyond" in Greek and "materials". Metamaterials (MTMs) are new artificial materials with unusual electromagnetic properties that are not found in natural materials. All natural materials such as glass or diamonds have positive electrical permittivity, magnetic permeability, and an index of refraction. But these new artificially fabricated materials, which are also called negative-index materials (NIM), double negative (DNG) materials, or left-handed (LH) materials have negative parameters (Kshetrimayum and others, 2004:44-46).

With these unusual material parameters, new kinds of low profile antennas and microwave components / devices can be created for the wireless communication and defense industries. Using MTMs offers novel possibilities of guiding radio frequency (RF) flux to the receiver coil, permitting a clear image to be obtained where none might be otherwise detectable (Kshetrimayum, 2004:44-46).

2.3.1 Introduction and History of Metamaterials

What is metamaterial? With most of the natural materials being used by scientists, and the eagerness to find better media for electromagnetic applications, scientists were forced to fabricate structures or use composite materials with physically resemble response functions that do not naturally occur or are not readily available in nature (Engheta and Ziolkowski, 2006).

Electromagnetic MTMs are artificially homogeneous electromagnetic structures with unusual properties not readily available in nature (Caloz and Itoh, 2006). MTMs have excellent electromagnetic features, such as reflecting incident waves in phase, and absorbing surface waves (Yang and Rahmat-Samii, 2003a:2691-2703).

The idea of artificial materials for electromagnetic applications has a long history dating back to Jadagis Chunder Bose in 1898. He worked and experimented on the constructed twisted elements that exhibit properties, known today as chiral characteristics (Alu and others, 2006:23-36). After Bose's discovery, artificial dielectrics were explored in the 1950s and 1960s for lightweight microwave antenna lenses. In 1967, Russian physicist Viktor Veselago theoretically investigated the substances with simultaneously negative values of permittivity ε and the permeability μ, and concluded that they may exist .

More than 30 years later, the first left-handed (LH) material was conceived and demonstrated by Smith and colleagues at the University of California, San Diego. The LH material was artificially made, and not a natural substance (Caloz and Itoh, 2006).

In the 1990s, the development of electromagnetic band gap (EBG) structured materials, single-negative (SNG) and double-negative (DNG) materials, and their fascinating properties have driven the interest in MTMs (Engheta and Ziolkowski, 2006).

Much research has been done in this area and several terms have been defined for these artificial materials. Left-handed (LH), double-negative (DNG), negative-refractive-index (NRI), backward-wave, Veselago medium, and negative phase velocity medium are all used to define these material substances (Caloz and Itoh, 2006).

MTMs are classified with the help of the constitutive parameters of electromagnetic materials which are the permittivity ε and the permeability μ. Relative permittivity ε_r and relative permeability μ_r of an electromagnetic material is related to the free space permittivity ε_0 and permeability μ_0 by

$$\varepsilon_0 = \varepsilon / \varepsilon_r = 8{,}854.10^{-12} \tag{1.1}$$

$$\mu_0 = \mu / \mu_r = 4\pi.10^{-7} \tag{1.2}$$

And the wave number k is defined by

$$k = \pm\omega\sqrt{\varepsilon_r.\mu_r} \tag{1.3}$$

Wave number is also related to the refractive index in some references, which is defined by

$$n = \pm\sqrt{\varepsilon_r.\mu_r} \tag{1.4}$$

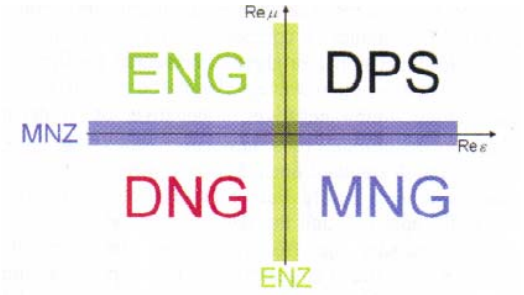

Figure 1. Four combinations of permittivity and permeability.

In equation 1.4, the sign of the relative permittivity ε_r and relative permeability μ_r is used to classify MTMs. Four combinations in the pair (ε_r, μ_r) are (+,+), (+,-), (-,+), and (-,-).

In Figure 1, four combinations of material parameters are shown (Alu and others, 2007:25). The real permittivity (ε) is on the x-axis and the real permeability (μ) is on the y-axis.

The combination of (+,+) is called Double Positive (DPS),

The combination of (-,+) is called Epsilon (ε) Negative (ENG),

The combination of (+,-) is called Mu (μ) Negative (MNG),

The combination of (-,-) is called Double Negative (DNG) (Alu and others, 2006:23-36).

The combinations of the first three, (+/+), (+/-), and (-/+), are well known in conventional materials, but the fourth combination, (-/-), with simultaneously negative permittivity and permeability, are novel materials which do not exist in nature. These materials are called double-negative materials (Caloz and Itoh, 2006).

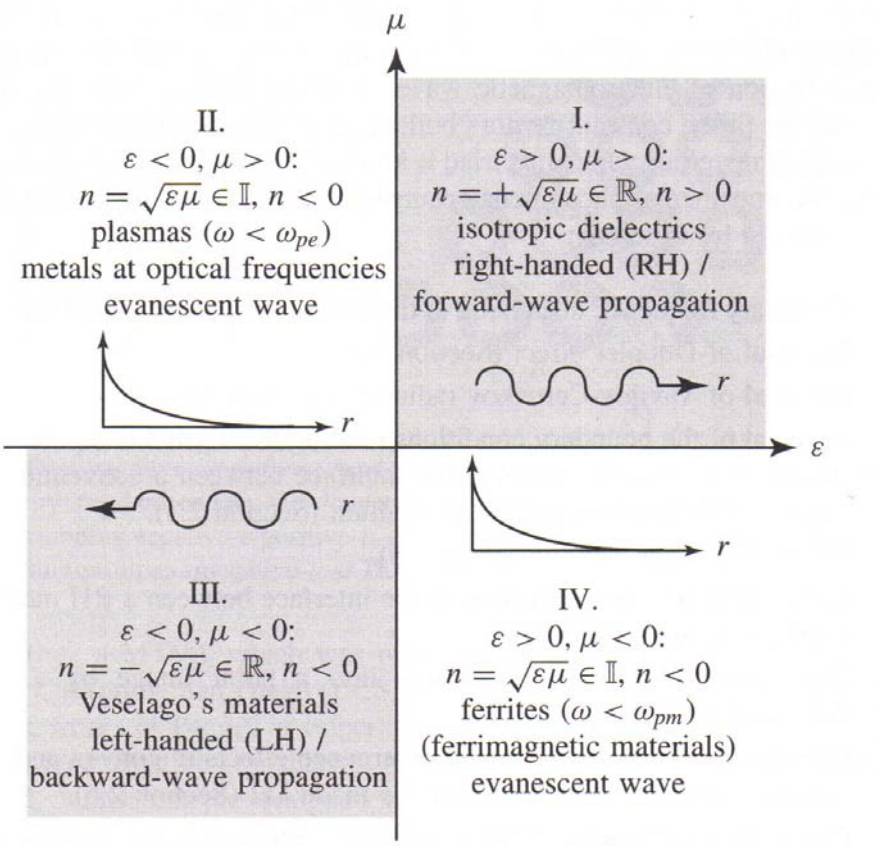

Figure 2. Permittivity-permeability (ε , μ) and refractive index (n) diagram.

In Figure 2, four combinations of the permittivity (ε), the permeability (μ), and the refractive index (n) are shown (Caloz and Itoh, 2006). In region I, both ε and μ are positive. Isotropic dielectrics are examples of this region. The double-negative materials are shown in region III. In this region both ε and μ are negative. Veselago materials are given as examples.

2.3.2 Double-Negative (DNG) Metamaterials

Double-negative materials are an example of electromagnetic composite media, such as chiral materials, omega materials, wire media, bianisotrophic media, linear and nonlinear media. Local and nonlocal media have been studied by many scientists all over the world.

The idea of complex materials, in which both permittivity and the permeability possess negative real values at certain frequencies, has received considerable attention. Vaselago investigated the plane-wave propagation in a material whose permittivity and permeability were assumed to be simultaneously negative. He demonstrated that in such a medium, a monochromatic uniform plane wave in the direction of the Poynting vector is antiparallel to the direction of the phase velocity. This is contrary to the case of the plane-wave propagation in conventional simple media (Engheta and Ziolkowski, 2006).

Vaselago called these materials left-handed (LH) to express that these types of materials would allow the propagation of electromagnetic waves with in the electric field, magnetic field, and with the phase constant vectors building a left-handed triad, compared to conventional materials where the triad is known to be right-handed (RH) (Caloz and Itoh, 2006).

Veselago predicted some basic features of LH materials as follows:

a. Necessary frequency dispersion of the constitutive parameters.
b. Reversal of Doppler Effect.
c. Reversal of Vavilov-Cerenkov radiation.

d. Reversal of boundary conditions relating to the normal components of the electric and magnetic fields at the interface between a conventional right-handed (RH) medium and a LH medium.
e. Reversal of Snell's law.
f. Subsequent negative refraction at the interface between a RH medium and a LH medium.
g. Transformation of a point source into a point image by a LH slab.
h. Interchange of convergence and divergence effects in convex and concave lenses, respectively, when the lens is made LH.
i. Plasmonic expression of the constitutive parameters in resonant-type LH media (Veselago, 1968).

2.3.3 Electromagnetic Bandgap (EBG) Metamaterials

After the 1980s and 1990s, artificial electromagnetic materials, such as electromagnetic band-gap (EBG) structures, photonic crystals, and double negative (DNG) structures have been investigated. These structures are also classified as MTMs that have special electromagnetic features such as reflecting incident waves in phase and absorbing surface waves. These man-made structures are made of well known perfect electric conductor (PEC) materials but they behaved as a perfect magnetic conductor (PMC) material. These novel features of the EBG motivated scientists to study antenna and propagation fields (Yang and Rahmat-Samii, 2003a:2691-2703).

EBG structures have been used for enhancing antenna performance because of the frequency band gap of the surface-wave suppression. EBG structures as a ground plane are used to achieve low profile broadband antennas that are useful for many antenna applications (Yang and Rahmat-Samii, 2003:2691-2703).

The reflection phase feature of an EBG structure is unusual. The reflection phase is defined as the phase of the reflected electric field at the reflecting surface, and it is normalized to the phase of the incident electric field at the reflecting surface. The PEC reflects the incident plane wave with a 180 degrees reflection phase, while the PMC, which does not exist in nature, reflects the incident plane wave in phase. There have been many studies to realize a PMC-like structure. Recent studies have indicated that EBG structures can satisfy the PMC-like condition in a certain frequency band, in fact that EBG structures are more than a PMC surface (Yang and Rahmat-Samii, 2003a:2691).

The reflection phase of an EBG surface varies continuously from 180 degrees to negative 180 degrees versus frequency, where the reflection phase is only 180 degrees for a PEC surface or 0 degrees for a PMC surface. This property of the EBG structures makes it useful for many electromagnetic applications. One of the potentially important applications of this surface is its usage as a ground plane of a wire antenna for a low profile design, which is desirable in many wireless communication systems (Yang and Rahmat-Samii, 2003a:2691-2703).

The mushroom-like structures were designed as EBG structures. The mushroom-like structure is known to have an effective band gap for surface-wave propagation. This structure is useful to optimize an antenna radiation pattern (Yang and Rahmat-Samii, 2003a:2691-2703).

2.4 High Impedance Ground Plane (HIGP)

The high impedance ground plane (HIGP) contains two metallic conductors and an artificial substrate with the artificial substrate located between two conductors, and two conductors connected to each other by vias.

In figure 3, 7 by 7 square-shaped HIGP design is shown (Linton and Scanlon, 2006). The HIGP was designed for use on surface mounted antennas. This has been developed with the objective of higher radiation efficiency and compact operation.

2.4.1 Electromagnetic Properties of HIGP

To enable physically small but electrically large antennas at Very High Frequency (VHF) and Ultra High Frequency (UHF), a metamaterial high impedance ground plane has to be created. The HIGP offers the possibility of high negative permittivity substrates over a narrow band, which will make the dimensions of the patch antenna smaller (Linton and Scanlon, 2006).

Radiation incident on the patch antenna will cause surface currents to flow on the outer metallic skin patch. For optimum antenna radiation, the substrate thickness for full reflection from the ground plane is λ/4 (Sievenpiper, 1999a:2059). This is impossible in compact antennas in all frequencies. Only in the highest frequencies can this substrate thickness be used. In figure 3, a square patch HIGP is shown (Linton and Scanlon, 2006:33).

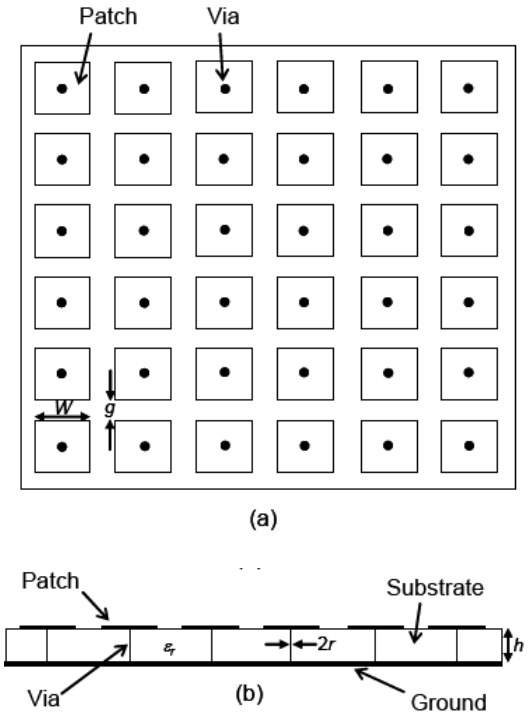

Figure 3. High Impedance Ground Plane: (a) Top View (b) Side View

When the frequency gets higher, the thickness of the substrate gets smaller. Over a narrow frequency band, however, a HIGP can be used to make an ultra thin substrate which retains the properties of the $\lambda/4$ substrate height separation (Linton and Scanlon, 2006:32).

Sievenpiper's design of metallic structures as a HIGP has the following interesting characteristics over a particular frequency band known as the electronic band-gap (EBG):

a. It reflects waves in-phase

b. It does not allow surface currents to propagate

These characteristics are novel, since typical metal surface reflects waves with a 180° phase shift and permits the propagation of alternating currents on the surface (Sievenpiper, 1999b:2073). Researches in AFIT using high impedance surfaces as ground planes for low-profile antennas has also demonstrated the advantages of such surfaces (Golla, 2001; Saville, 2000; Schloer 1999).

A low-profile antenna such as a patch antenna over a ground plane has some design limitations due to the metal ground plane. A metal ground plane acts as a PEC. In this case if the patch is brought close to the metal ground plane which behaves as a PEC, the image current induced in the metal ground cancels the current in the radiating element. To avoid this, the distance between radiating element and ground plane should be at least a quarter of a wavelength ($\lambda/4$). This limits the reduction in height of the antenna that can be achieved. When the surface currents flowing in the ground reach the edge of the metal, they will radiate from the metal causing interference with the intended radiated wave. The remedy of these two problem areas is replacing the metal ground plane with a HIGP.

A HIGP is a periodic lattice of horizontal metal patches positioned over a solid metal sheet and connected to the sheet by vertical conducting vias. The space between patches and the ground plane may be filled with a dielectric substrate for convenience of the fabrication. Square patches were chosen for the ground plane in figure 3, however, there can be a number of other geometrical shapes and may have a non-periodic array pattern. The parameters used to tailor the characteristics of the surface in figure 3 are:

W: the patch width,

g: the gap width between patches,

h: the substrate thickness,

ε_r : the substrate permittivity,

r: the via radius.

2.4.2 High Impedance Surface Lumped-Element Approximation

When the dimensions of the lattice are small compared to the wavelength of the illuminating energy, the surface can be modeled using lumped-circuit elements, such as a parallel LC circuit, as shown in Fig.4 (Sievenpiper, 1999a:2060; Linton and Scanlon, 2006:34).

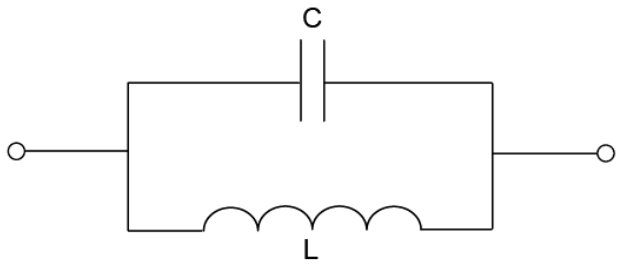

Figure 4. Lumped-Element Equivalent Circuit of the HIGP

The inductance arises from the current flowing between patches through the vias and the capacitance arises from the proximity of adjacent patches (Linton and Scanlon, 2006:34). At resonance the impedance of a parallel LC circuit is

$$Z = \frac{j\omega L}{1-\omega^2 LC} \tag{1.5}$$

$$\omega = \frac{1}{\sqrt{LC}} \tag{1.6}$$

At the resonant frequency the impedance of the surface becomes very high and purely real. Over the bandwidth of the surface, centered at the resonant frequency, both TE and TM surface waves are suppressed. At frequencies below the lower band-edge the surface impedance is inductive, TM surface waves can propagate, and at frequencies higher than the upper band-edge the surface impedance is capacitive and TE surface waves can propagate.

If a HIGP is used as a substrate of an antenna, suppression of surface waves will improve the antenna efficiency and reduce the sidelobe level that is caused by the diffreaction of surface waves at the edges of the substrate (Yablonovitch, 1994:173). When a thick substrate with higher dielectric constant value instead of a HIGP is used to increase the bandwidth of the antenna, power losses due to the surface waves become as high as 60% of the radiated power (Gonzalo and others, 1999:2132).

The bandwidth of the HIGP is the frequency range over which the reflected wave is in-phase with the incident wave. This occurs when the phase of the reflected wave is between 90° and –90°. The bandwidth is also the frequency range over which surface currents are suppressed (Linton and Scanlon, 2006:35). It is defined as

$$BW = \frac{1}{\eta_0}\sqrt{\frac{L}{C}} \tag{1.7}$$

In equation (1.7), η_0 is the impedance of the incident wave (usually the impedance of free-space); approximate values of the capacitance and inductance for the HIGP structure shown in figure 3 are :

$$C = \frac{W\varepsilon_0(1+\varepsilon_r)}{\pi}\cosh^{-1}\left(\frac{2W+g}{g}\right) \tag{1.8}$$

$$L = \mu_0 h \tag{1.9}$$

Equations (1.7)−(1.9) allow the approximate design of a HIGP using lumped elements. It is important to know the effect of each of the design parameters on the resonant frequency and bandwidth of the HIGP for an appropriate design (Linton and Scanlon, 2006:35).

2.5 Conclusion

Electrically small and efficient antennas are being designed and developed. But to improve better antennas make scientists discover novel areas. In this case HIGPs can be used to develop more efficient antennas. By using MTMs, physically small but electrically large, low-profile antennas can be developed. The HIGP as a MTMs for surface mount antennas let scientists create broadband, low-profile antennas which work on conducting surfaces. These broadband, low-profile antennas with high impedance ground planes can be used on the surfaces of the unmanned aerial vehicles, aircraft, and spacecraft.

Chapter 3 Methodology

3.1. Chapter Overview

The purpose of this chapter is to identify the method to achieve the goal of the research. Fabrication of HIGP samples, surface wave measurements, narrowband and broadband antenna return loss and gain measurements are detailed.

3.2. Method to Achieve Research Goal

In this research, mushroom-like HIGP samples with different elements were analyzed. Many techniques were reviewed in the literature to find the most appropriate method for testing ground planes and antennas (Brown, 1993; Colburn and Rahmat-Samii, 1990; Compton and others, 1987; Golla, 2001; Gonzalo, 1999; Linton, 2006; Yang and Rahmat-Samii, 2003a:2691-2703). Finally, square patch HIGP samples were designed similarly as in (Yang and Rahmat-Samii, 2003a) as a starting point. The proportion of the design parameters was taken directly from this work, but additionally three different design frequencies were chosen. Square patch HIGP samples were designed, built, and analyzed to be able to reach the same results. Thus, we could verify our measurements. The experimental measurement results were also compared to the simulation results.

After the fabrication of basic HIGPs, a circular patch hexagonal HIGP, a square patch HIGP and two novel HIGP samples were built. These samples were designed and optimized in Ansoft's commercial full-wave solver HFSS (High Frequency Structure Simulator) as another research (Dogrul, 2008). The optimized samples were tested and analyzed as a final step.

Analysis proceeded in three steps:

- Surface Wave Measurements
- Narrowband Antenna Measurements
- Broadband Antenna Measurements

In the first step, the band gap of surface wave suppression was analyzed by measuring surface waves on square patch HIGPs. It's known that mushroom-like structures have effective band gaps for the surface-wave propagation. Identification of the band gap of these structures is important to determine the operational frequencies of the desired HIGP/antenna system. However, the surface wave band gap of the structure cannot guarantee the effective radiation of the low profile antenna alone. Complicated interactions occur between the wire antenna and the HIGP surface, and electromagnetic waves are not restricted to surface waves that propagate in the horizontal plane (Yang and Rahmat-Samii, 2003a:2691).

For these reasons, in the second and the third step HIGPs were tested with narrowband and broadband antennas. Dipole antennas were chosen for narrowband antenna, since there are many studies on dipoles with electromagnetic band gap structures (Kominami, 1985:600-607; Sievenpiper, 1999c:1245-1248; Yang and Rahmat-Samii, 2003a:2691-2703). A variety of dipole antennas in different lengths were located $0.03\,\lambda_{8GHz}/0.035\,\lambda_{8GHz}/0.04\,\lambda_{8GHz}$ over the HIGPs. Thus, the radiation performance of each HIGP/dipole antenna was characterized in a far field anechoic chamber.

In broadband antenna measurements, a log-periodic antenna as in (DuHamel and Ore, 1958:139-151) with two HIGP samples and two bow-tie antenna/HIGP combinations were analyzed. First, a square patch HIGP and a circular patch hexagonal HIGP were built for the log-

periodic antenna. The same measurement techniques as in narrowband antenna measurements were applied.

Second, two novel HIGP designs were tested. Specifically, two different multi-scale triangular-patch mushroom HIGP samples with a bow-tie were analyzed. Several bow-ties and integrated antennas were reviewed for the fabrication (Kiminami, 2004:152-153; Loi, 1998:137-140; Rutledge, 1983:550-557; Yang and Rahmat-Samii, 2003b:2936-2946). The sizes and periodicities were designed, so that the two samples have band-gaps that appear successively in frequency.

A broadband horn antenna was used for the calibration of the anechoic chamber measurements. The frequency band was considered between 2–18 GHz for measurements, because the equipment in the laboratory only operates in this frequency band. The calibration data was collected twice a day, once at the beginning and once at the end.

3.3. Fabrication of HIGP Samples

Desired HIGP samples were designed by using Isopro Software (v.2.5), and samples were built using the T-Tech's Quick Circuit System. Tools used for the fabrication which are also provided by T-Tech, are shown below in Table 1.

Table 1. T-Tech Tool Set

Drill Bits (inch)	Stub Endmills (inch)
0.021	0.015
0.026	0.020
0.032	0.031
0.040	0.040

Materials chosen to use for the fabrication were RT/duroid 5880, RT/duroid 5870, RT/duroid 6002 and RT/duroid 6010. These materials are teflon based fiberglass high frequency laminates which were produced by Rogers Corporation. The permittivity of materials is shown in Table 2.

Table 2. Permittivity of High Frequency Laminates

Material Name	Permittivity
RT/Duroid 5880	2,2
RT/Duroid 5870	2,33
RT/Duroid 6002	2,94
RT/Duroid 6010	10,02

For square patch HIGP samples, three main design frequencies, 8 GHz, 10 GHz, and 12 GHz, were chosen. Design parameters of HIGP samples, such as patch width and gap width, were considered proportional to the wavelength of these frequencies.

For example, 7 by 7 square patch designs, shown on the first row of figure 5, were built proportional to the wave length of 8 GHz. The frame size of the sample was λ_{8GHz} by λ_{8GHz}, which is 37.5 mm by 37.5 mm. The patch width of the design is $0.12\,\lambda_{8GHz}$, which is 4.5 mm, and the gap width is $0.02\ \lambda_{8GHz}$, which is 0.75 mm. According to design parameters (Yang and Rahmat-Samii, 2003:2691-2703), the height of 7 by 7 square patch designs should have been 0.75 mm ($0.02\,\lambda_{8GHz}$), but since we used RT/Duroid 5880, produced by Rogers Corporation, we had only 7 different height choices, they were 0.005" (0.127mm), 0.010"(0.254mm), 0.015"(0.381mm), 0.020"(0.508mm), 0.031"(0.787mm), 0.062"(1.575mm), and 0.125"(3.175mm). For this reason, the thickest value of 0.125" (3.175mm) was chosen so as to be able to get better bandwidth and band gap.

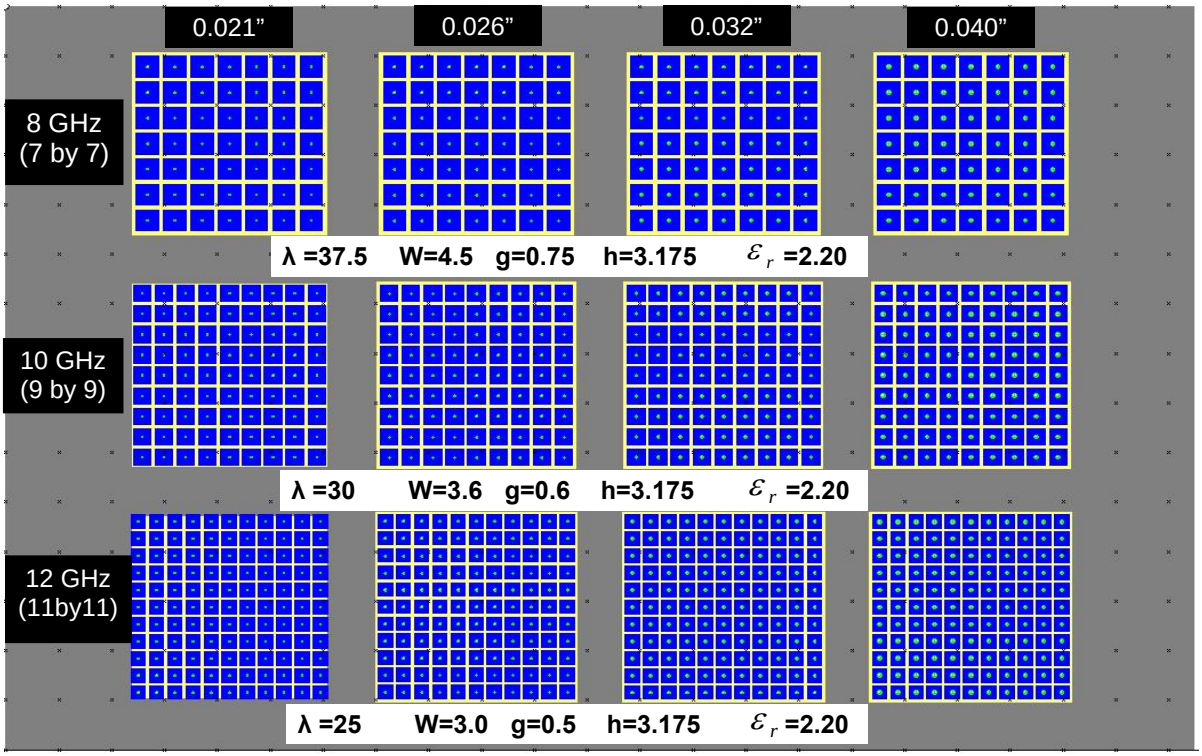

Figure 5. Square Patch HIGP Samples

Square patch HIGP samples designed in Isopro (v.2.5.) are shown in figure 5 above. In this figure, numbers at the first row show the radius of drill bits that were used for the fabrication. The patch width (W), the gap width (g) and the height (h) are chosen as explained above. The substrate permittivity is $\varepsilon_r = 2.20$.

One of the square patch designs is detailed in figure 6 below.

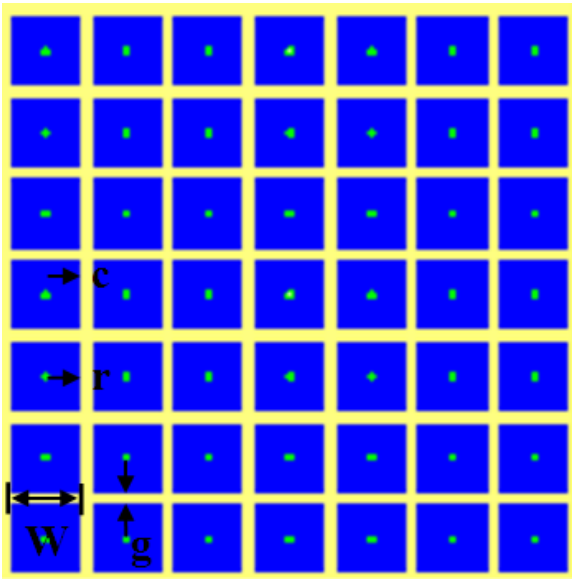

a) Top View

b) Side View

W = Patch Width (0.12 λ)
g = Gap Width (0.02 λ)
h = Substrate Thickness
r = Via Radius
c = Copper Cladding
ε_r = Substrate Permittivity

Figure 6. Detailed Square Patch HIGP Design

In figure 6a, the top view of the HIGP with patch width, gap width, via radius, and copper cladding parameters is shown; in figure 6b, the side view of the structure with substrate thickness and permittivity parameters is shown. Design parameters of square HIGP samples are shown in Table 3 below.

Table 3.Square Patch HIGP Design Parameters

	λ (mm)	W (mm)	g (mm)	h (mm)	ε_r (duroid5880)
8 GHz	37.5	4.5	0.75	3.175	2.20
10 GHz	30	3.6	0.6	3.175	2.20
12 GHz	25	3	0.5	3.175	2.20

After square patch HIGP samples were designed, a 9 by 16 -inch RT/Duroid5880 board, with a thickness of 0.125" (3.175 mm) was used for the fabrication. After the RT/Duroid5880 board was patterned as in figure 5, it was plated at the Air Force Research Laboratory (AFRL). By plating the board, square patches on the surface were connected to a conductive (copper) backward layer.

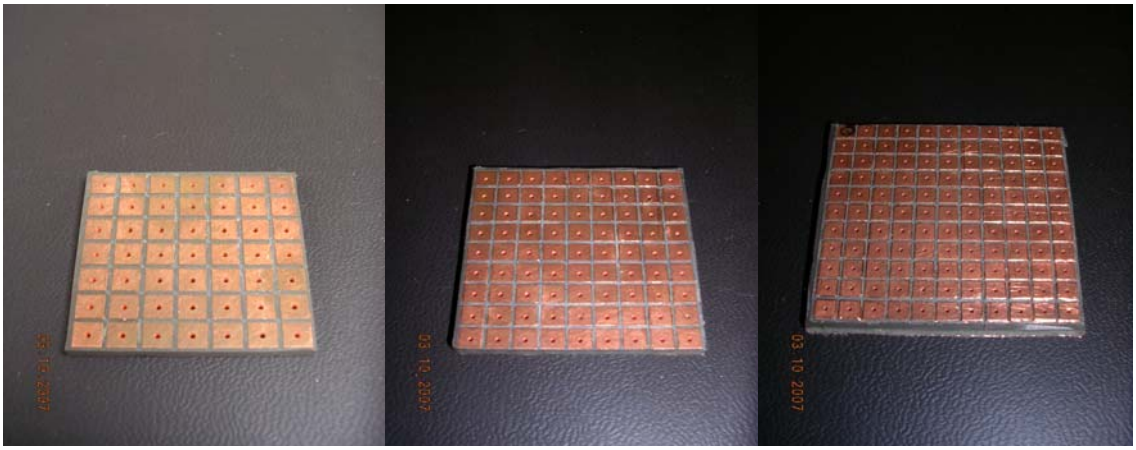

(a) (b) (c)

Figure 7. Square Patch HIGP Samples, a) 7 by 7 square patch HIGP, b) 9 by 9 square patch HIGP, c) 11 by 11 square patch HIGP.

Subsequently, square patch mushroom structures were completed. Pictures of the fabricated samples are shown in figure 7. In figure 7a, 7b, and 7c, top views of 7 by 7, 9 by 9 and 11 by 11 square patch HIGPs are shown.

Two new HIGP samples for broadband antenna measurements and two novel HIGP samples were then designed. A multi-scale triangular-patch HIGP, with planar bow-tie (side length of 7.6 mm) antenna, is shown in figure 8a. Another multi-scale triangular patch HIGP, with planar bow-tie (16 mm. side length) antenna, is shown in figure 8b. The 11 by 11 square patch optimized HIGP is shown in figure 8c, and the circular patch hexagonal HIGP is shown in figure 8d. Four totally samples were built as shown in figure 8.

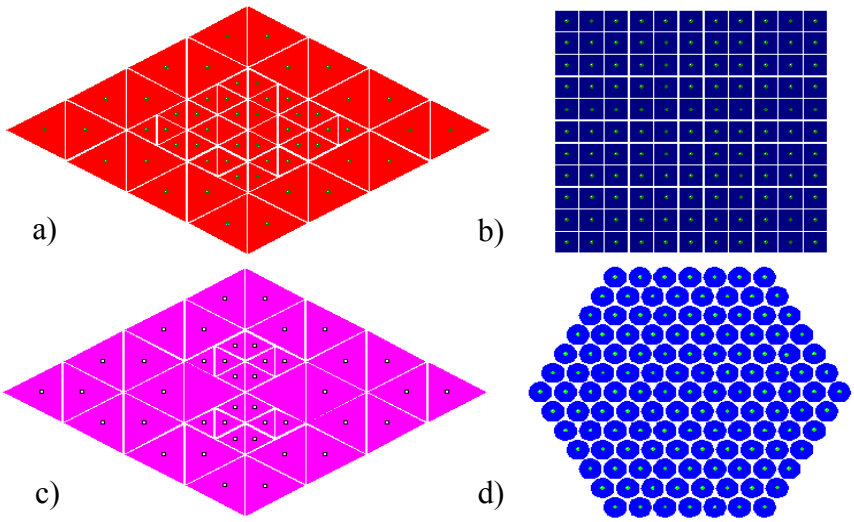

Figure 8. HIGP Designs
a) Triangular-patch HIGP with planar 7.6 mm-bow-tie antenna,
b) Triangular-patch HIGP with planar 16 mm-bow-tie antenna,
c) 11 by 11 square patch optimized HIGP,
d) Circular patch hexagonal HIGP

Samples were drilled first on the 9 by 16-inch RT/Duroid5880 board using a 0.032-inch drill bit. The 0.032-inch drill bit was chosen due to the HFSS optimization. After the board was drilled, it was sent to AFRL for the plating process. Finally, the HIGP designs were directly printed on the plated board using a milling machine as shown in figure 9.

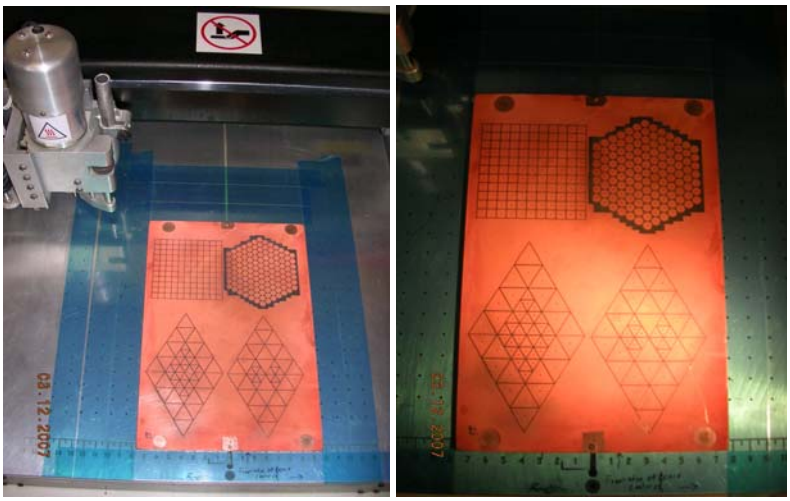

a) b)

Figure 9. Printed RT/Duroid Board, a) Top View, b) Close View.

3.4. Surface Wave Measurements

The Agilent E8362B Network Analyzer, is shown in figure 10, was used for the analysis of surface wave measurements. Surface waves on square patch HIGP samples were measured horizontally and diagonally. The frequency range was limited to 0-20 GHz.

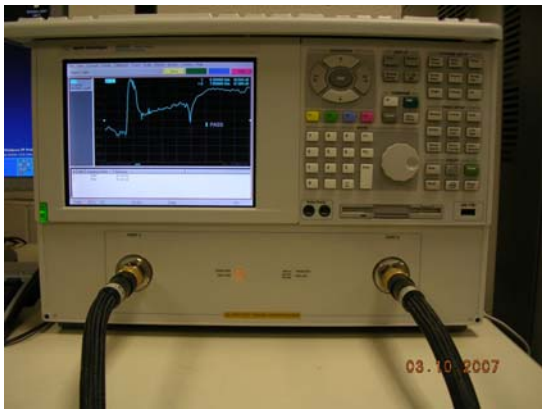

Figure 10. Agilent E8362B Network Analyzer

Copper wires and SMA connectors, as shown in figure 11, were connected to HIGP samples. The outer conductor of the copper wires was shorted to the back side of the ground plane, and the center connector was extended through the front side and connected to the square patch as shown in figure 12, and figure 13.

Figure 11. Square HIGP Samples and Copper Wires

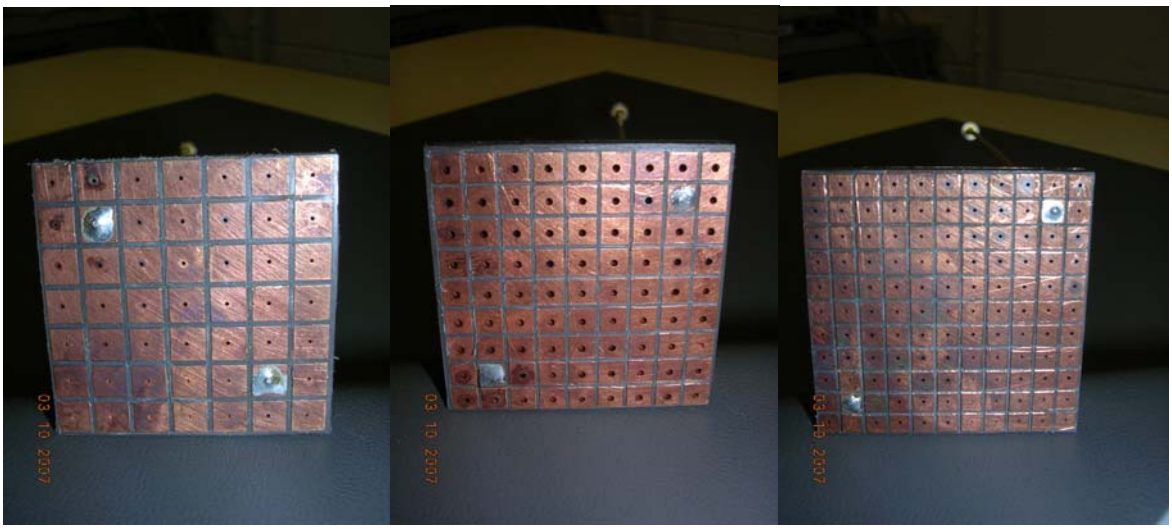

(a) (b) (c)

Figure 12. Diagonal Surface Wave Measurements
a) 7 by 7 HIGP, b) 9 by 9 HIGP, c) 11 by 11 HIGP

In diagonal surface wave measurements, copper wires were diagonally connected to two square patches, which are located one patch before the corner as shown in figure 12. Selected patches were drilled at their centroids, then the center connector was extended through the ground plane and soldered to the patch element, the outer conductor was shorted to the ground plane.

After both copper wires were connected to selected square patches, samples were connected to port1 and port2 of the network analyzer as shown in figure 14. After the calibration of the network analyzer, the S_{21} data was taken. The data was analyzed in Matlab (v.2007a) and results were analyzed in chapter 4. In horizontal surface wave measurements, another copper wire was horizontally connected to the ground plane as shown in figure 13. Two horizontal wires were connected to the network analyzer and the third connector was connected to the 50 Ohm terminator. The data was analyzed in Matlab (v.2007a) and results are shown in chapter 4.

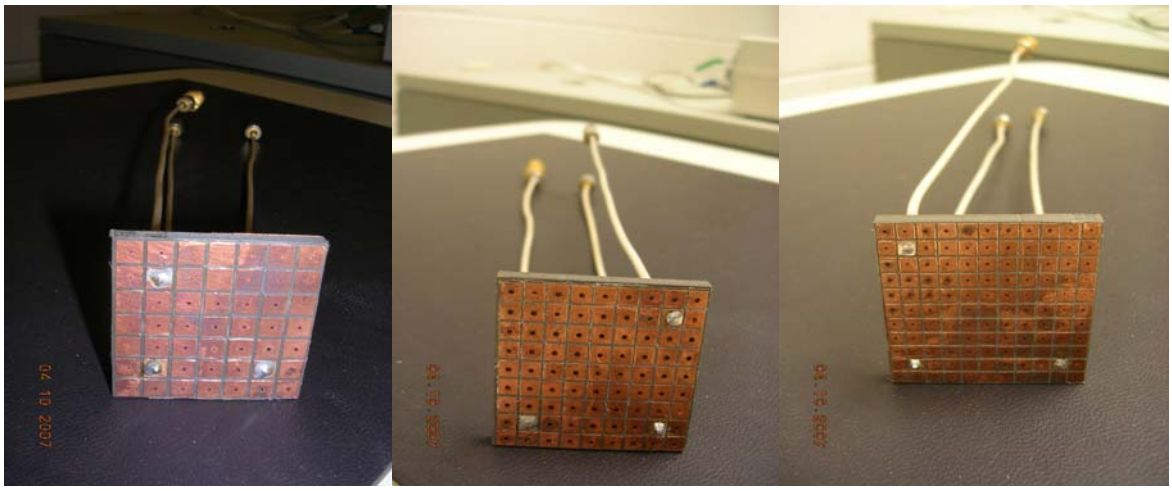

(a) (b) (c)

Figure 13. Horizontal Surface Wave Measurements
a) 7 by 7 HIGP, b) 9 by 9 HIGP, c) 11 by 11

The 50 ohm terminator used in the horizontal surface wave measurements is shown in figure 14.a. Figure 14 also shows the horizontal connection of the HIGP samples.

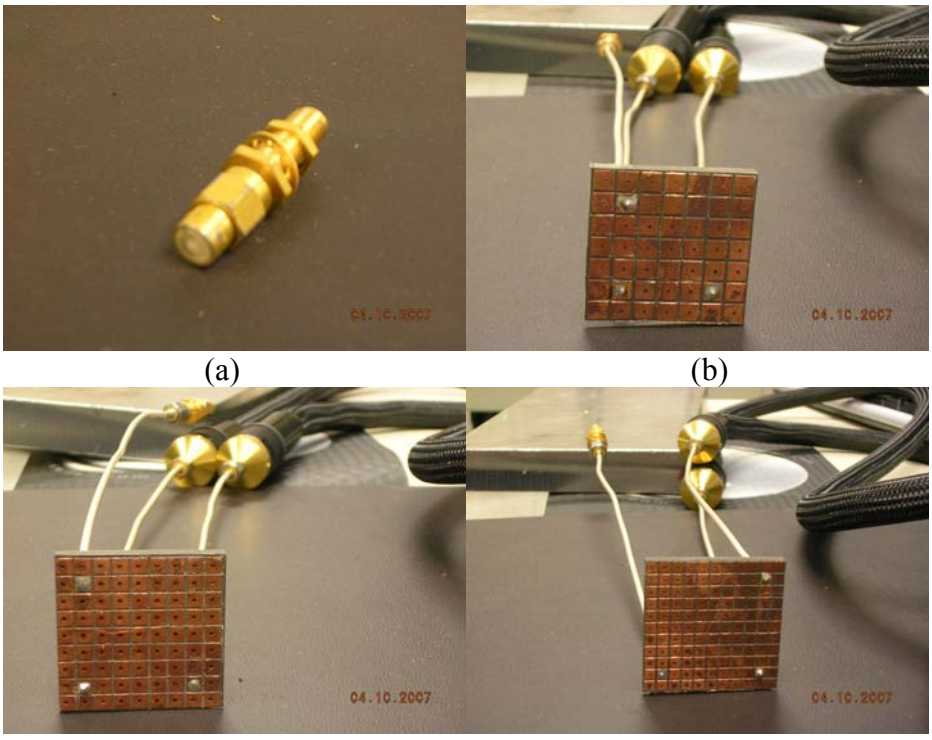

(a) (b)

(c) (d)

Figure 14. HIGPs Connected to Network Analyzer
a) 50 Ohm terminator, b) 7 by 7, c) 9 by 9, d) 11 by 11

3.5. Narrowband Antenna Measurements

Dipole antennas were chosen as a narrowband antenna. To understand the behavior of dipole antennas, in different lengths, over HIGP samples, radiation mechanisms were examined.

The AFIT anechoic chamber was used for narrowband antenna measurements. Three different dipole lengths were chosen for each of the HIGP samples. Totally, twelve dipole antennas, the lengths of which are proportional to the wavelength of design frequencies, are shown in Table 4 below.

Table 4. Length of Dipole Antennas

DIPOLE LENGTH	HIGP SAMPLES		
	8GHz (7 by 7)	10 GHz (9 by 9)	12GHz (11 by 11)
λ (mm)	**37.5**	**30**	**25**
0.4	15	12	10
0.5	18.75	15	12.5
0.7	26.25	21	17.5

Dipole antennas were built by connecting two copper wires parallel. Each dipole was positioned in the center of the HIGP. The front view of a dipole antenna and HIGP sample is shown in figure 15.a. The outer conductors of the wires were soldered to each other and the inner conductors were used as a dipole antenna. HIGP samples were drilled in the middle and the dipole antennas were passed through samples. The outer conductors were soldered to the back side of the HIGP sample as shown in figure 15.b. A 3-dB hybrid coupler with 180° phase difference is shown in figure 16 was used for measurements. This helped to feed the antenna in a balanced way, the frequency band was considered between 2–18 GHz for the measurements.

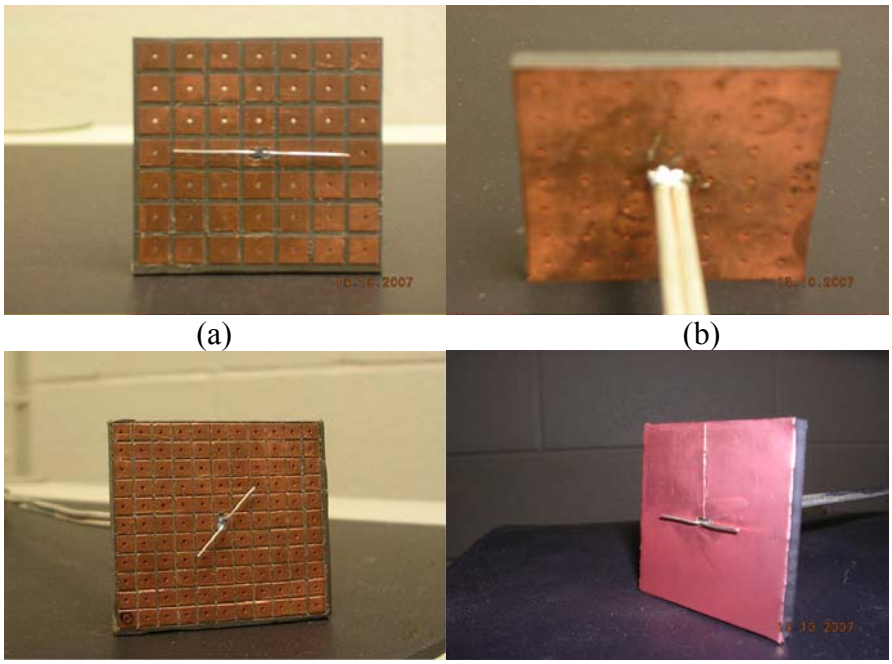

(a) (b)

(c) (d)

Figure 15. HIGP/Dipole Antenna Designs
a) Horizontally located dipole antenna over HIGP (Front View);
b) Horizontally located dipole antenna over HIGP (Back View);
c) Diagonally located dipole antenna over HIGP (Front View);
d) Horizontally located dipole antenna over PEC.

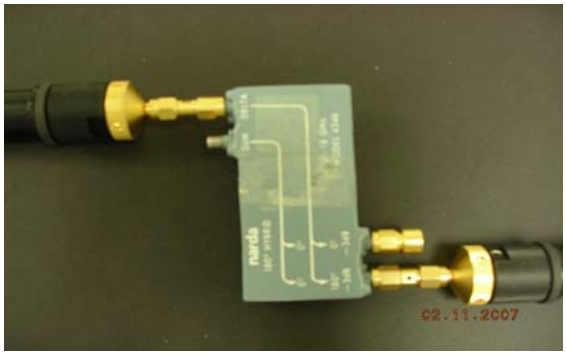

Figure 16. Hybrid Coupler

Dipole antenna/HIGP samples, with hybrid coupler, were put into Styrofoam and mounted on a maneuverable stand located in the middle of the anechoic chamber as shown in figure 17.

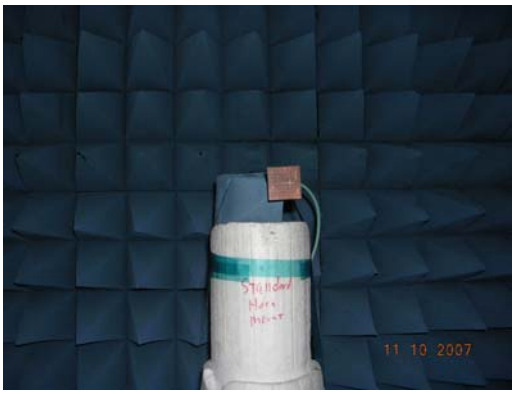

Figure 17. Dipole Antenna/HIGP Measurement in the Anechoic Chamber.

Dipoles were measured in three different ways. In the first two measurements, dipoles were mounted horizontally and diagonally as in figure 18. In the third measurement, the HIGP was covered with a copper tape and the dipole antenna horizontally located over the copper-covered HIGP as in figure 18.d. Thus PEC/dipole data was taken for comparison.

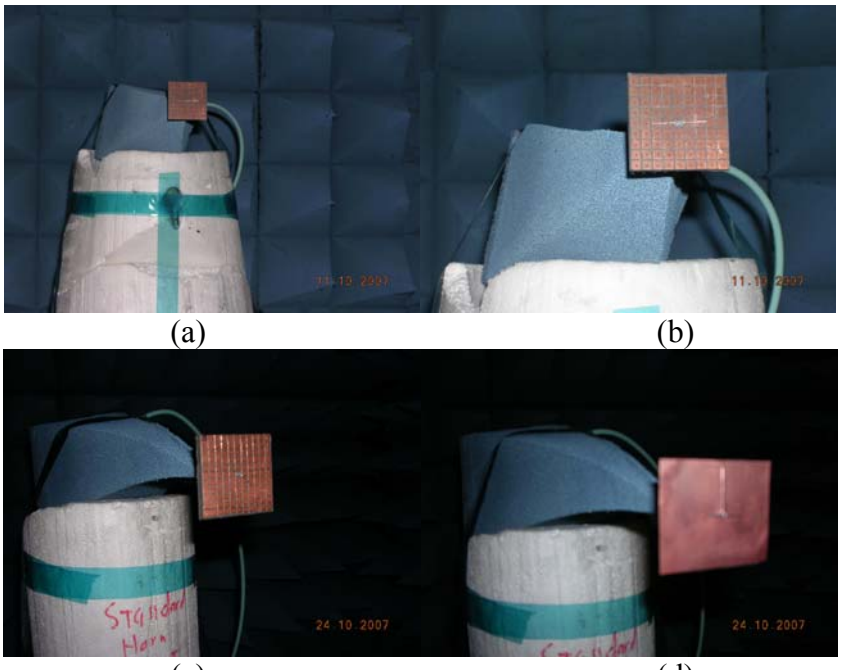

(a) (b)

(c) (d)

Figure 18. HIGP/Dipole Antenna Anechoic Chamber Measurements
a) Horizontally Located Dipole Antenna over HIGP;
b) Horizontally Located Dipole Antenna over HIGP (Close View);
c) Diagonally Located Dipole Antenna over HIGP;
d) Horizontally Located Dipole Antenna over PEC.

Table 5. List of Narrowband Antenna Measurements

HIGP	Dipole Length		Measurement
7 by 7	**0.4λ**	15 mm	Dipole V/H
		15 mm	Diagonal Dipole V/H
		15 mm	PEC Dipole V/H
	0.5λ	18.75 mm	Dipole V/H
		18.75 mm	Diagonal Dipole V/H
		18.75 mm	PEC Dipole V/H
	0.7λ	26.25 mm	Dipole V/H
		26.25 mm	Diagonal Dipole V/H
		26.25 mm	PEC Dipole V/H
9 by 9	**0.4λ**	12 mm	Dipole V/H
		12 mm	Diagonal Dipole V/H
		12 mm	PEC Dipole V/H
	0.5λ	15 mm	Dipole V/H
		15 mm	Diagonal Dipole V/H
		15 mm	PEC Dipole V/H
	0.7λ	21 mm	Dipole V/H
		21 mm	Diagonal Dipole V/H
		21 mm	PEC Dipole V/H
11 by 11	**0.4λ**	10 mm	Dipole V/H
		10 mm	Diagonal Dipole V/H
		10 mm	PEC Dipole V/H
	0.5λ	12.5 mm	Dipole V/H
		12.5 mm	Diagonal Dipole V/H
		12.5 mm	PEC Dipole V/H
	0.7λ	17.5 mm	Dipole V/H
		17.5 mm	Diagonal Dipole V/H
		17.5 mm	PEC Dipole V/H

A total of fifty four narrowband antenna measurements, for three different HIGP samples, were completed as shown in Table 5. The results of these measurements are detailed in chapter 4. The upper case letters ‘V/H’ stand for vertical/horizontal, which means the transmitter antenna, was vertically and horizontally set. HIGP/dipole antenna samples were set as a receiver antenna.

The S_{21} data was taken and calibrated afterwards. Radiation patterns of dipoles were examined to better understand the behavior of each dipole over square patch HIGP.

The DRH-0118 broadband, double ridged horn antenna, which is linearly polarized, was used for the calibration of the anechoic chamber measurements. The DRH-0118 broadband antenna, as shown in figure 19, was used while the calibration data was being taken. The broadband horn antenna operates over a frequency of 1 to 18 GHz, and the HIGP/dipole antenna samples were tested over the frequency of 2-18 GHz. Thus calibration measurements were applied between 2-18 GHz, twice a day, one at the beginning and one at the end. The data, of vertical-vertical broadband horn antenna measurement, was compared to the theoretical data. The difference between the measured and the theoretical data was added to the data of HIGP/dipole antenna measurements.

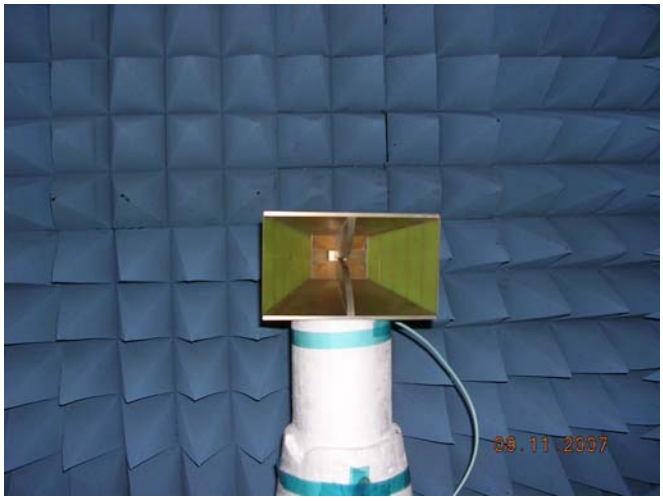

Figure 19. The DRH-0118 Broadband, Double Ridged Horn Antenna

3.6. Broadband Antenna Measurements

The AFIT's far-field anechoic chamber was used for broadband antenna measurements. A log-periodic antenna was chosen as a broadband antenna. In figure 20, the picture of the chosen log-periodic broadband antenna is shown. To understand the different behavior of a broadband antenna over the HIGP samples, first the log-periodic antenna was measured in the anechoic chamber to obtain the free space radiation pattern. Then two different HIGP samples with the log-periodic, detailed below, were analyzed. The optimized samples were designed to provide maximum band gap and bandwidth in the desired frequency range.

Figure 20. The Log-periodic Broadband Antenna

The first HIGP sample, shown in figure 21 was designed as an 11 by 11 square patch HIGP. The square patch design was printed on a RT/duroid 5880 board. The substrate permittivity (ε_r) is 2.2. This design is similar to the starting HIGP designs that were used in the narrowband antenna measurements, but with different parameters. In Table 6, design parameters of the square patch HIGP sample are shown.

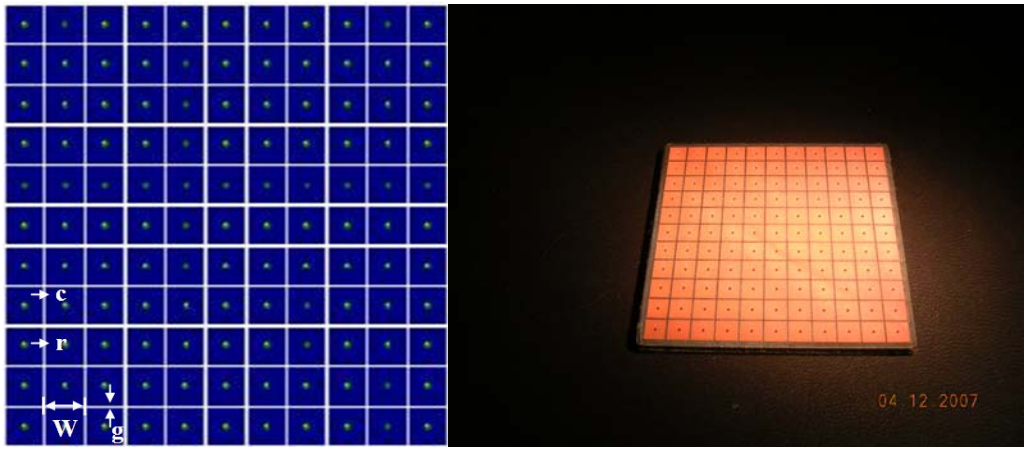

a) b)

Figure 21. 11 by 11 Square Patch HIGP, a) HFSS Design, b) Fabricated HIGP

Table 6. Design Parameters of the 11 by 11 Square Patch HIGP

Parameters	Length (mm/inch)
Patch Width (W)	5.5 / 0.2165
Gap Width (g)	0.4 / 0.0157
Substrate Thickness (h)	3.175 / 0.125
Via Radius (r)	0.0406 / 0.016
Copper Cladding (c)	0.035 / 0.0014

The patch width of the design is 5.5 mm and the gap width is 0.4 mm as shown in Table 6. The parameters used are the optimized parameters using Ansoft's HFSS v.10. In this design, the patch width was increased, whereas the gap width was decreased. It is anticipated that the increase in patch width and the decrease in gap width provide better bandwidth and band gap. A log-periodic broadband antenna was mounted on the square patch HIGP sample, and it was measured in the anechoic chamber as shown in figure 22.

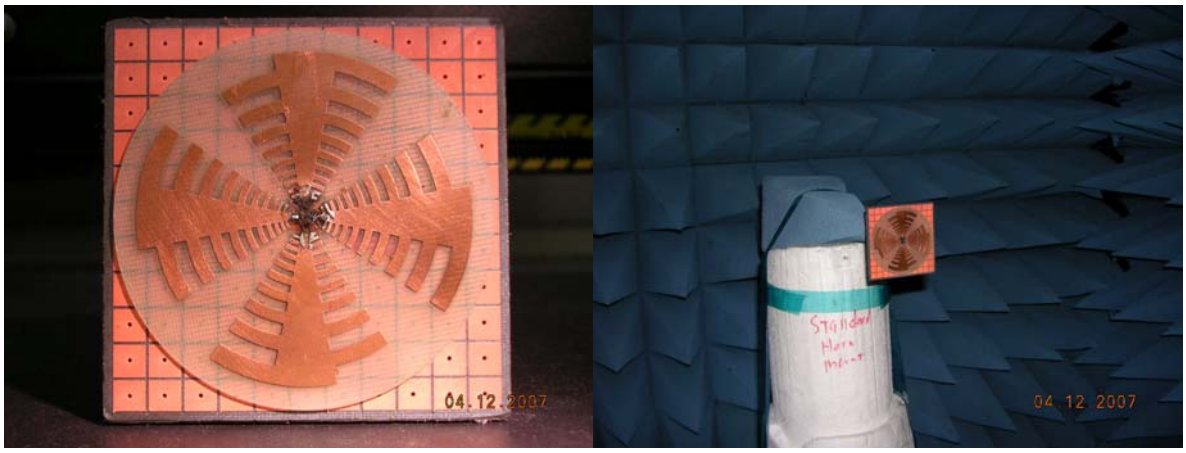

b) b)

Figure 22. 11 by 11 Square Patch HIGP/Log-periodic Antenna Combination
a) Log-periodic Antenna over 11 by 11 Square Patch HIGP,
b) Log-periodic Antenna over 11 by 11 Square Patch HIGP Measurement

The second HIGP sample was designed as a circular patch hexagonal structure as shown in figure 23a. In this design the diameter of a circle (i.e. the patch width) is 5.5 mm and the minimum gap between two circles (i.e. the gap width) is 0.4 mm. The circular patch hexagonal square patch design was printed on a RT/Duroid 5880 board as shown in figure 23b. The behavior of the circular patches and the hexagonal structure were analyzed and compared to the square patch sample.

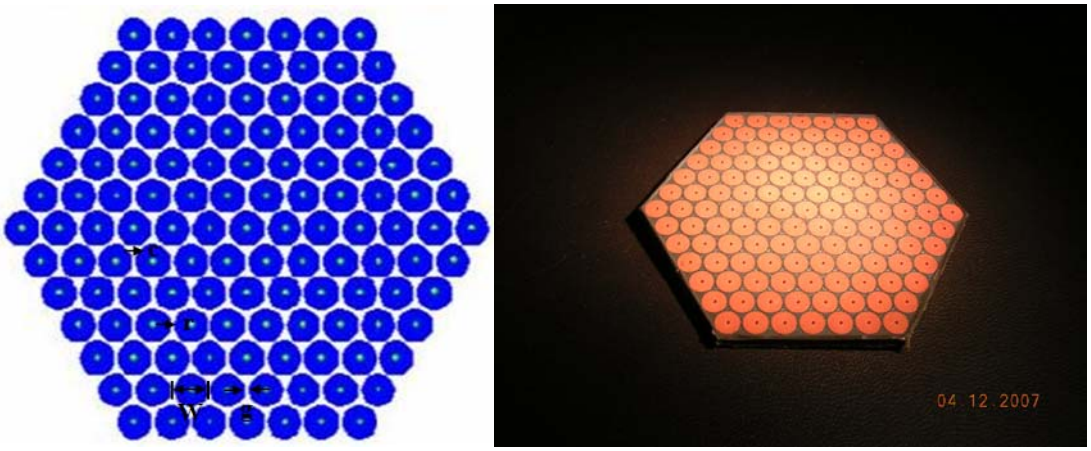

a) b)

Figure 23. Circular Patch Hexagonal HIGP, a) HFSS Design, b) Fabricated HIGP

In Table 7, design parameters of the circular patch hexagonal HIGP sample are shown.

Table 7. Design Parameters of the Circular Patch Hexagonal HIGP

Parameters	Length (mm/inch)
Patch Width (W)	5.5 / 0.6299
Gap Width (g)	0.4 / 0.0157
Substrate Thickness (h)	3.175 / 0.125
Via Radius (r)	0.0406 / 0.016
Copper Cladding (c)	0.035 / 0.0014

The same log-periodic broadband antenna was mounted on the circular patch hexagonal HIGP. Only two horizontal arms of the log-periodic were excited via a hybrid coupler. The HIGP/antenna combination was measured horizontally in the anechoic chamber as shown in figure 24 and the gain of the antenna was measured after calibration.

a) b)

Figure 24. Circular Patch Hexagonal HIGP/Log-periodic Antenna Combination
a) Log-Periodic Antenna over the Circular Patch Hexagonal HIGP
b) Log-Periodic Antenna/11 by 11 Circular Patch Hexagonal HIGP Measurement

3.7. Novel HIGP Design Measurements

Square shaped elements have mostly been used in the construction of mushroom structure HIGPs. For this reason, two multi-scale triangular patch HIGPs were developed as novel designs. Two equilateral triangles with side lengths of 16 mm and 7.6 mm were used. A bow-tie antenna was chosen since it is relatively broadband, and its triangular arms allow for its natural integration into the HIPG structure. Thus, a bow-tie antenna was located in the center of the HIGP structure. Two multi-scale periodic HIGP samples, along with the active bow-tie antennas were printed directly onto a RT/Duroid 5880 substrate with a permittivity of ε_r=2.2 to form the HIGP-antenna combinations. The connections of the mushroom elements were formed by drilling vias at the centroids of the HIGP elements. Furthermore, the bow-tie antenna was excited by a balanced coaxial feed using two coaxial lines fed with 180^o phase difference. The design parameters are shown in Table 8 below.

Table 8. Design Parameters of Multi-scale Triangular Patch HIGP Designs

Parameters	Length (mm/inch)
Patch Width (W_1)	7.6 / 0.2992
Patch Width (W_2)	16 / 0.6299
Gap Width (g)	0.4 / 0.0157
Substrate Thickness (h)	3.175 / 0.125
Via Radius (r)	0.0406 / 0.016
Copper Cladding (c)	0.035 / 0.0014

We used triangular mushroom element HIGPs made from two different size elements. They have a combined large band-gap that extends across the operation bandwidth of a simple bow-tie antenna.

In the first design, a 16 mm-bow-tie antenna was located in the middle of multi-scale triangular mushrooms. The bow-tie was vertically covered with smaller triangular mushrooms (with side lengths of 7.6mm) and larger mushrooms (with side lengths of 16mm) were located on the sides as shown in figure 25.

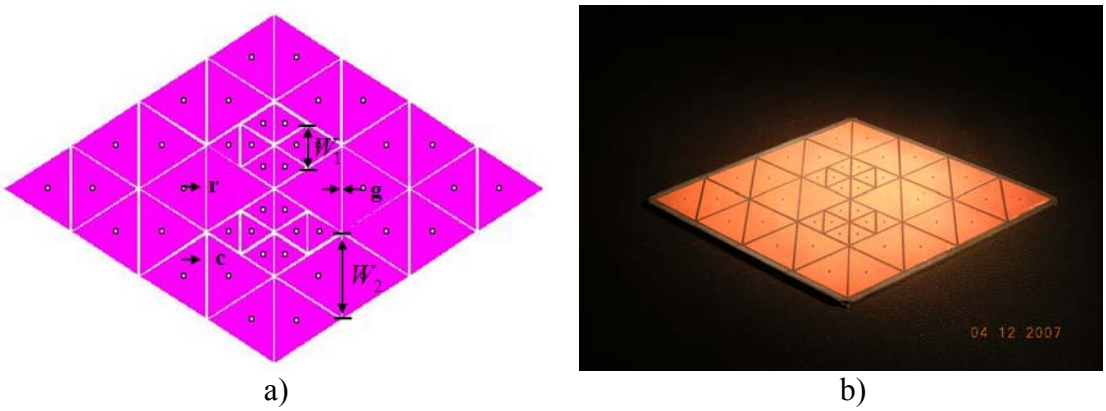

a) b)

Figure 25. Multi-scale Triangular-patch HIGP with 16 mm-Bow-tie Antenna
a) HFSS Design, b) Fabricated Sample

The return loss and the radiation pattern of the bow-tie were tested. The radiation pattern of the combination was measured in the anechoic chamber as shown in figure 26.

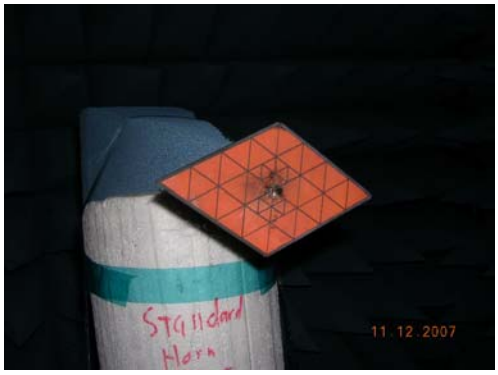

Figure 26. Triangular-patch HIGP with 16 mm-Bow-tie Antenna Measurement

In the final design, a 7.6 mm-bow-tie antenna was located in the center of multi-scale triangular mushrooms. The bow-tie was surrounded with smaller triangular mushrooms (with side lengths of 7.6mm). Larger mushrooms (with side lengths of 16mm) were located to the edges of the substrate. The resulting composite antenna geometry is shown in figure 27.

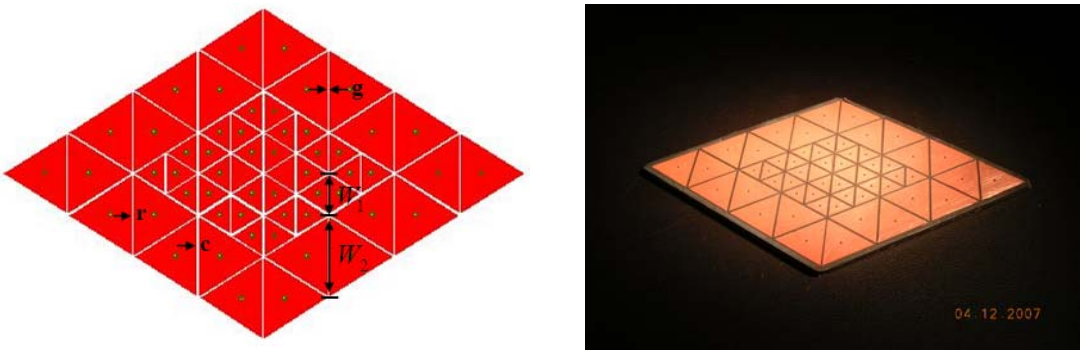

a) b)

Figure 27. Multi-scale Triangular-patch HIGP with 7.6 mm-Bow-tie Antenna
a) HFSS Design, b) Fabricated Sample

The radiation pattern of the HIGP/bow-tie combination was measured in the anechoic chamber as shown in figure 28. The return loss of the composite antenna was also characterized from 2 to 10 GHz using Agilent E8362B network analyzer. Return loss results were compared to the bow-tie antenna performance in free-space and on a PEC ground plane.

Figure 28. Triangular-patch HIGP with 16 mm-Bow-tie Antenna Measurement

Chapter 4 Results and Analysis

4.1. Chapter Overview

Results based on the data gathered through experimental measurements are analyzed and presented in this chapter in three phases. Moreover some results are compared to HFSS simulations and were verified. In the first phase results of square patch HIGP surface wave measurements are analyzed. The second phase analyzes the behavior of different length dipoles as narrowband antennas over the square patch HIGP samples. The last phase analyzes behaviors of a log-periodic and two bow-tie broadband antennas over different HIGP surfaces.

4.2. Results of Surface Wave Measurements

Diagonal and horizontal surface waves for 7 by 7, 9 by 9, and 11 by 11 HIGP samples were measured and analyzed to understand the surface wave suppression of different-size square patch mushroom structures, and to find out surface wave frequency band gap. Each of the surface wave measurement results were compared to HFSS (v.10) simulation results to verify our measurements. It is seen that similar results were obtained from both experiment and simulation.

HIGP analysis included both surface wave measurements and antenna measurements. Same samples used in surface wave measurements were also used in narrowband antenna measurements. Resonant frequencies of dipoles over square patch

HIGPs are expected to be similar to reference (Yang and Rahmat-Samii, 2003a:2691-2703). For this reason, band gaps occurring in 10GHz +/- 6 GHz frequency ranges were of interest.

The result of the 7 by 7 square HIGP diagonal surface wave measurement is shown in figure 29. The HIGP sample had a band gap from 5.70 GHz to 13.80 GHz, better than -20 dB with 8.10 GHz-bandwidth. Another band gap between 0-5 GHz, better than -20dB with a 5 GHz-bandwidth is also noticed. Similar figures were obtained from simulation. In figure 30, the result of the HFSS simulation is shown. A band gap better than-20 dB from 4.5 GHz to 12 GHz with a 7.5 GHz bandwidth is easily noticed. A similar band gap is also seen between 0-4.5 GHz as in the experimental result.

The 9 by 9 square patch HIGP diagonal surface wave measurement result is shown in figure 31. The HIGP structure had a band gap from 6.70 GHz to 15.50 GHz , better than -40 dB with 8.80 GHz-bandwidth. The simulation result is shown in figure 32. A similar band gap from 5.8 GHz to 15.5 GHz, better than -40 dB with a 9.7 GHz bandwidth is noticed. Another noticeable band gap between 1-5.5 GHz is also seen.

The 11 by 11 square HIGP diagonal surface wave measurement result is shown in figure 33. The HIGP sample had a band gap from 7.20 GHz to 16.60 GHz, better than -50 dB with a 9.40 GHz-bandwidth. Figure 34 shows the simulation result. A similar band gap from 6 GHz to 16 GHz, better than -50 dB with a 10 GHz-bandwidth is noticed. Another band gap between 1-5.5 GHz as in 9 by 9 diagonal surface wave simulation result is also noticed.

The result of the 7 by 7 square HIGP horizontal surface wave measurement is shown in figure 35. The HIGP sample had a band gap from 5.70 GHz to 13.80 GHz

better than -20 dB with an 8.10 GHz-bandwidth as in the diagonal measurement. Another band gap between 0-5 GHz, better than -20dB, with a 5 GHz-bandwidth is seen. A similar figure was obtained from simulation. Figure 36 shows the simulation results. A band gap from 5 GHz to 11.5 GHz, better than -20 dB, is noticed. A similar band gap is also seen between 1-4.5 GHz at the experimental results.

The 9 by 9 square HIGP horizontal surface wave measurement results are shown in figure 37. The HIGP sample had a band gap from 6.70 GHz to 15.00 GHz better than -40 dB with 8.30 GHz-bandwidth. The simulation results are shown in figure 38. A similar band gap from 6.5 GHz to 13.2 GHz, better than -40 dB, with a 6.7 GHz bandwidth is noticed. Another noticeable band gap between 1-6 GHz is also seen.

The 11 by 11 square HIGP horizontal surface wave measurement results are as shown in figure 39. The HIGP sample had a band gap from 7.20 GHz to 16.60 GHz, better than -50 dB with a 9.40 GHz bandwidth. Figure 40 shows the simulation results. Similar band gap from 6.5 GHz to 13 GHz, better than -50 dB with a 7.5 GHz bandwidth is noticed. Another band gap between 1-5.5 GHz is also seen.

All surface wave measurement results of square patch HIGP samples are listed below in Table 9.

Table 9. HIGP Surface Wave Measurements Results

HIGP	Experiment		Simulation	
	Band Gap (GHz)	**Bandwidth (GHz)**	**Band Gap (GHz)**	**Bandwidth (GHz)**
7 by 7 Diagonal	5.70 – 13.80	8.10	4.50 – 12.00	7.50
9 by 9 Diagonal	6.70 – 15.50	8.80	5.80 – 15.50	9.70
11 by 11 Diagonal	7.20 – 16.60	9.40	6.00 – 16.00	10.00
7 by 7 Horizontal	5.70 – 13.80	8.10	5.00 – 11.50	6.50
9 by 9 Horizontal	6.70 – 15.00	8.30	6.50 – 13.20	6.70
11 by 11 Horizontal	7.20 – 16.60	9.40	6.50 – 13.00	7.50

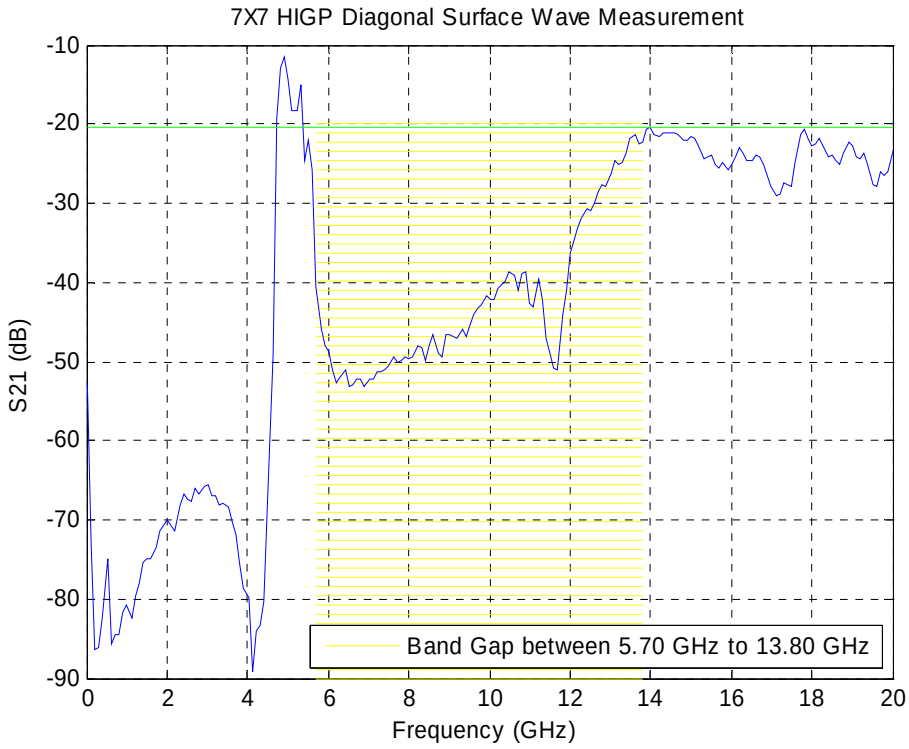

Figure 29: 7 by 7 HIGP Diagonal Surface Wave Result

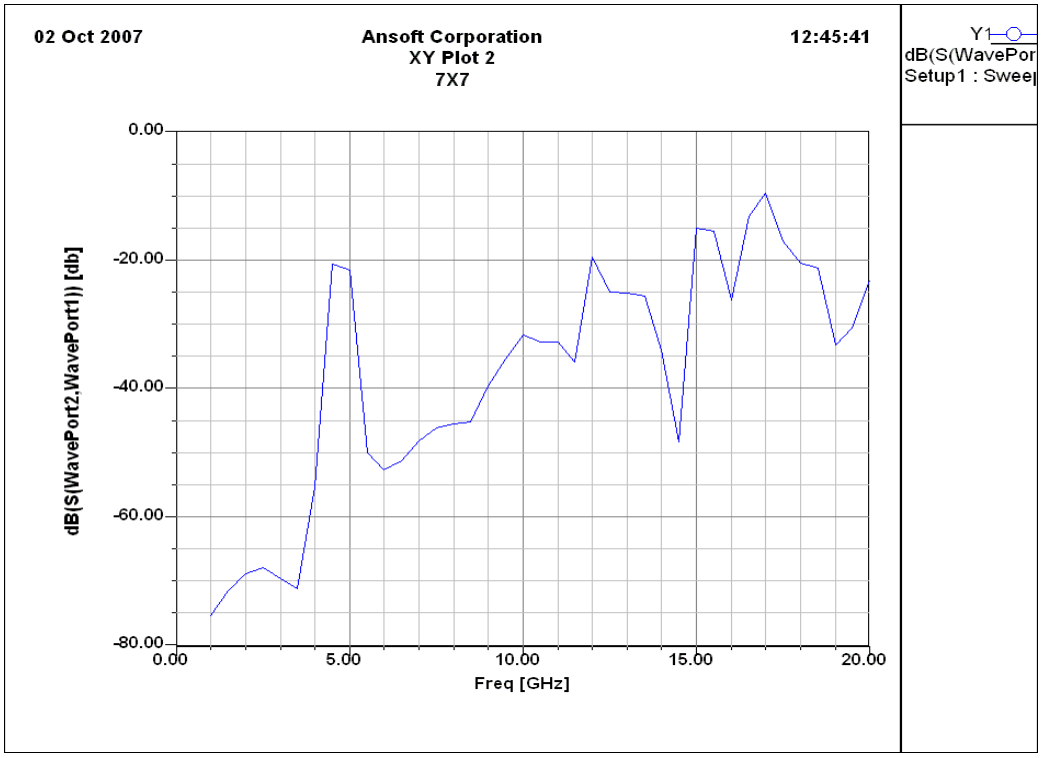

Figure 30: 7 by 7 HIGP Diagonal Surface Wave HFSS Result

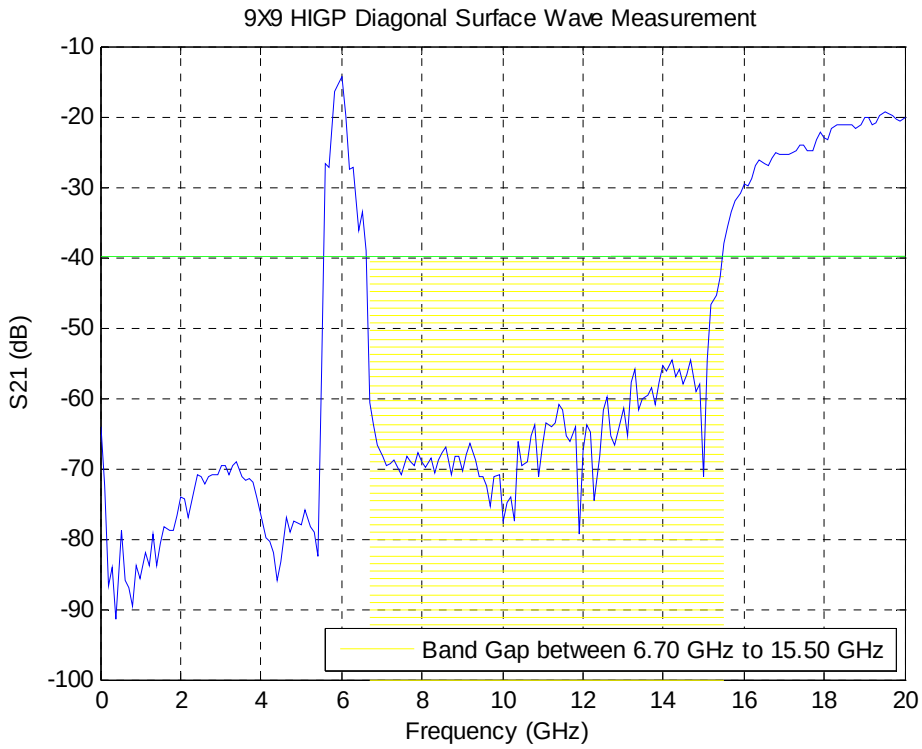

Figure 31: 9 by 9 HIGP Diagonal Surface Wave Result

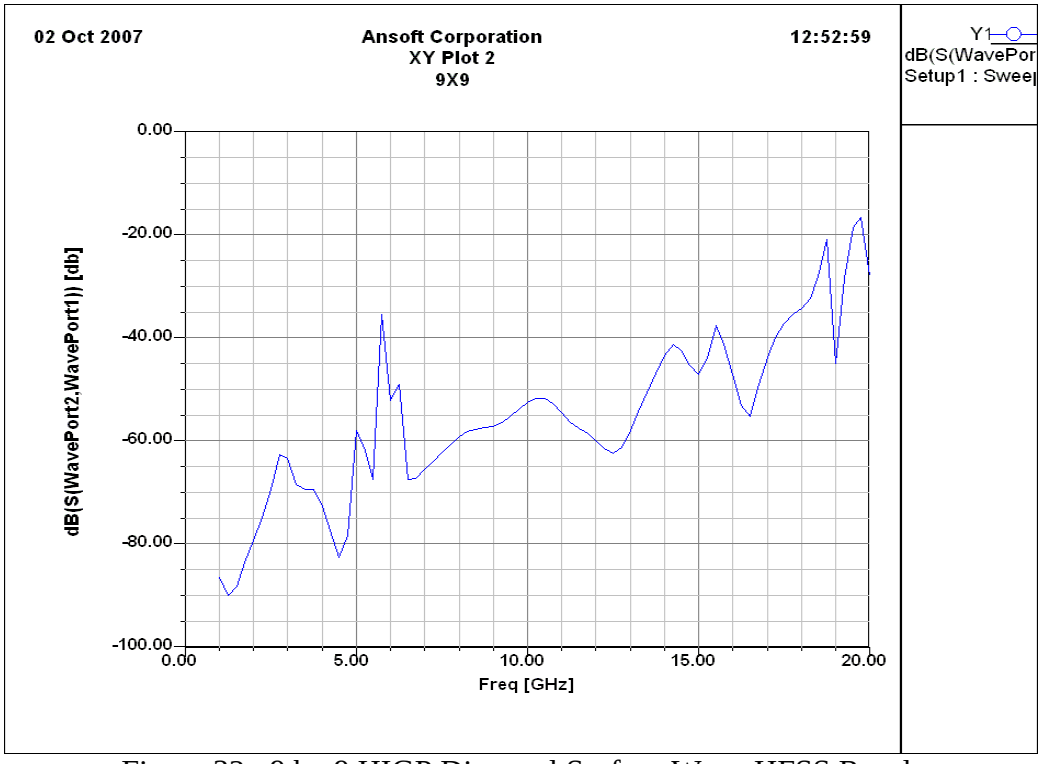

Figure 32: 9 by 9 HIGP Diagonal Surface Wave HFSS Result

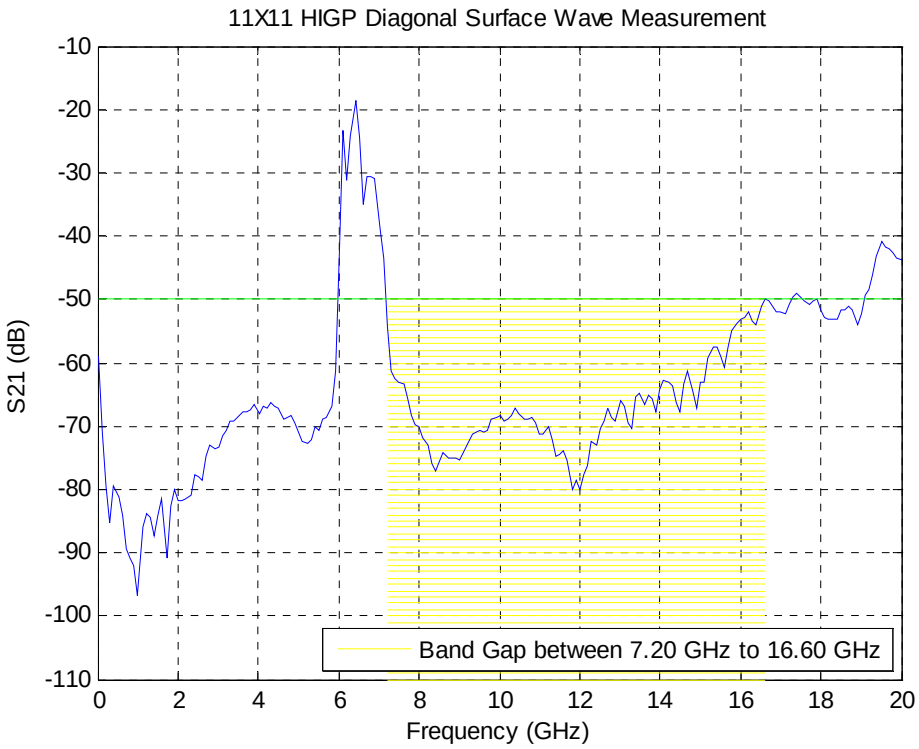

Figure 33: 11 by 11 HIGP Diagonal Surface Wave Result

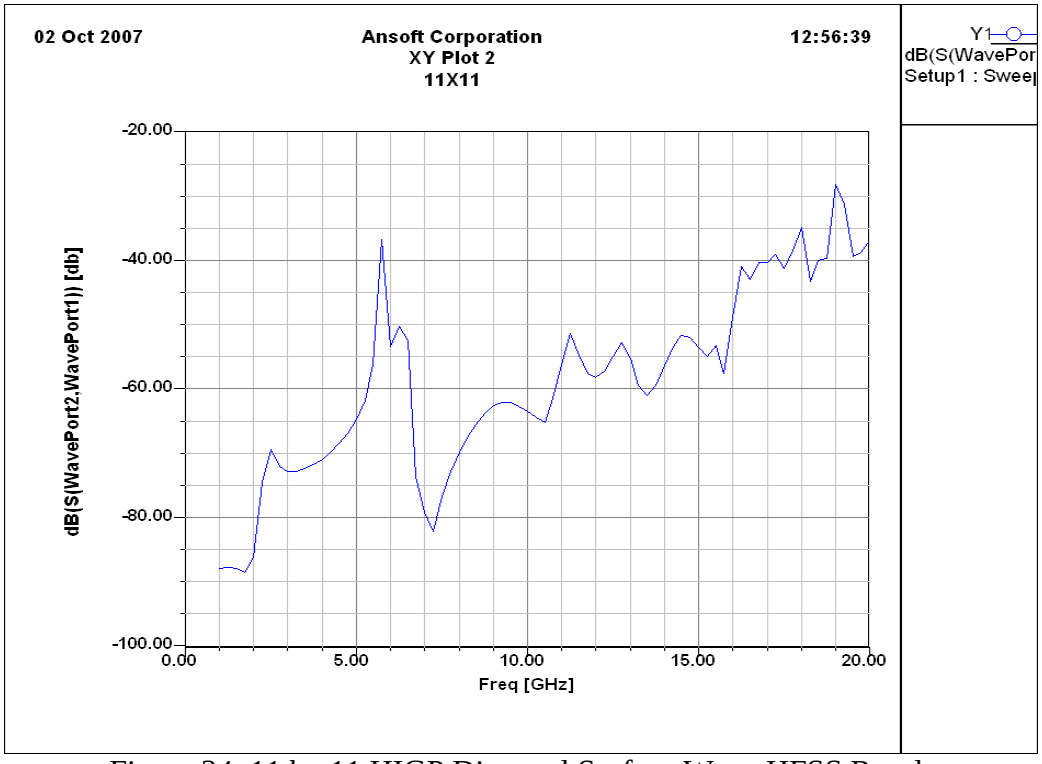

Figure 34: 11 by 11 HIGP Diagonal Surface Wave HFSS Result

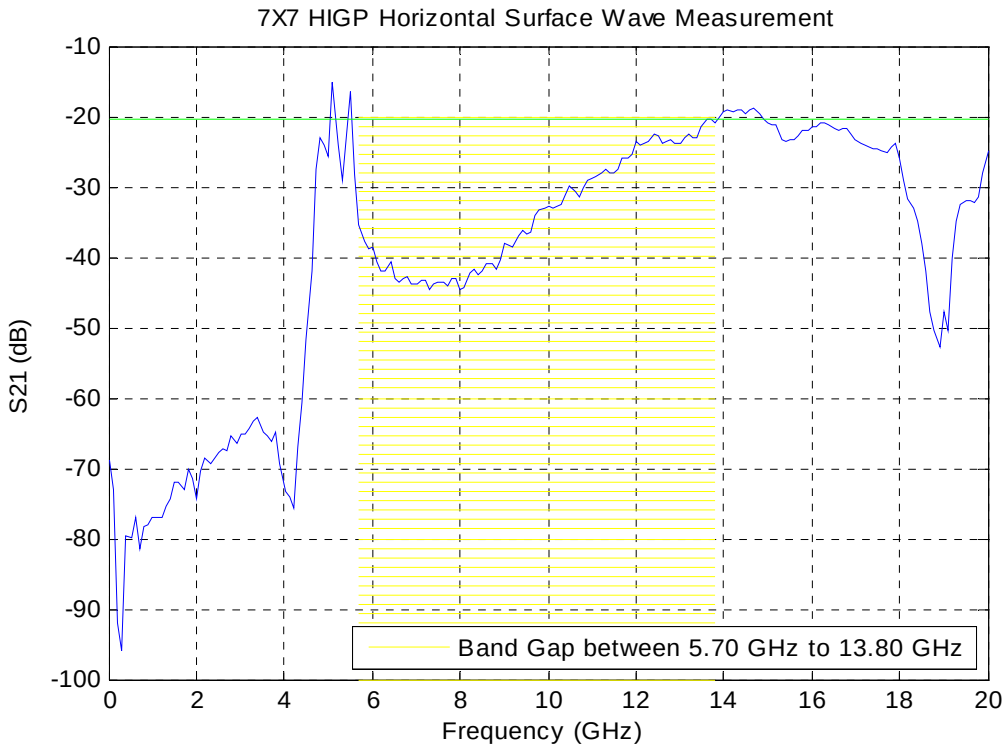

Figure 35: 7 by 7 HIGP Horizontal Surface Wave Result

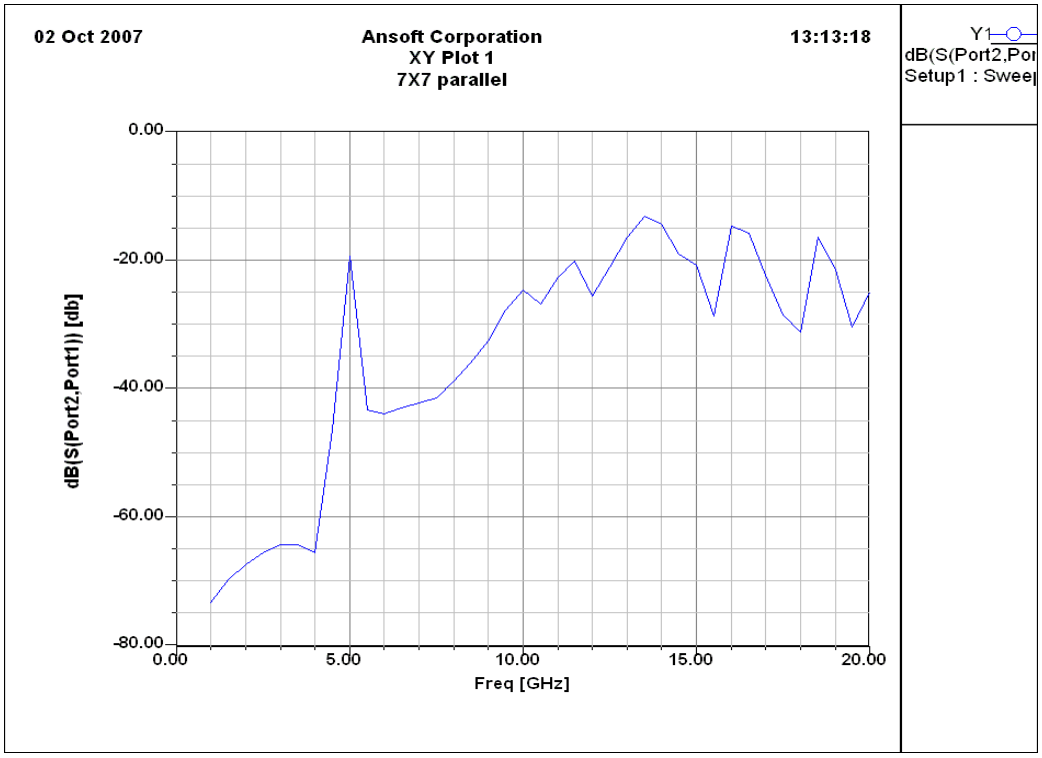

Figure 36: 7 by 7 HIGP Horizontal Surface Wave HFSS Result

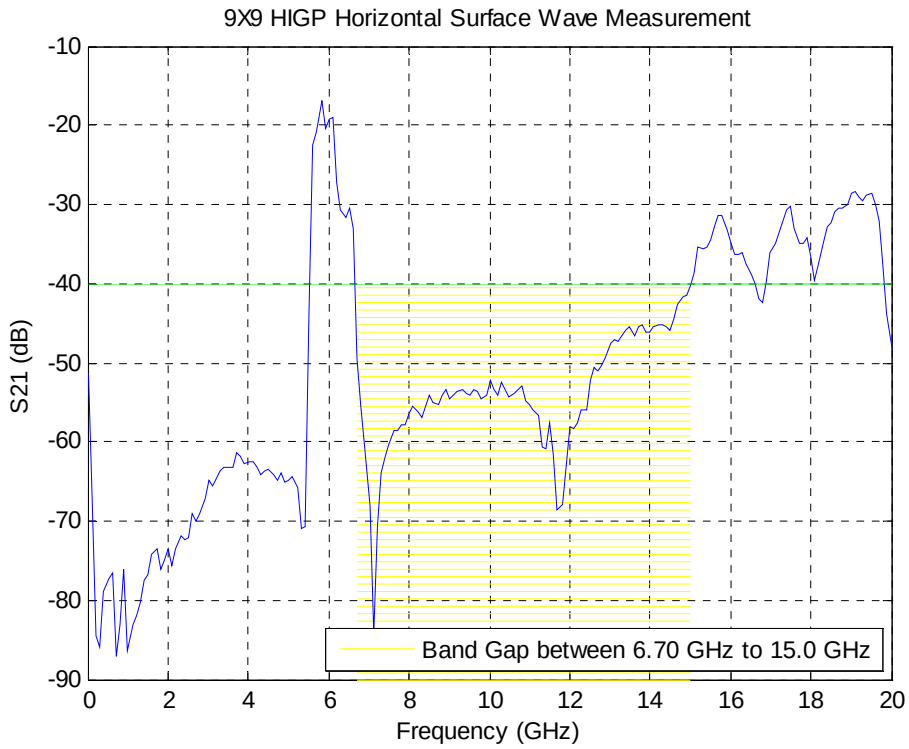

Figure 37: 9 by 9 HIGP Horizontal Surface Wave Result

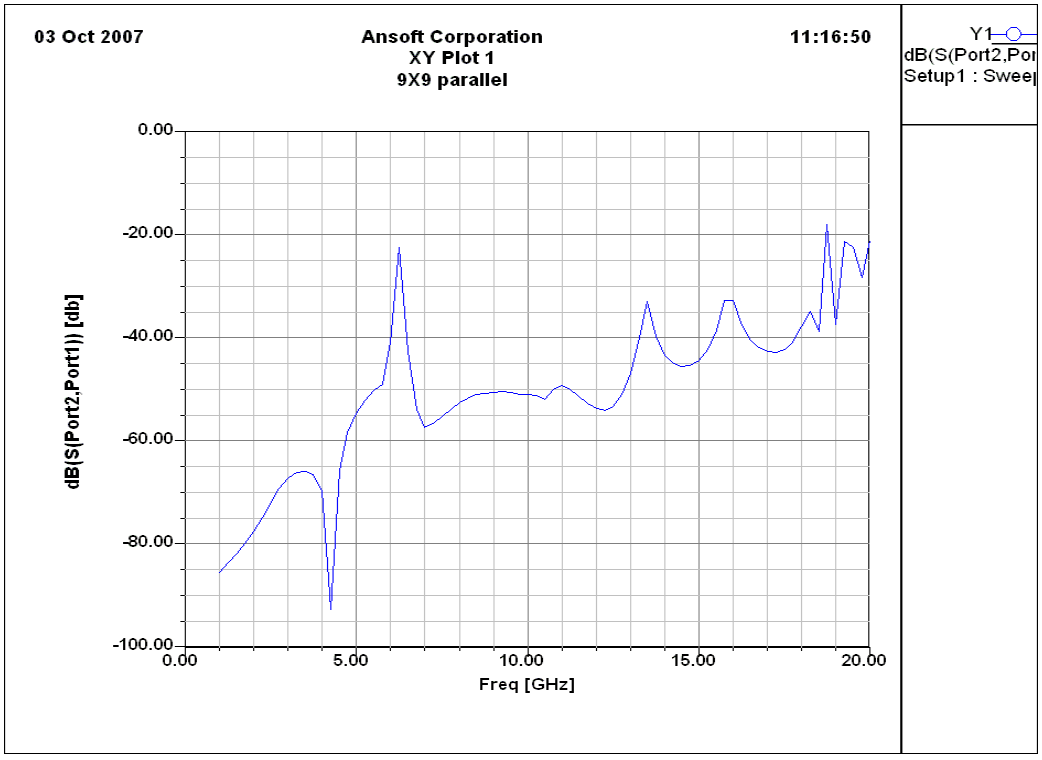

Figure 38: 9 by 9 HIGP Horizontal Surface Wave HFSS Result

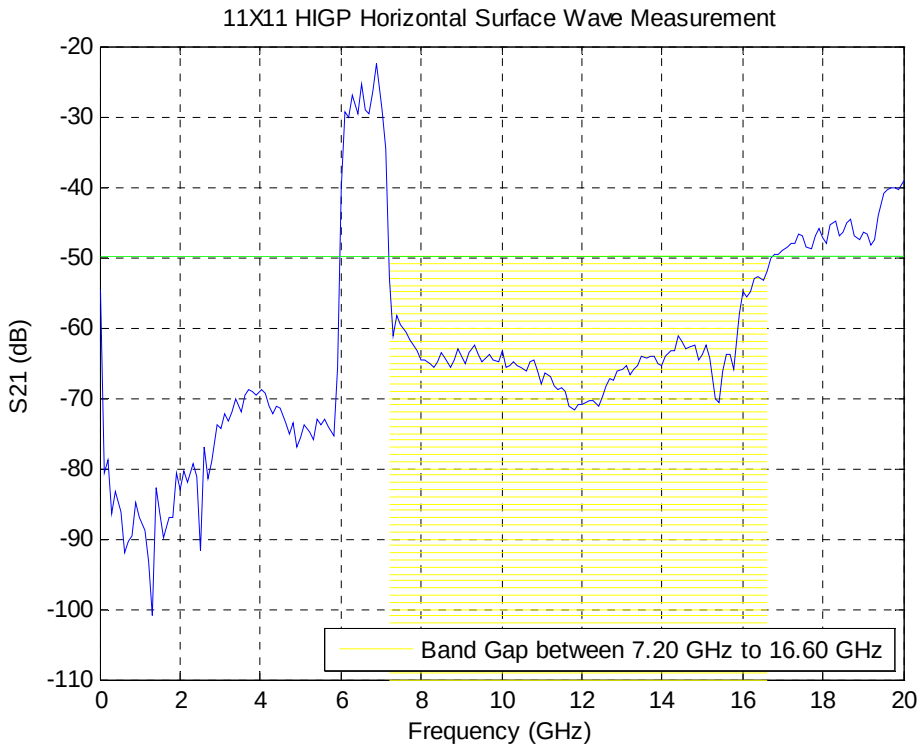

Figure 39: 11 by 11 HIGP Horizontal Surface Wave Result

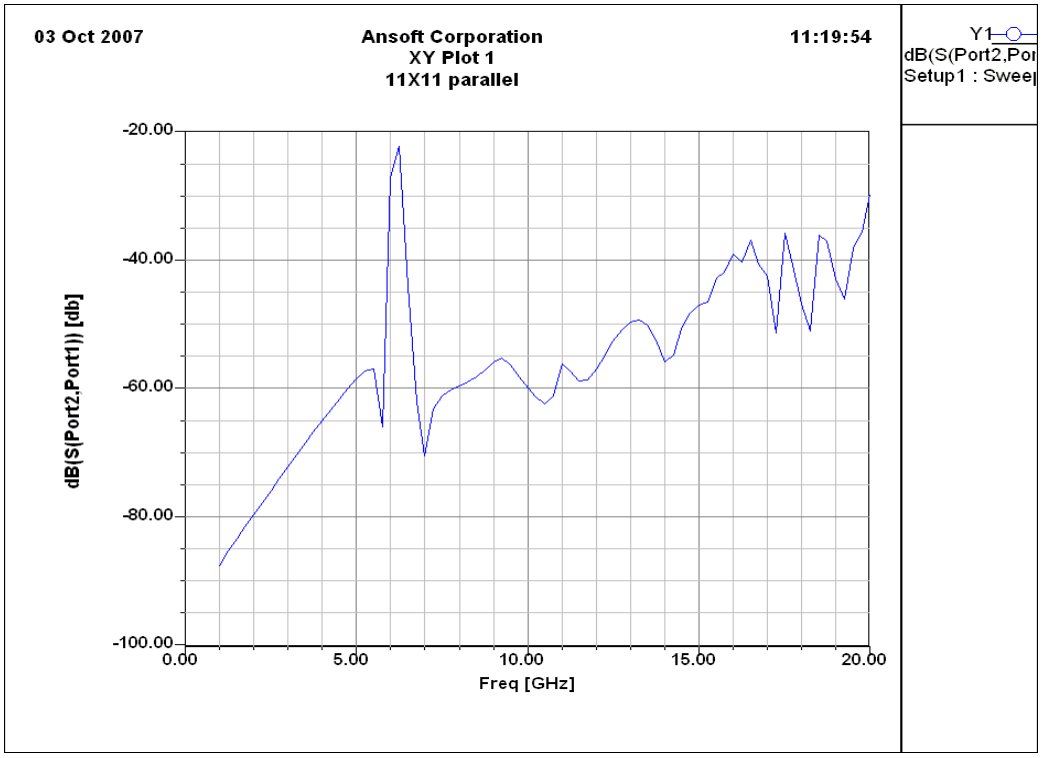

Figure 40: 11 by 11 HIGP Horizontal Surface Wave HFSS Result

4.3. Results of Narrowband Antenna Measurements

In this phase, the same square-patch HIGP samples were tested with three different length dipole antennas. The list of dipole antenna lengths were given in Table 4 and the list of measurements are shown in Table 5 in chapter 3.

First, the return loss data of HIGP/dipole combinations was taken from 2 GHz to 18 GHz. Band gaps which have a return loss better than -10 dB are identified to find out the resonant frequencies of the dipoles. Dipoles are well matches at resonant frequencies. Thus, the frequencies which provide the minimum return loss were chosen for use in the radiation pattern figures in gain measurements.

The result of each gain measurement is analyzed in three figures. The three dimensional dipole antenna pattern is shown in the first figure, the gain performance of the antenna is shown in the second figure, and the radiation pattern at the maximum impedance match point is given in the third figure.

In the three dimensional antenna pattern figures the frequency range from 2 GHz to 18 GHz and the angle range from -90° to 90° were taken. In gain performance figures the data at 0° is plotted which means both transmitter and the receiver antennas were head on to each other. In radiation pattern figures, frequencies, which give better return loss results were chosen and radiation pattern figures were plotted at this frequency in the -90° to 90° angle range. The frequency band, which gives better return loss result, is also known as an input-match frequency band. It is expected that the operational frequency band of our HIGP/antenna combinations should be the overlap of the surface-wave frequency band and the input-match frequency band.

4.3.1. 7 by 7 HIGP/Dipole Antenna Return Loss Measurements

The result of the 7 by 7 HIGP/0.4 λ_{8GHz} -dipole antenna return loss measurement is shown in figure 41. The dipole shows a return loss better than -10 dB from 8 to 12 GHz and from 13 to 14.5 GHz. Better return loss values were obtained at 10.5 GHz, and 13.7 GHz.

The result of the 7 by 7 HIGP/0.5 λ_{8GHz} -dipole antenna return loss measurement is shown in figure 42. The dipole shows a return loss better than -15 dB from 10 to 12 GHz and from 13 to 14 GHz. Better return loss values were obtained at 10.5 GHz, and 13.7 GHz.

The result of the 7 by 7 HIGP/0.50.7 λ_{8GHz} -dipole antenna return loss measurement is shown in figure 43. The dipole shows a return loss better than -15 dB from 8 to 12 GHz and from 13 to 14 GHz. Better return loss values were obtained at 10.5 GHz, and 13.7 GHz.

a) 7 by 7 HIGP with 0.4 λ_{8GHz} -Dipole Return Loss Measurement

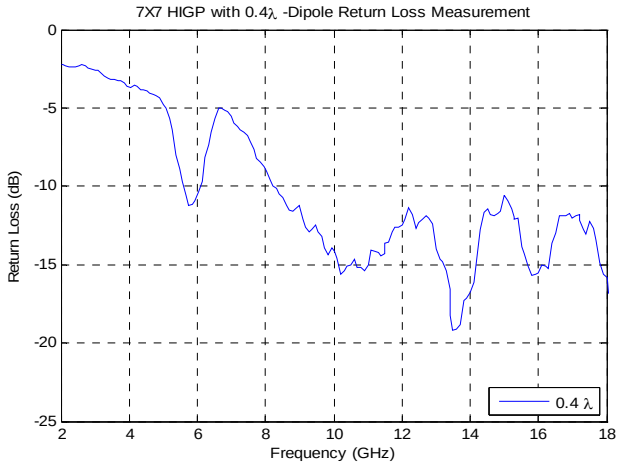

Figure 41: 7 by 7 HIGP with 0.4 λ_{8GHz} -Dipole Return Loss Result

b) 7 by 7 HIGP with 0.5 λ_{8GHz} -Dipole Return Loss Measurement

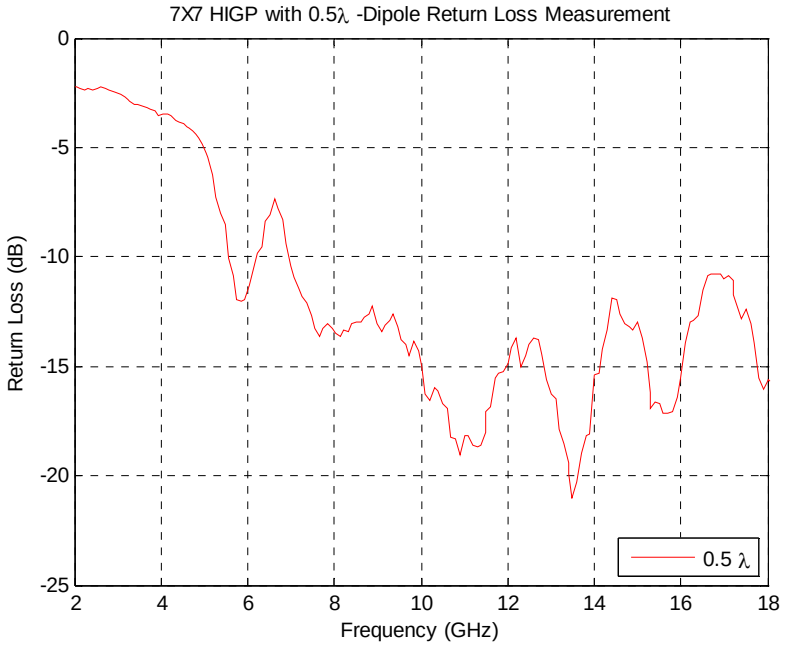

Figure 42: 7 by 7 HIGP with 0.5 λ_{8GHz} -Dipole Return Loss Result

c) 7 by 7 HIGP with 0.7 λ_{8GHz} -Dipole Return Loss Measurement

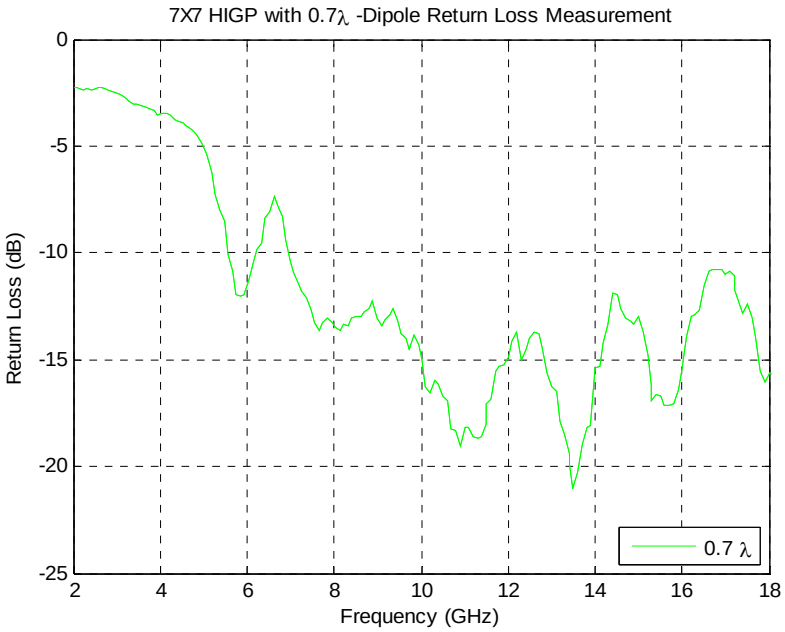

Figure 43: 7 by 7 HIGP with 0.7 λ_{8GHz} -Dipole Return Loss Result

4.3.2. 7 by 7 HIGP/Dipole Antenna Gain Measurements

Figure 44 shows the results of the 7 by 7 HIGP/0.4 λ_{8GHz}-dipole measurements. The HIGP/antenna combination had better gain from 6.8 to 11.1 GHz with a 4.3 GHz bandwidth. Figure 45 shows the results of the 7 by 7 HIGP/0.5 λ_{8GHz}-dipole antenna measurements. The HIGP/antenna combination had better gain from 6.6 to 11.1 GHz with a 4.5 GHz bandwidth. Figure 46 shows the results of the 7 by 7 HIGP/0.7 λ_{8GHz}-dipole antenna measurements. The HIGP/antenna combination had better gain from 6.5 to 11.1 GHz with a 4.6 GHz bandwidth.

Figure 47 shows the comparison of the gain performance of 0.4 λ_{8GHz}, 0.5 λ_{8GHz}, and 0.7 λ_{8GHz} dipoles over the 7 by 7 HIGP. The 0.7 λ_{8GHz} had better gain than other dipoles. Especially in the frequency range between 6.8 and 11.1 GHz, HIGP provides almost 10 dB gain. Figure 48 shows the comparison of the gain performance of 0.4 λ_{8GHz}, 0.5 λ_{8GHz}, and 0.7 λ_{8GHz} dipoles over the PEC. The 0.7 λ_{8GHz} dipole had better gain than 0.4 λ_{8GHz}, 0.5 λ_{8GHz} dipoles, but especially in low frequencies dipoles have much less gain than the dipoles over the HIGP, due to the conducting surface.

Figure 49 shows the comparison of the radiation pattern of 0.4 λ_{8GHz}, 0.5 λ_{8GHz}, and 0.7 λ_{8GHz} dipoles over the 7 by 7 HIGP. The 0.7 λ_{8GHz} dipole had better radiation pattern at 10.5 GHz, better than 8 dB. Figure 50 shows the comparison of the radiation pattern of 0.4 λ_{8GHz}, 0.5 λ_{8GHz}, and 0.7 λ_{8GHz} dipoles over the PEC at 10.5 GHz. The 0.7 λ_{8GHz} dipole had better gain than the other dipoles, but it's seen that HIGP provides much better gain.

a) 7 by 7 HIGP with 0.4 λ_{8GHz} -Dipole Horizontal Measurement

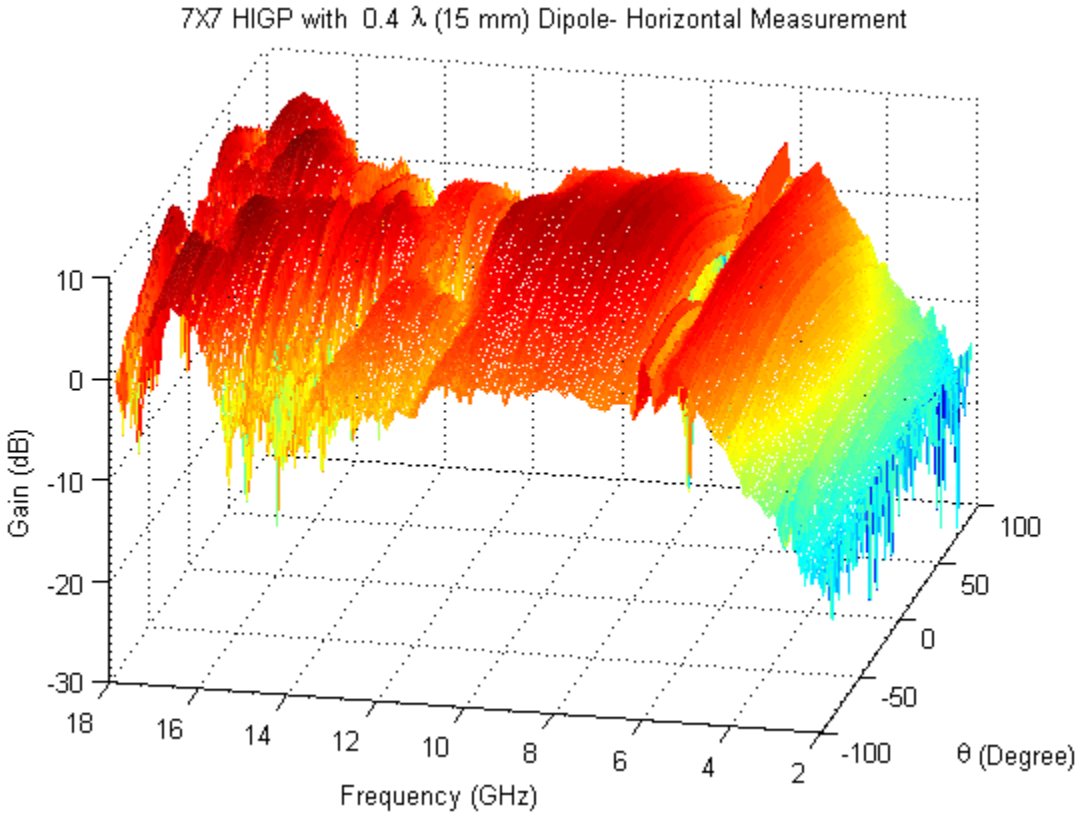

a) 7 by 7 0.4 λ_{8GHz} -Dipole Antenna Pattern

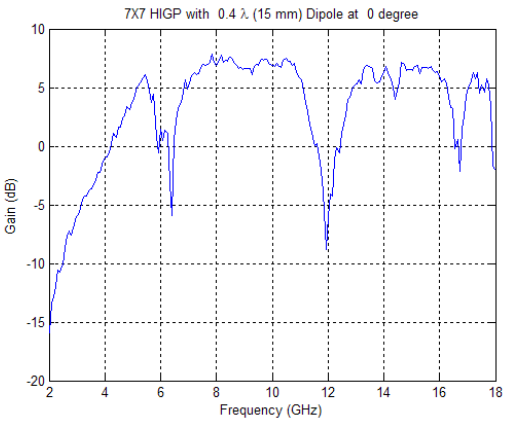

b) Gain Performance

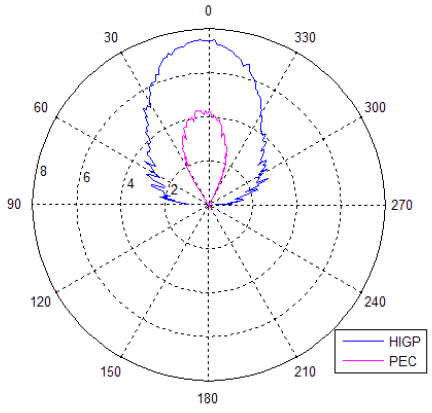

c) Radiation Pattern at 10.5 GHz

Figure 44: 7 by 7 Square Patch HIGP with 0.4 λ_{8GHz} -Dipole Measurement

b) 7 by 7 HIGP with 0.5 λ_{8GHz} (18.75 mm) Dipole Horizontal Measurement

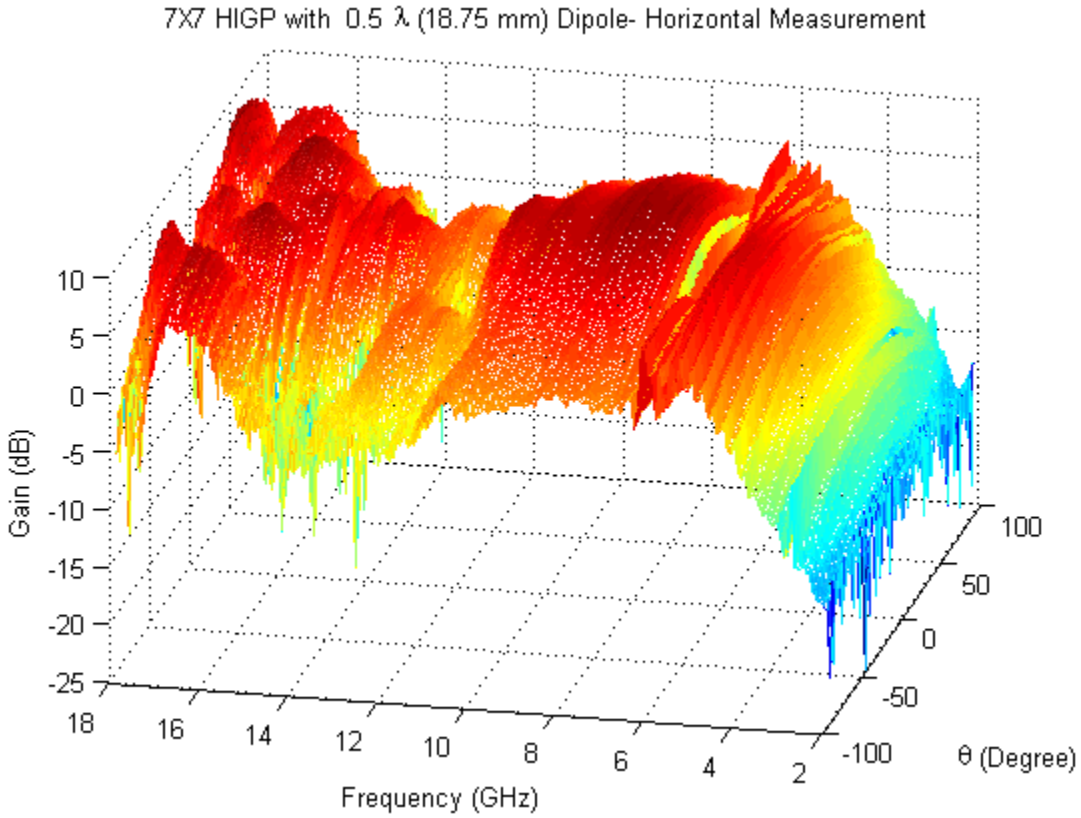

a) 7 by 7 0.5 λ_{8GHz} -Dipole Antenna Pattern

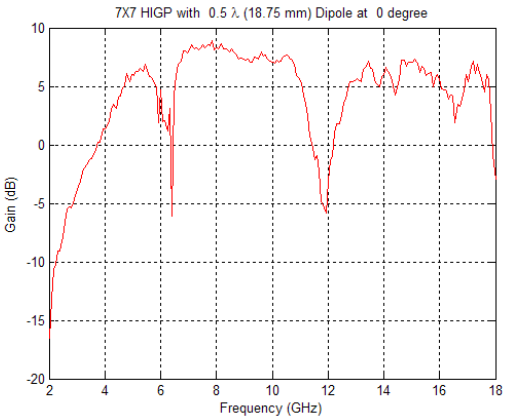

b) Gain Performance

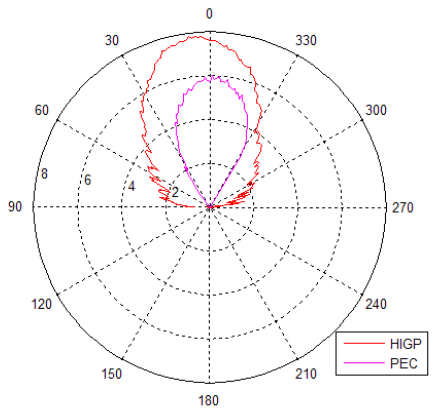

c) Radiation Pattern at 10.5 GHz

Figure 45: 7 by 7 Square Patch HIGP with 0.5 λ_{8GHz} -Dipole Horizontal Measurement

c) 7 by 7 HIGP with 0.7 λ_{8GHz} (26.25 mm) Dipole Horizontal Measurement

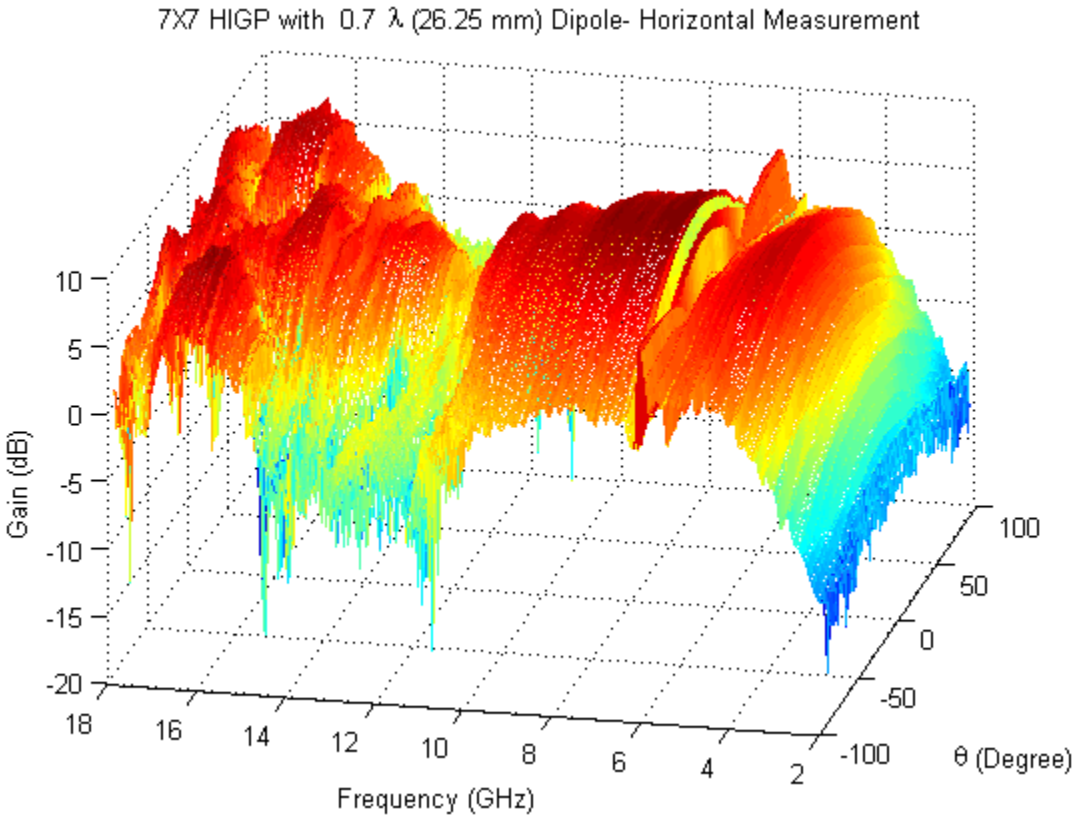

a) 7 by 7 0.7 λ_{8GHz} Dipole Antenna Pattern

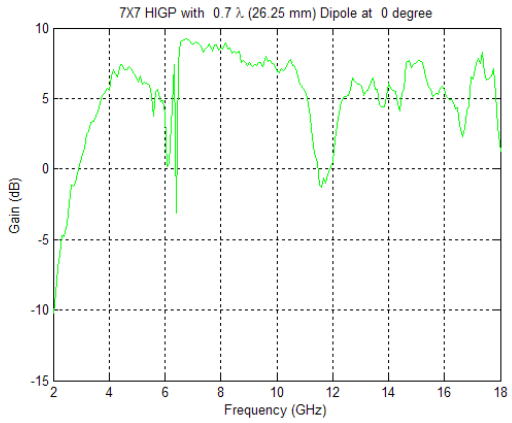

b) Gain Performance

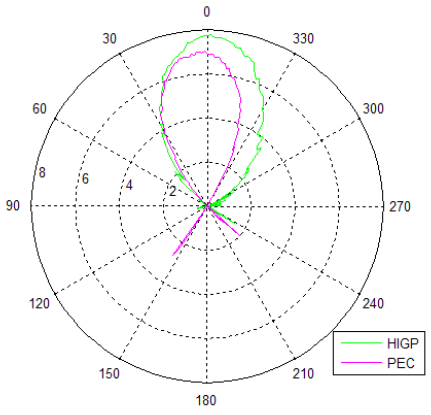

c) Radiation Pattern at 10.5 GHz

Figure 46: 7 by 7 Square Patch HIGP with 0.7 λ_{8GHz} -Dipole Horizontal Measurement

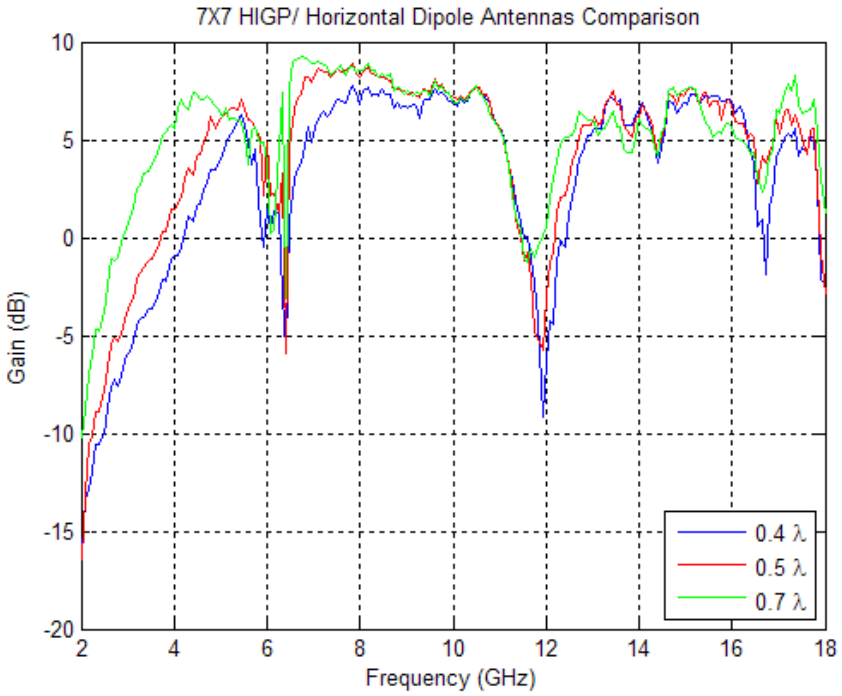

Figure 47: 7 by 7 HIGP/Dipole Gain Performance Comparison

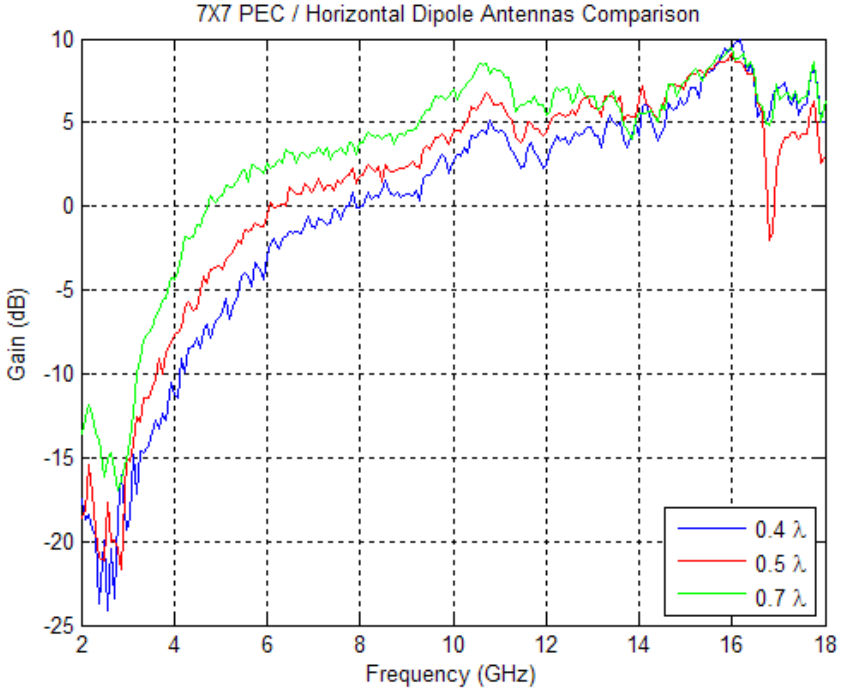

Figure 48: 7 by 7 PEC/Dipole Gain Performance Comparison

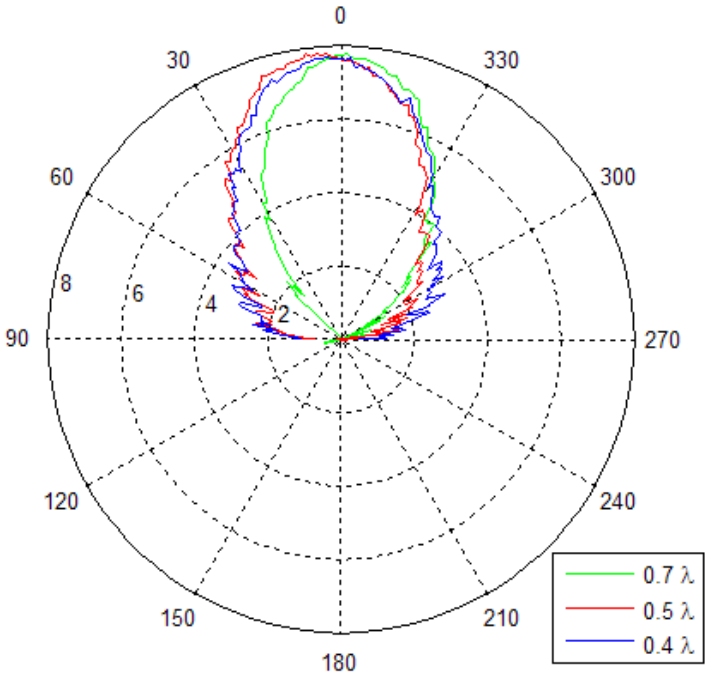

Figure 49: 7 by 7 HIGP/ Dipole Radiation Pattern Comparison

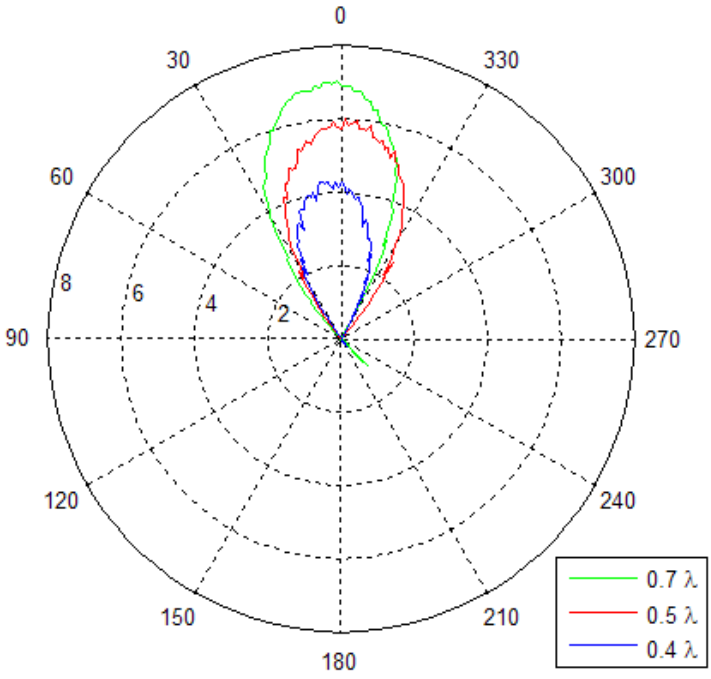

Figure 50: 7 by 7 PEC/ Dipole Radiation Pattern Comparison

4.3.3. 9 by 9 HIGP/Dipole Antenna Return Loss Measurements

The results of the 9 by 9 HIGP/0.4 λ_{10GHz} -dipole antenna return loss measurement are shown in figure 51. The dipole shows a return loss better than -10 dB from 13 to 15 GHz. Better return loss values obtained at 10.5 and 14 GHz.

The results of the 9 by 9 HIGP/0.5 λ_{10GHz} -dipole antenna return loss measurement are shown in figure 52. The dipole shows a return loss better than -15 dB from 13 to 14.5 GHz. Better return loss value obtained at 10.5 and 14 GHz.

The results of the 9 by 9 HIGP/0.50.7 λ_{10GHz} -dipole antenna return loss measurement are shown in figure 53. The dipole shows a return loss better than -15 dB from 13 to 14.5 GHz and from 10.5 to 11.5 GHz. Better return loss values were obtained at 10.5, and 14 GHz.

a) 9 by 9 HIGP with 0.4 λ_{10GHz} -Dipole Return Loss Measurement

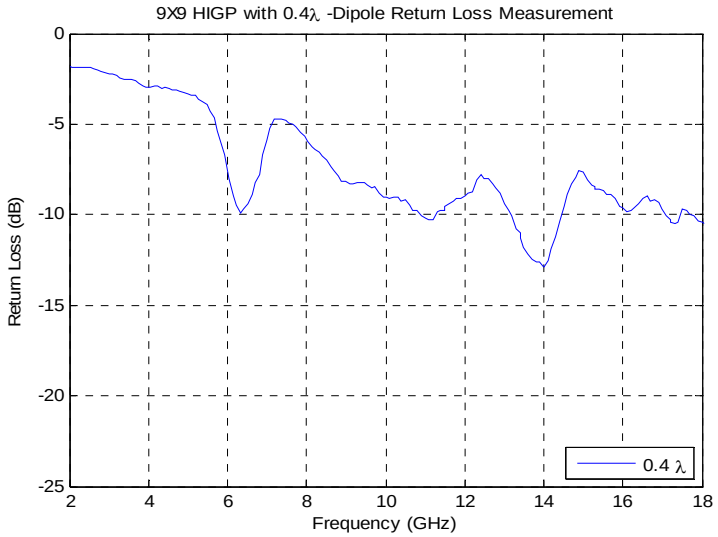

Figure 51: 9 by 9 HIGP with 0.4 λ_{10GHz} -Dipole Return Loss Result

b) 9 by 9 HIGP with 0.5 λ_{10GHz} -Dipole Return Loss Measurement

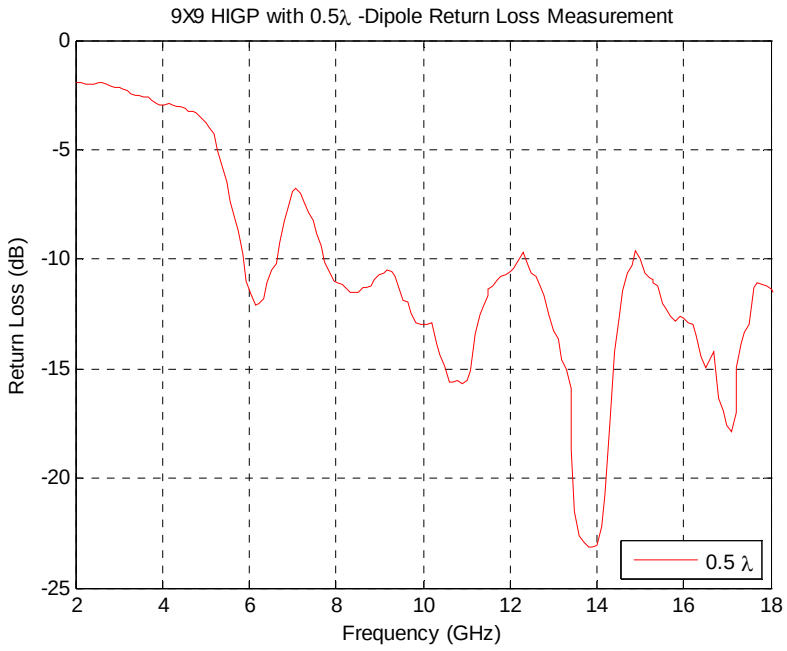

Figure 52: 9 by 9 HIGP with 0.5 λ_{10GHz} -Dipole Return Loss Result

c) 9 by 9 HIGP with 0.7 λ_{10GHz} -Dipole Return Loss Measurement

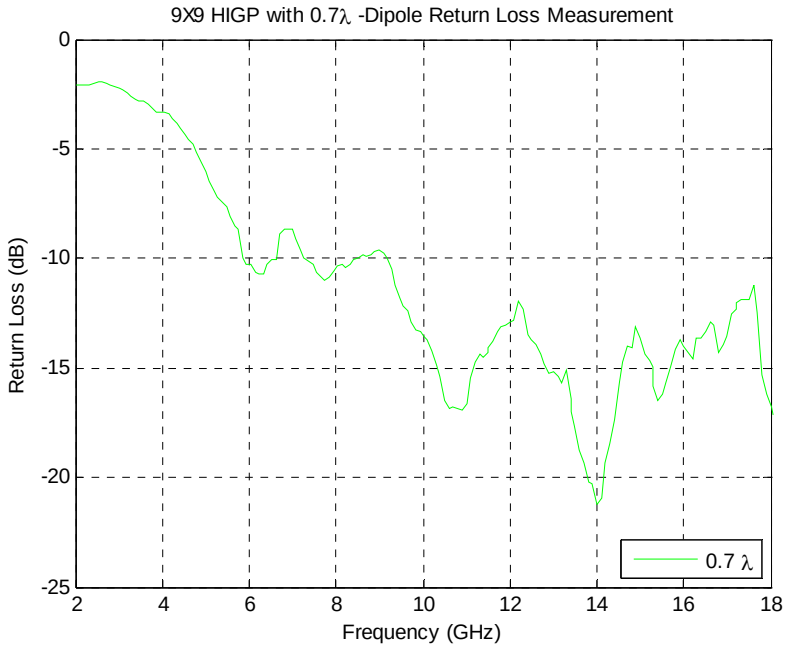

Figure 53: 9 by 9 HIGP with 0.7 λ_{10GHz} -Dipole Return Loss Result

4.3.4. 9 by 9 HIGP/Dipole Antenna Gain Measurements

Figure 54 shows the results of the 9 by 9 HIGP/0.4 λ_{10GHz} -dipole antenna measurements. The HIGP/antenna combination had better gain from 7.6 GHz to 10.9 GHz with a 3.3 GHz bandwidth. Figure 55 shows the results of the 9 by 9 HIGP/0.5 λ_{10GHz} -dipole antenna measurements. The HIGP/antenna combination had better gain from 7.0 GHz to 11.0 GHz with a 4.0 GHz bandwidth. Figure 56 shows the results of the 9 by 9 HIGP/0.7 λ_{10GHz} -dipole antenna measurements. The HIGP/antenna combination had better gain from 6.9 GHz to 11.1 GHz with a 4.2 GHz bandwidth.

Figure 57 shows the comparison of the gain performance of 0.4 λ_{10GHz} **,** 0.5 λ_{10GHz} **,** and 0.7 λ_{10GHz} dipoles over 9 by 9 HIGP. According to the comparison, the 0.7 λ_{10GHz} **(**21 mm**)** dipole had better gain from 6.9 GHz to 11.1 GHz better than 9dB. Figure 58 shows the comparison of the gain performance of 0.4 λ_{10GHz} **,** 0.5 λ_{10GHz} **,** and 0.7 λ_{10GHz} dipoles over PEC. According to the comparison, the 0.7 λ_{10GHz} **(**21 mm**)** dipole looks better compared to the 0.4 λ_{10GHz} -dipole, and 0.5 λ_{10GHz} -dipole. But since the ground plane is a conducting surface, dipoles have much less gain at low frequencies.

Figure 59 shows the comparison of the radiation pattern of 0.4 λ_{10GHz} **,** 0.5 λ_{10GHz} **,** and 0.7 λ_{10GHz} dipoles over 9 by 9 HIGP. According to the comparison, the 0.7 λ_{10GHz} **(**21 mm**)** dipole had better radiation pattern at 10.5 GHz, better than 9 dB. Figure 60 shows the comparison of the radiation pattern of 0.4 λ_{10GHz} **,** 0.5 λ_{10GHz} **,** and 0.7 λ_{10GHz} dipoles over 9 by 9 PEC. Even, the 0.7 λ_{10GHz} dipole had better gain compared to the others, dipoles over the PEC surface have less gain than the dipoles over the HIGP.

a) 9 by 9 HIGP with 0.4 λ_{10GHz} (12 mm) Dipole Horizontal Measurement

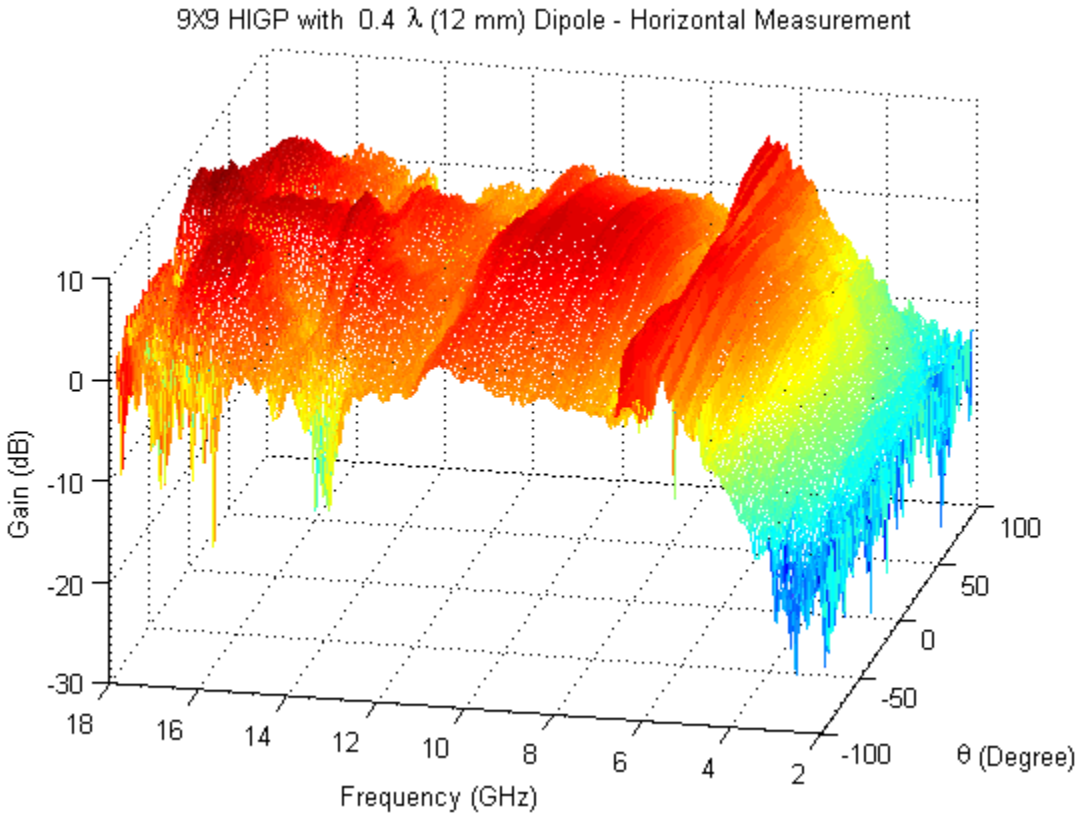

a) 9 by 9 0.4 λ_{10GHz} Dipole Antenna Pattern

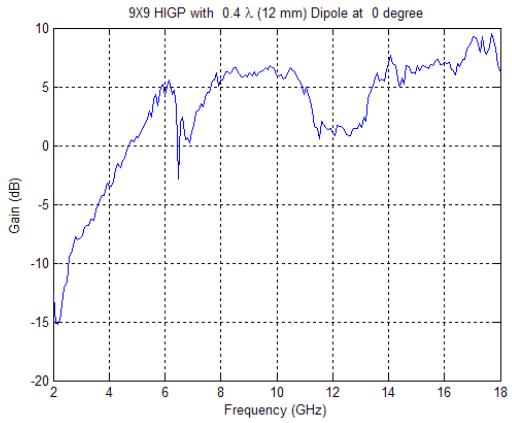

b) Gain Performance

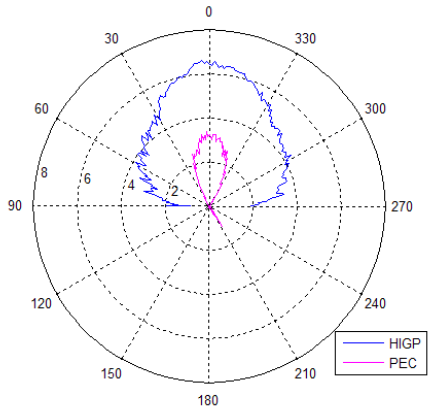

c) Radiation Pattern at 10.5 GHz

Figure 54: 9 by 9 Square Patch HIGP with 0.4 λ_{10GHz} -Dipole Horizontal Measurement

b) 9 by 9 HIGP with 0.5 λ_{10GHz} (15 mm) Dipole Horizontal Measurement

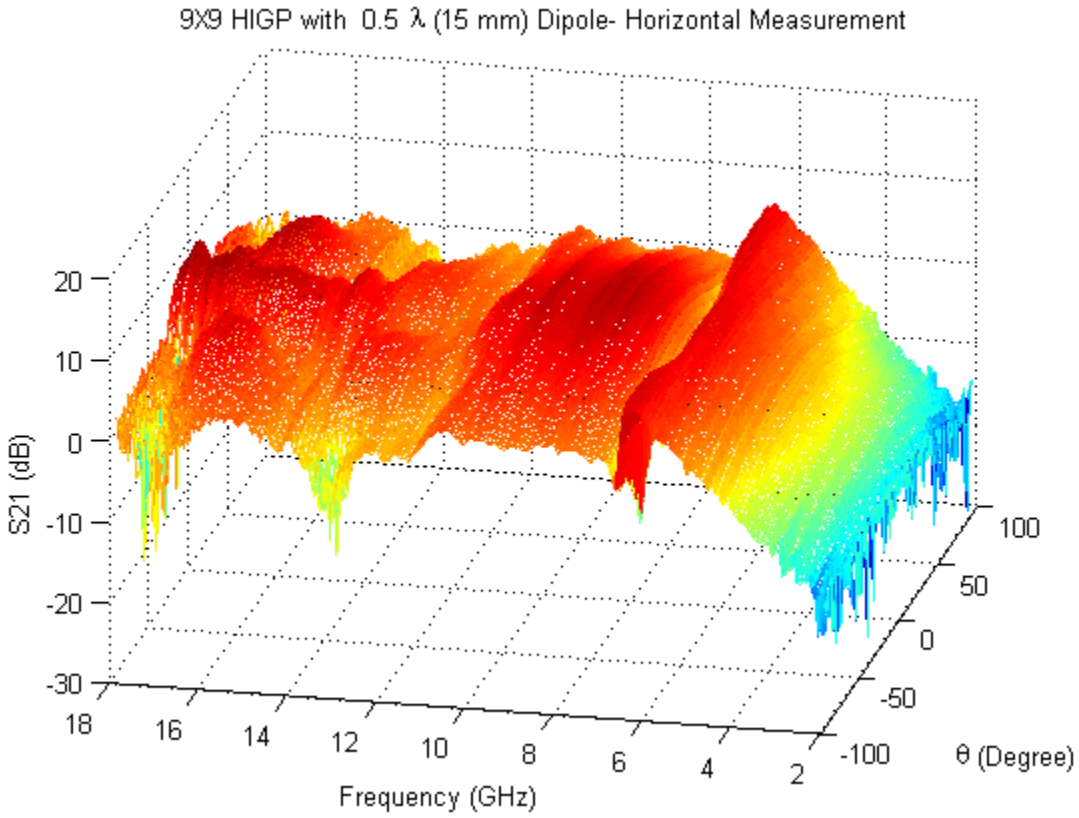

a) 9 by 9 0.5 λ_{10GHz} Dipole Antenna Pattern

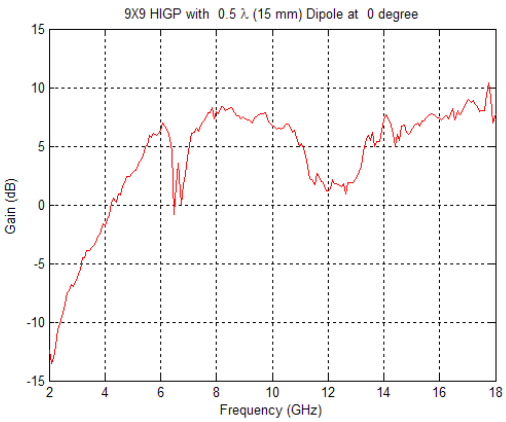

b) Gain Performance

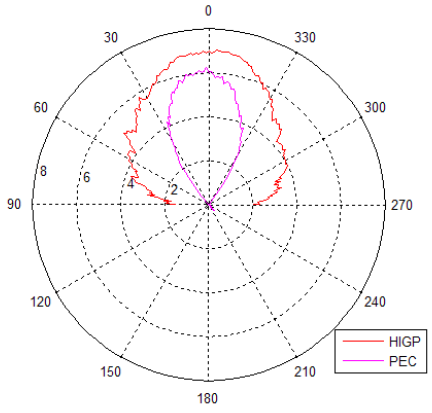

c) Radiation Pattern at 10.5 GHz

Figure 55: 9 by 9 Square Patch HIGP with 0.5 λ_{10GHz} -Dipole Horizontal Measurement

c) 9 by 9 HIGP with 0.7 λ_{10GHz} (21 mm) Dipole Horizontal Measurement

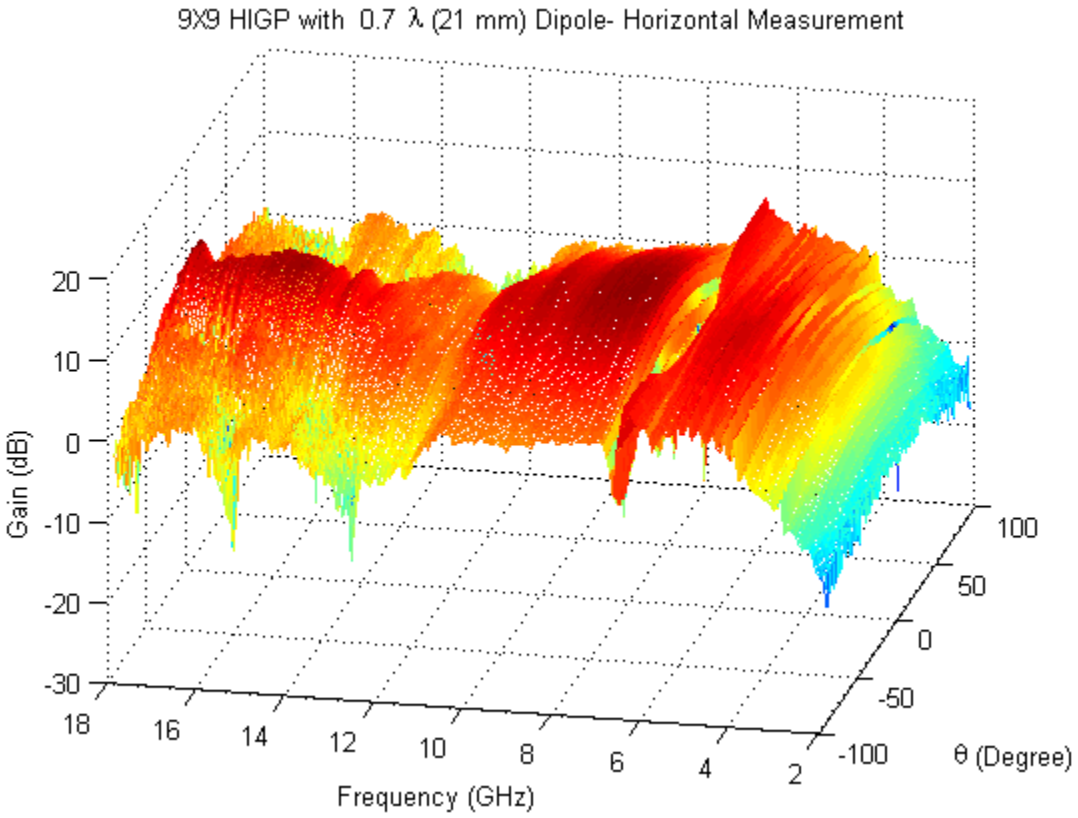

a) 9 by 9 0.7 λ_{10GHz} Dipole Antenna Pattern

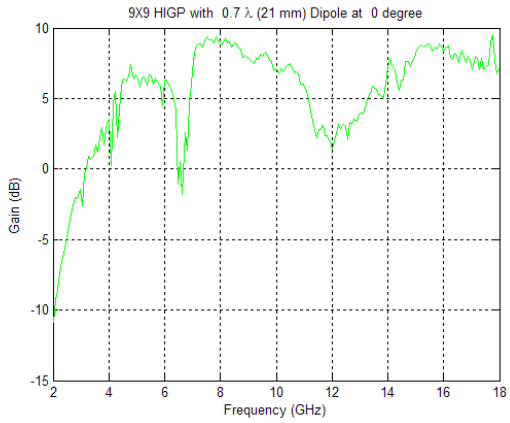

b) Gain Performance

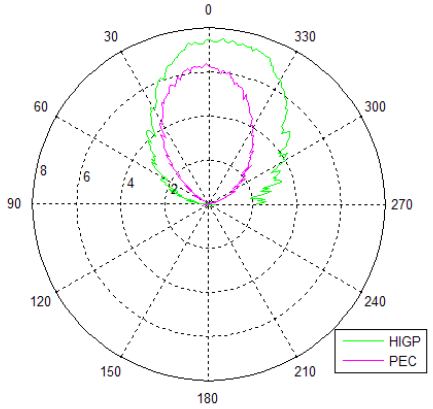

c) Radiation Pattern at 10.5 GHz

Figure 56: 9 by 9 Square Patch HIGP with 0.7 λ_{10GHz} -Dipole Horizontal Measurement

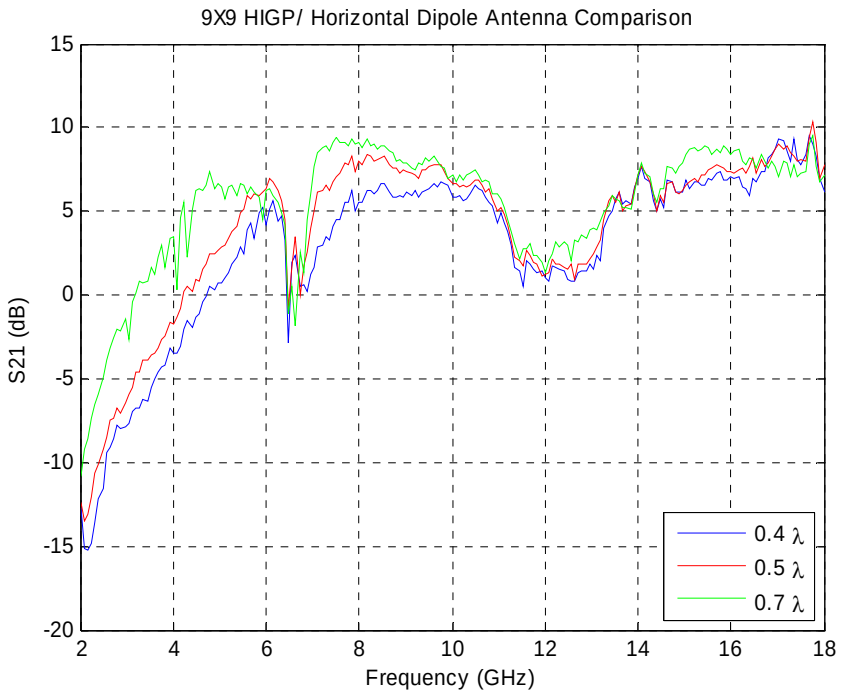

Figure 57: 9 by 9 HIGP/ Dipole Gain Performance Comparison

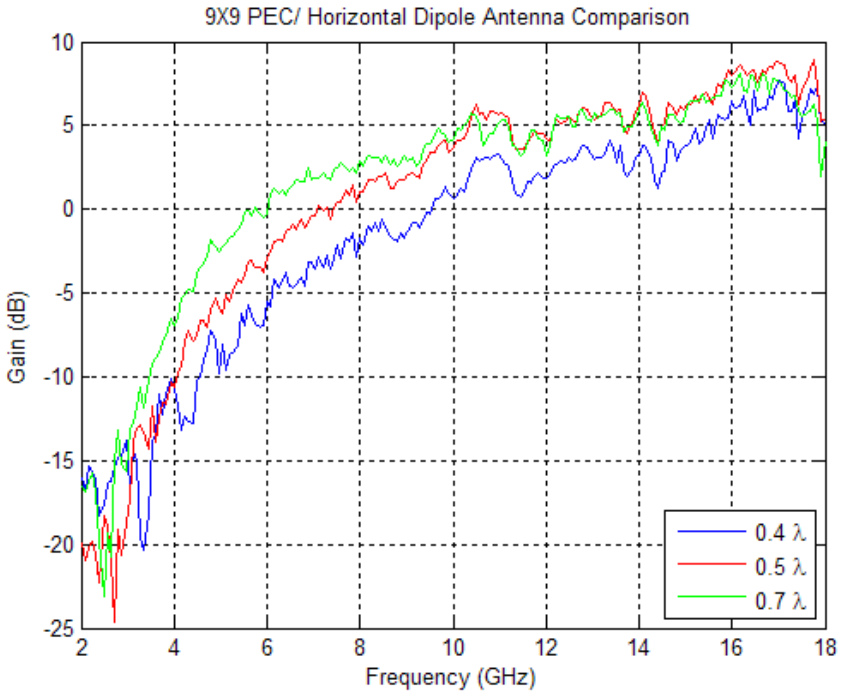

Figure 58: 9 by 9 PEC/ Dipole Gain Performance Comparison

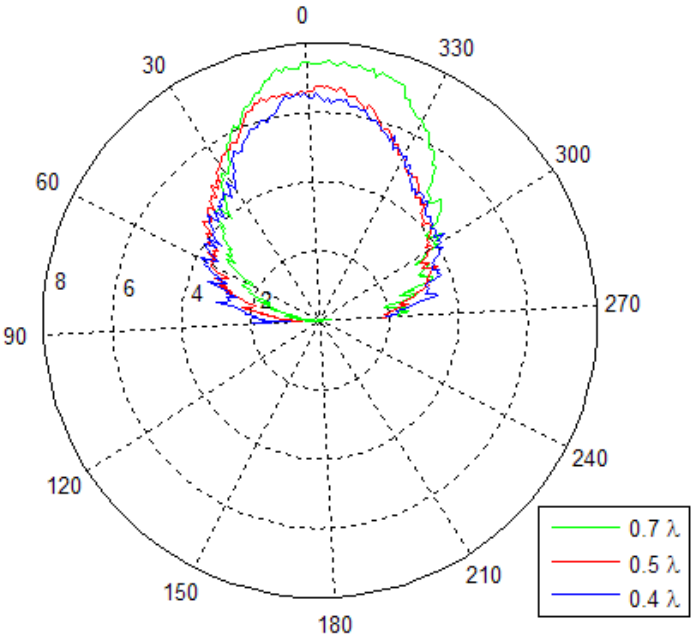

Figure 59: 9 by 9 HIGP/ Dipole Radiation Pattern Comparison

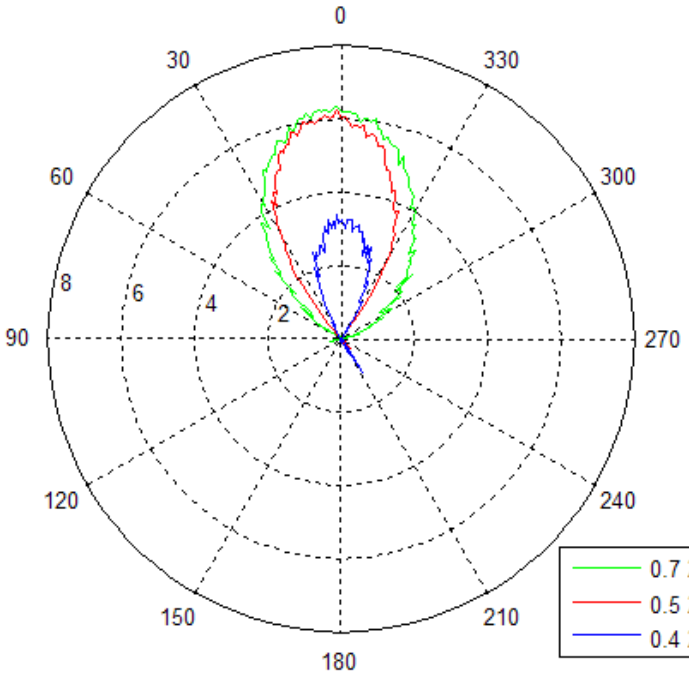

Figure 60: 9 by 9 PEC/ Dipole Radiation Pattern Comparison

4.3.5. 11 by 11 HIGP/Dipole Antenna Return Loss Measurements

The results of the 11 by 11 HIGP/0.4 λ_{12GHz} -dipole return loss measurement are shown in figure 61. The dipole shows a return loss better than -10 dB, from 6.5 to 7.5 GHz, and from 13.5 to 15 GHz. Better return loss were obtained at 7 and 14 GHz.

The results of the 11 by 11 HIGP/0.5 λ_{12GHz} -dipole return loss measurement are shown in figure 62. The dipole shows a return loss better than -14 dB, from 7 to 7.5 GHz, from 13.5 to 15 GHz, and from 17 to 18 GHz. The best return loss values were obtained at 7 GHz, and 14 GHz.

The results of the 11 by 11 HIGP/0.7 λ_{12GHz} -dipole return loss measurement are shown in figure 63. The dipole shows a return loss better than -14 dB, from 6 to 7.5 GHz, and from 16 to 18 GHz. Better return loss value were obtained at 7, 14, and 17.5 GHz.

a) 11 by 11 HIGP with 0.4 λ_{12GHz} -Dipole Return Loss Measurement

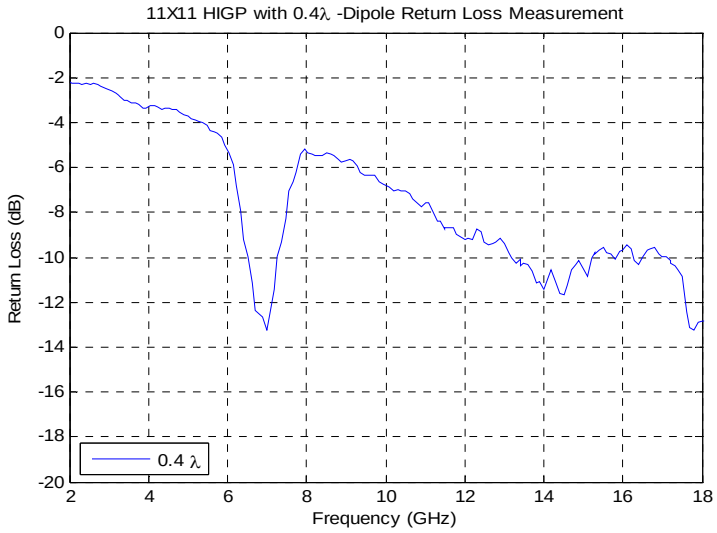

Figure 61: 11 by 11 HIGP with 0.4 λ_{12GHz} -Dipole Return Loss Result

b) 11 by 11 HIGP with 0.5 λ_{12GHz} -Dipole Return Loss Measurement

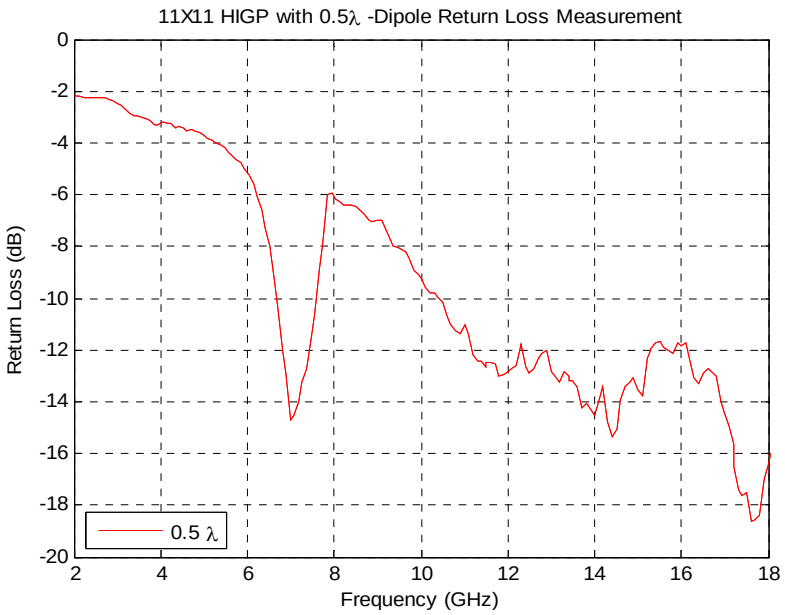

Figure 62: 11 by 11 HIGP with 0.5 λ_{12GHz} -Dipole Return Loss Result

c) 11 by 11 HIGP with 0.7 λ_{12GHz} -Dipole Return Loss Measurement

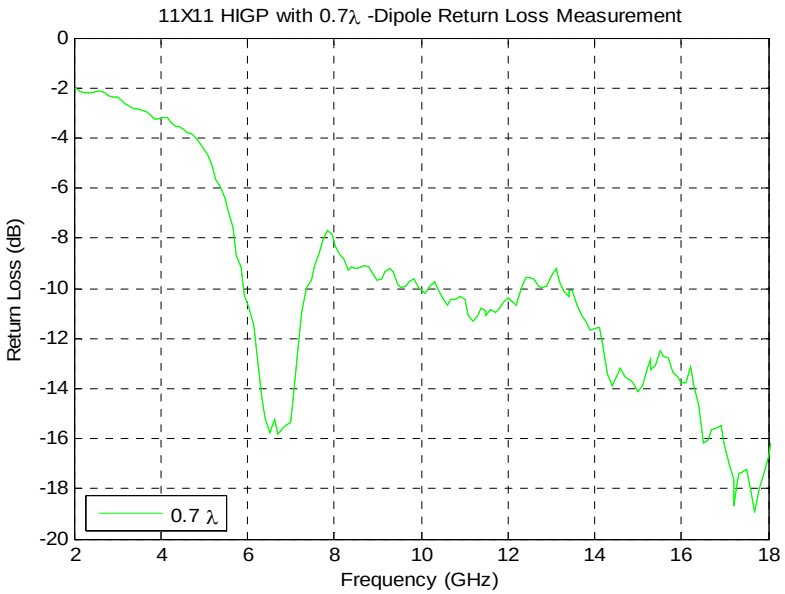

Figure 63: 11 by 11 HIGP with 0.7 λ_{12GHz} -Dipole Return Loss Result

4.3.6. 11 by 11 HIGP/Dipole Antenna Gain Measurements

Figure 64 shows the results of the 11 by 11 HIGP/0.4 λ_{12GHZ}-dipole antenna measurements. The HIGP/antenna combination had better gain from 8.15 GHz to 11.15 GHz with a 3.0 GHz bandwidth.

Figure 65 shows the results of the 11 by 11 HIGP/0.5 λ_{12GHZ}-dipole antenna measurements. The HIGP/antenna combination had better gain from 7.6 GHz to 11.2 GHz with a 3.6 GHz bandwidth.

Figure 66 shows the results of the 11 by 11 HIGP/0.7 λ_{12GHZ}-dipole antenna measurements. The HIGP/antenna combination had better gain from 7.45 GHz to 11.25 GHz with a 3.8 GHz bandwidth.

Figure 67 shows the gain performance comparison of $0.4\lambda_{12GHZ}$, $0.5\lambda_{12GHZ}$, and $0.7\lambda_{12GHZ}$ dipole over the 11 by 11 square patch HIGP. According to the comparison, the $0.7\lambda_{12GHZ}$ (17.5 mm) dipole had better gain from 7.45 GHz to 11.25 GHz better than 9dB.

Figure 68 shows the comparison of the gain performance of $0.4\lambda_{12GHZ}$, $0.5\lambda_{12GHZ}$, and $0.7\lambda_{12GHZ}$ dipoles over PEC. The $0.7\lambda_{12GHZ}$-dipole had better gain than the $0.4\lambda_{10GHz}$-dipole, and $0.5\lambda_{10GHz}$-dipole, but much less than the dipoles over the HIGP.

Figure 69 shows the radiation pattern comparison of $0.4\lambda_{12GHZ}$, $0.5\lambda_{12GHZ}$, and $0.7\lambda_{12GHZ}$ dipole over 11 by 11 square patch HIGP. According to the comparison, the $0.7\lambda_{12GHZ}$ (17.5 mm) dipole had better radiation pattern at 10.5 GHz, better than 8 dB.

Figure 70 shows the comparison of the radiation pattern of $0.4\lambda_{12GHZ}$, $0.5\lambda_{12GHZ}$, and $0.7\lambda_{12GHZ}$ dipole over 11 by 11 PEC. Even the $0.7\lambda_{12GHZ}$ dipole had better gain than the $0.4\lambda_{12GHZ}$-dipole, and $0.5\lambda_{12GHZ}$-dipole, the HIGP provide much better gain to the dipoles as expected.

As a result of all the measurement, we can say that, dipoles over the HIGP samples have much better gain than the dipoles over PEC surface. HIGP samples provide better than 9 dB gain to the dipoles, while PEC surface reduces the gain of the dipoles.

The gain performance of all HIGP/dipole combinations is so close in comparison. All dipoles operate well between 7 GHz and 11 GHz, and all dipoles receive better than 9 dB in these frequency range.

All the results of the narrowband antenna measurements over HIGP samples are listed below in Table 10.

Table 10. HIGP/Dipole Antenna Measurement Results

Dipole Length	7 by 7 HIGP		9 by 9 HIGP		11 by 11 HIGP	
	Band Gap (GHz)	**Bandwidth (GHz)**	**Band Gap (GHz)**	**Bandwidth (GHz)**	**Band Gap (GHz)**	**Bandwidth (GHz)**
0.4 λ	6.8 – 11.1	4.3	7.6 – 10.9	3.3	8.15 – 11.15	3.00
0.5 λ	6.6 – 11.1	4.5	7.0 – 11.0	4.0	7.60 – 11.20	3.60
0.7 λ	6.5 – 11.1	4.6	6.9 – 11.1	4.2	7.45 – 11.25	3.80

a) 11 by 11 HIGP with 0.4 λ_{12GHz} (10 mm) Dipole Horizontal Measurement

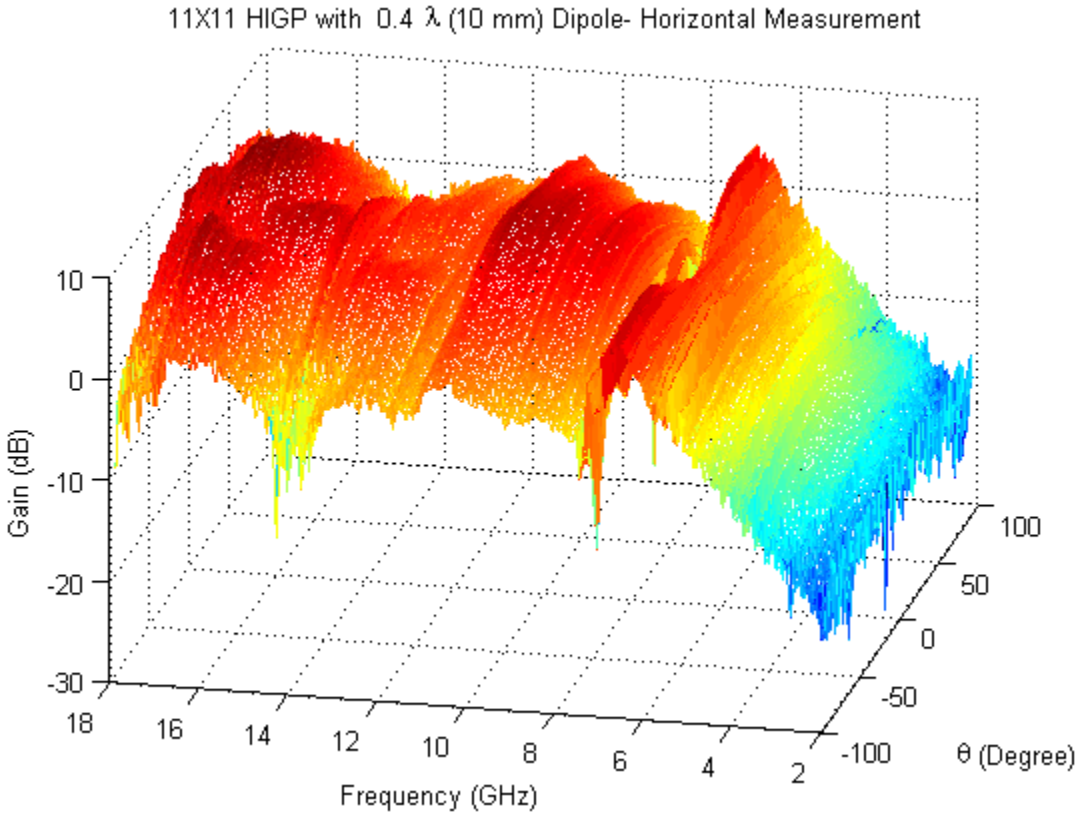

a) 11 by 11 0.4 λ_{12GHz} Dipole Antenna Pattern

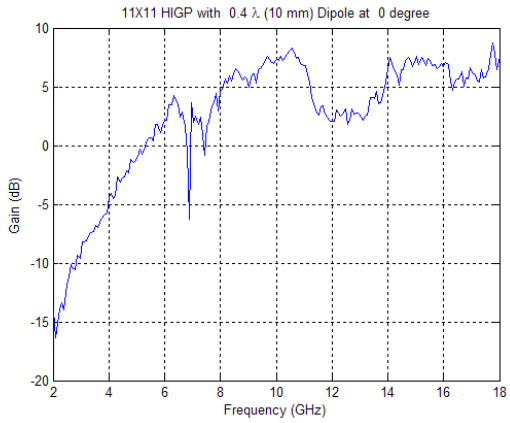

b) Gain Performance

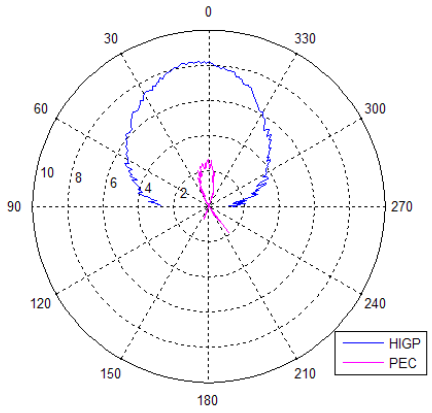

c) Radiation Pattern at 10.5 GHz

Figure 64: 11 by 11 Square Patch HIGP with 0.4 λ_{12GHz} -Dipole Horizontal Measurement

b) 11 by 11 HIGP with 0.5 λ_{12GHz} (12.5 mm) Dipole Horizontal Measurement

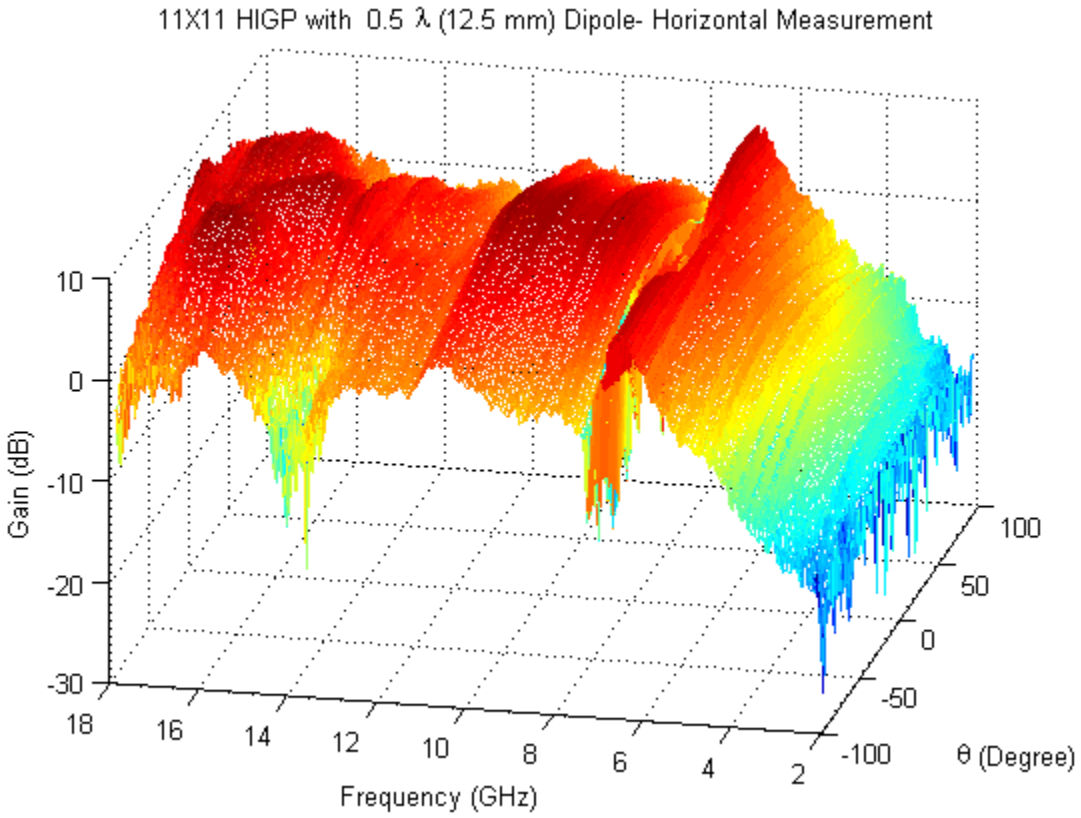

a) 11 by 11 0.5 λ_{12GHz} Dipole Antenna Pattern

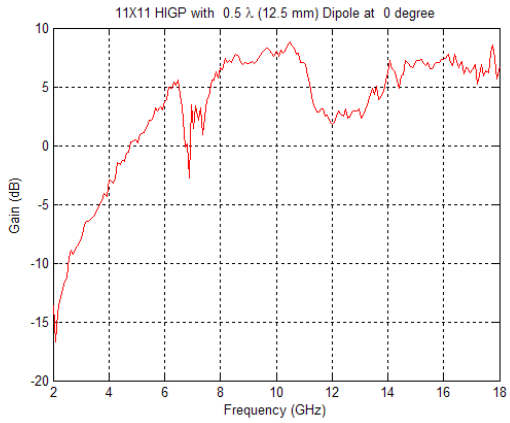

b) Gain Performance

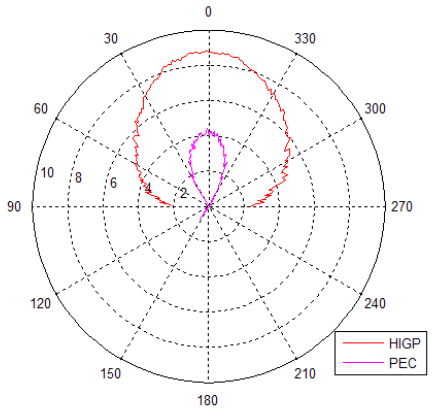

c) Radiation Pattern at 10.5 GHz

Figure 65: 11 by 11 Square Patch HIGP with 0.5 λ_{12GHz} -Dipole Horizontal Measurement

c) 11 by 11 HIGP with 0.7 λ_{12GHz} (17.5 mm) Dipole Horizontal Measurement

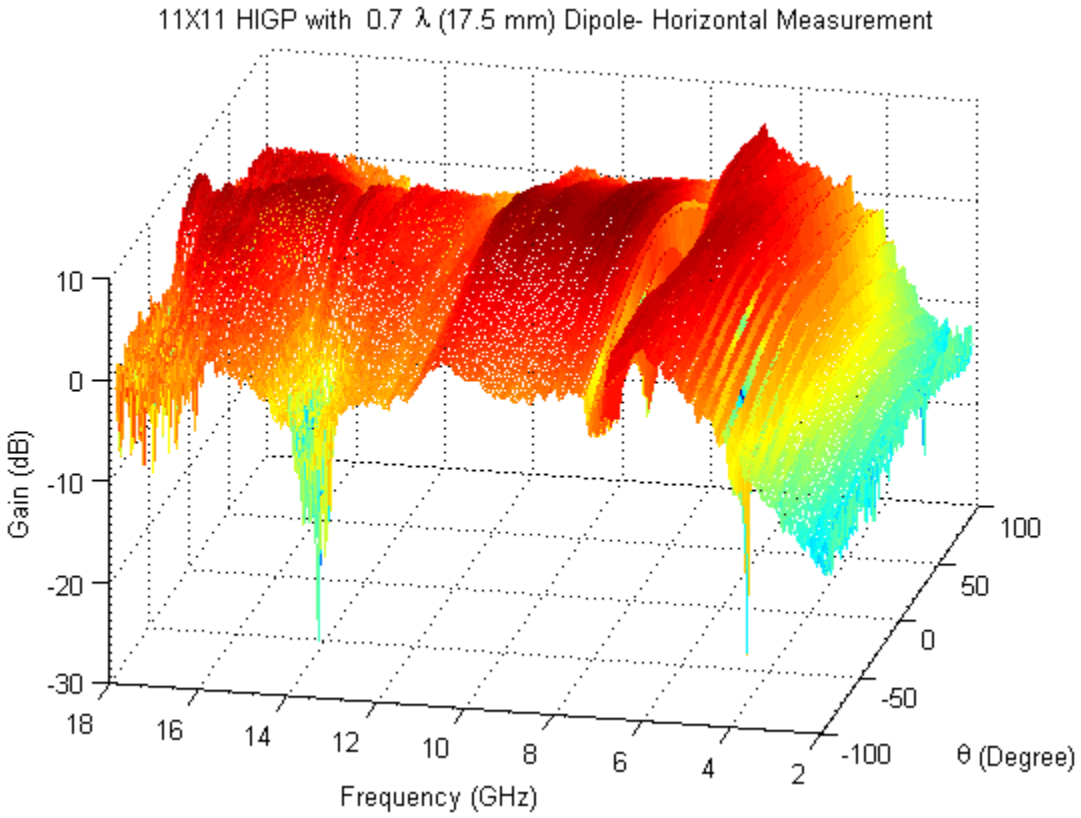

a) 11 by 11 0.7 λ_{12GHz} Dipole Antenna Pattern

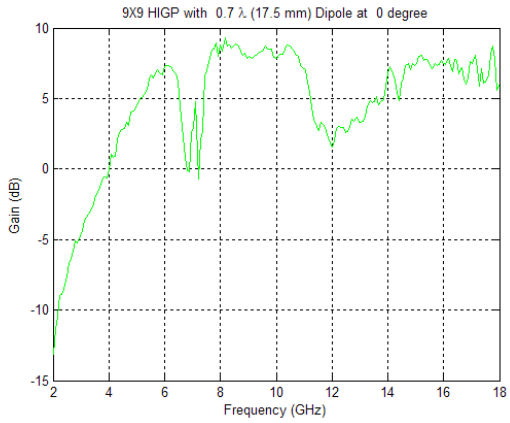

b) Gain Performance

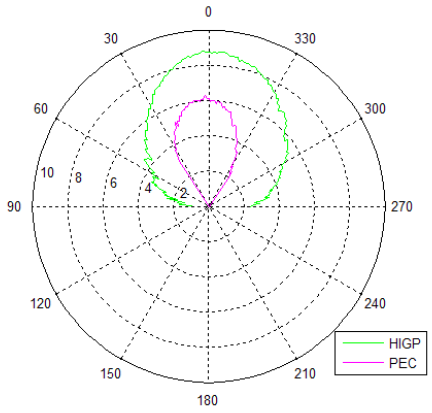

c) Radiation Pattern at 10.5 GHz

Figure 66: 11 by 11 Square Patch HIGP with 0.7 λ_{12GHz} -Dipole Horizontal Measurement

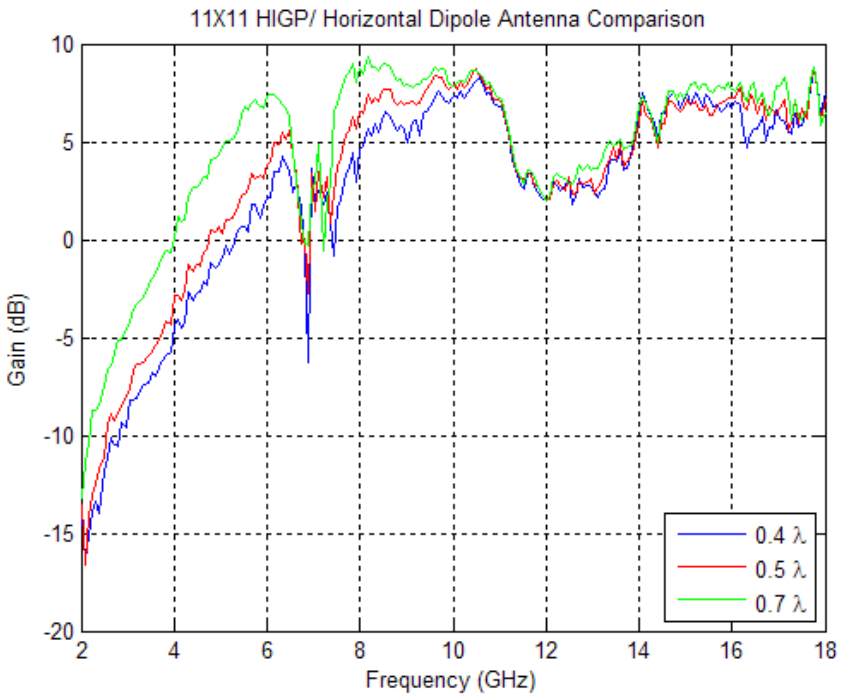

Figure 67: 11 by 11 HIGP/ Dipole Gain Performance Comparison

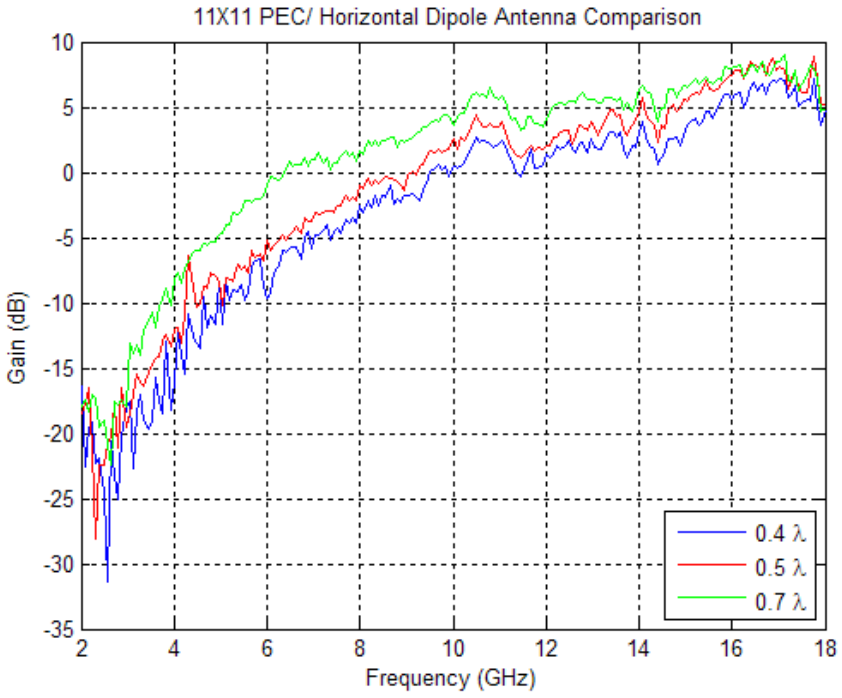

Figure 68: 11 by 11 PEC/ Dipole Gain Performance Comparison

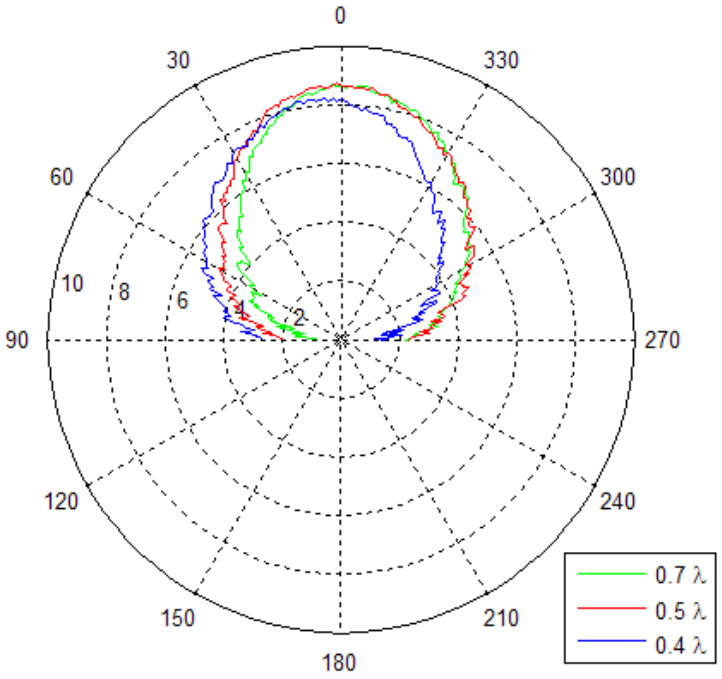

Figure 69: 11 by 11 HIGP/ Dipole Radiation Pattern Comparison

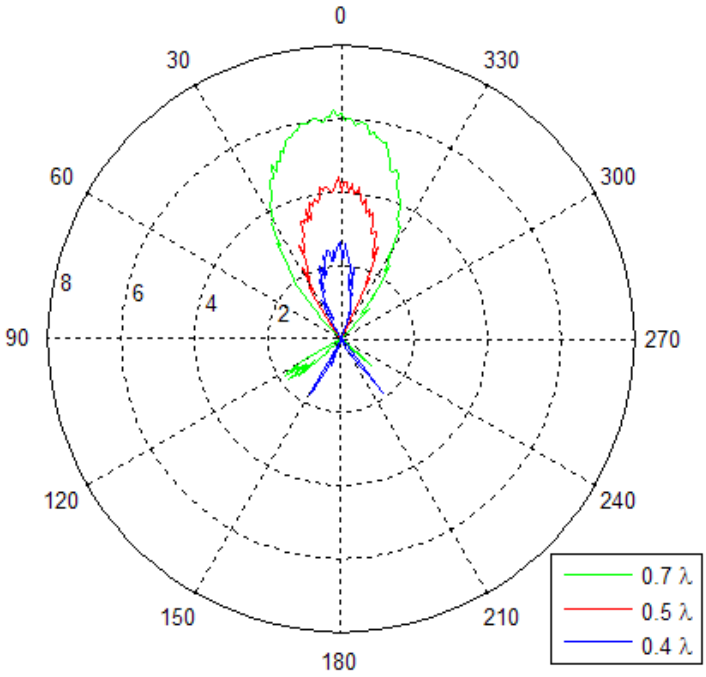

Figure 70: 11 by 11 PEC/ Dipole Radiation Pattern Comparison

4.4. Results of Broadband Antenna Measurements

In the third phase, four different HIGP samples with broadband antennas were tested and analyzed as explained in chapter three. In this phase, first a log-periodic antenna, with a square patch HIGP and with a circular patch hexagonal HIGP, was analyzed. Second, two multi-scale triangular-patch HIGP/bow-tie antenna combinations were analyzed.

The results of each measurement were analyzed in three figures as in the previous section. The three dimensional dipole antenna pattern is shown in the first figure (figure a), the gain performance of the antenna is shown in the second figure (figure b), and the radiation pattern of the antenna is given in the third figure (figure c).

4.4.1. Log-Periodic Antenna Measurements

In log-periodic antenna measurements, first, a log-periodic antenna in free space was analyzed. Figure 71 and figure 72 show the return loss and gain measurement results. According to the return loss, band gaps which have better than -10 dB return loss are well matched such as the band gap between 4.12-4.55 GHz and the band gap between 5.4-6 GHz. According to gain performance results, the log-periodic had so many peaks, as seen in figure 72a, due to the log-periodic arms of the antenna. Bandwidths of the peaks are approximately 2 GHz. Better gain performances are seen at 16 GHz (approximately 6 dB), at 3 GHz and at 5 GHz (5 dB). Since the log-periodic is well-matched at 4.5 GHz,

the radiation pattern is plotted at this frequency as shown in figure 72c. The log-periodic antenna had an approximately 6 dB gain at this frequency.

Second, the same log-periodic antenna was mounted over the square patch HIGP and the results are shown in figure 73 and figure 74. According to the return loss results in figure 73, band gaps, such as 4-4.5 GHz, 5-5.6 GHz, 6.2-9.2 GHz and 10.2-11.2 GHz are well matched. Same peaks as in free space are seen due to the arms of the log-periodic. But the log-periodic, with square patch HIGP, had gain performance better than 9 dB at 4.5 GHz. At this frequency, the log-periodic in free space had less than 6 dB gain. It's seen that the square patch HIGP provides 3-dB increase on gain performance.

Finally, the results of the log-periodic antenna, with circular patch hexagonal HIGP, are shown in figure 75 and figure 76. According to the return loss results in figure 75, band gaps, such as 2-2.8 GHz, 3.4-4.2 GHz, 5.4-6 GHz and 6-6.6 GHz are well matched. Figure 76 shows the results of the gain measurement. For this case, peaks were integrated between 5 GHz-8 GHz and 9 GHz-11 GHz. The integrated peaks were seen due to the effect of the circular periodic geometry. The log-periodic, with circular patch hexagonal HIGP, had gain performance better than 8 dB at 5.5 GHz. It's seen that the circular patch HIGP provides 2-dB increase on gain performance.

a) Log-Periodic Antenna in Free Space

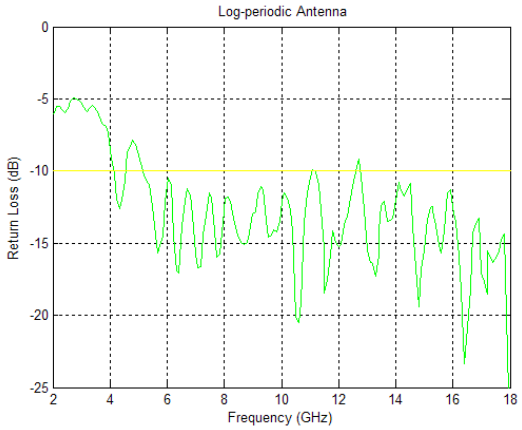

Figure 71. Log-periodic Antenna Free Space Return Loss Result

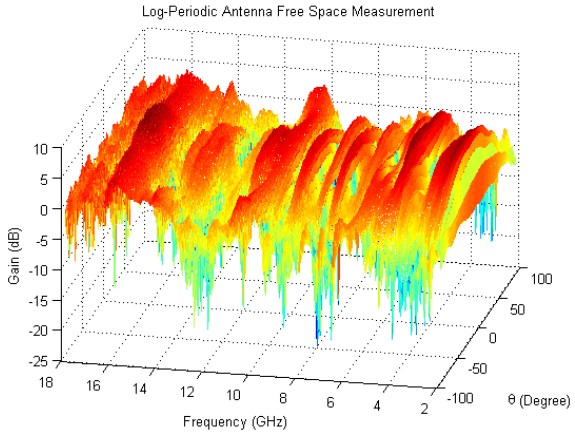

a) Log-Periodic Horizontal Antenna Pattern

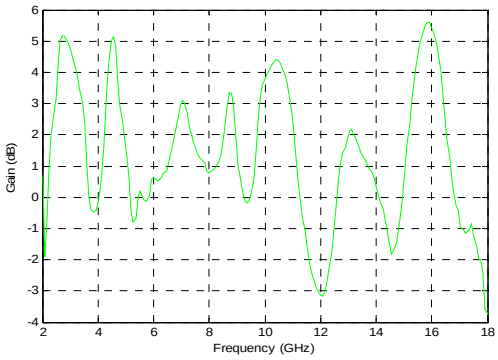

b) Gain Performance

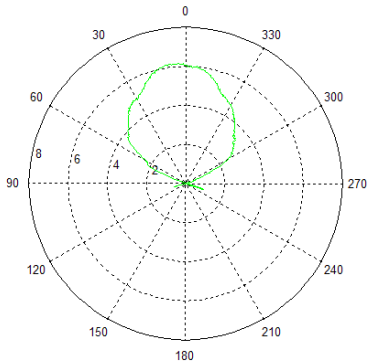

c) Radiation Pattern at 4.5 GHz

Figure 72. Log-periodic Antenna Free Space Measurement

b) Log-Periodic in Antenna Over 11 by 11 Square Patch HIGP

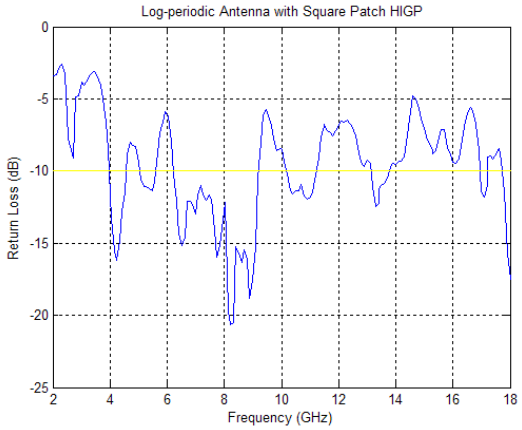

Figure 73. 11 by 11 Square HIGP/Log-periodic Antenna Return Loss Result

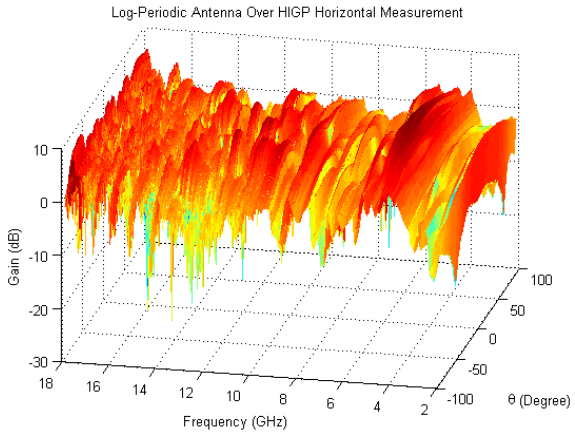

a) 11 by 11 Square HIGP /Log-periodic Antenna Pattern

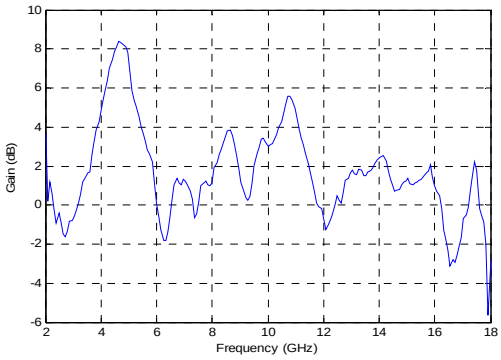

b) Gain Performance

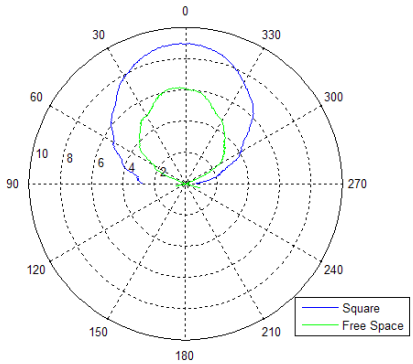

c) Radiation Pattern at 4.5 GHz

Figure 74. 11 by 11 Square HIGP/Log-periodic Antenna Measurement

c) Log-Periodic in Antenna over Circular Patch Hexagonal HIGP

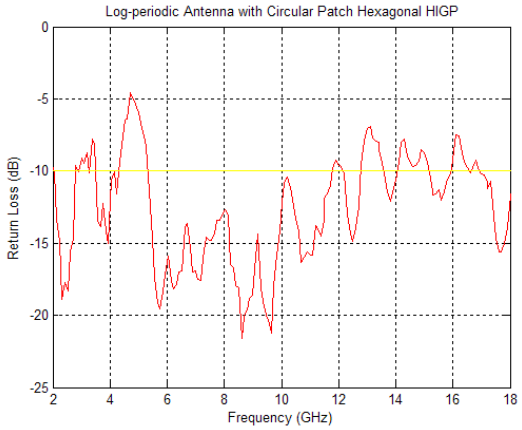

Figure 75. Circular Patch Hexagonal HIGP/Log-periodic Antenna Return Loss Result

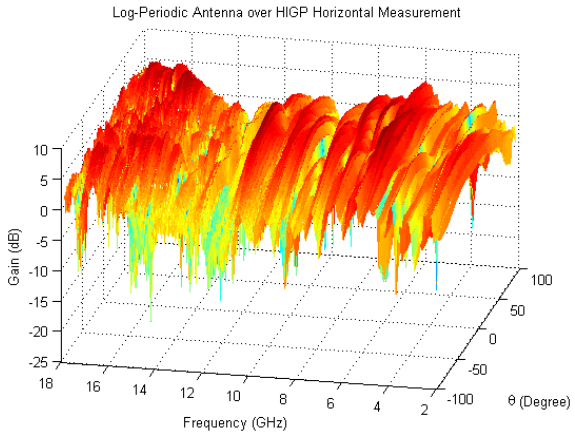

a) Circular Patch Hexagonal HIGP/Log-periodic Antenna Pattern

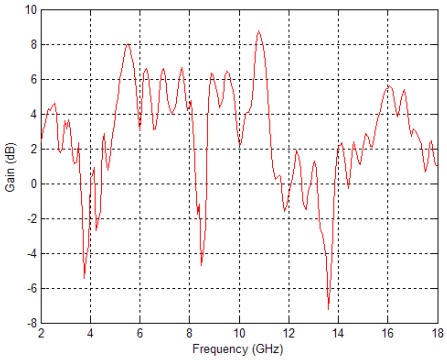

b) Gain Performance

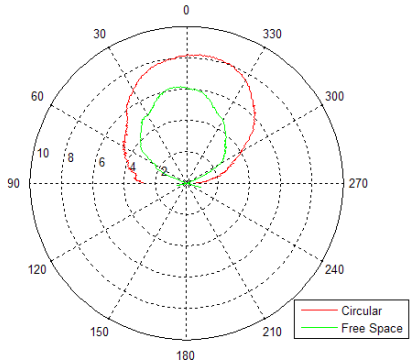

c) Radiation Pattern at 5.5 GHz

Figure 76. Circular Patch Hexagonal HIGP/Log-periodic Antenna Measurement

4.4.2. Bow-tie Antenna Measurements

In bow-tie antenna measurements, a 16mm-bow-tie and a 7.6mm-bow-tie were analyzed with a multi-scale triangular-patch HIGP. The multi-scale triangular patches and the same size bow-tie antenna were incorporated into a single structure. The results were also compared to the results of the bow-tie antenna in free space. The presented results include the return loss and the radiation patterns.

The 16mm-bow-tie antenna return loss measurement is shown in figure 77. Gain measurements are shown in figure 78. The three dimensional antenna pattern of the 16mm-bow-tie in free space is shown in figure 78a. The gain performance results are shown in figure 78b. The bow-tie is well-matched at 7 GHz and had a gain performance less than 5 dB. The radiation pattern at 7 GHz is shown in figure 78c.

The multi-scale triangular-patch HIGP/16mm-bow-tie combination was then analyzed as shown in figure 79 and figure 80. The return loss measurement is as shown in figure 79. The three dimensional antenna pattern of the combination is shown in figure 80a. Figure 80b shows the gain performance of the combination. The gain performance of the 16mm-bow-tie is enhanced via multi-scale triangular-patch HIGP. In figure 80c, the radiation pattern comparison of 16mm-bow tie with HIGP, in free space, and on a PEC surface are shown. The multi-scale triangular-patch HIGP/16mm-bow-tie combination is well-matched at 7 GHz and the bow-tie with HIGP had approximately 8 dB gain at 7 GHz. The gain performance of the HIGP/antenna combination is 3dB better than the gain performance of the bow-tie in free space and 4dB better than the gain performance of the bow-tie on a PEC surface.

The 7.6mm-bow-tie antenna free space measurement was analyzed as in figure 81 and figure 82. The return loss measurement results are shown in figure 81. The three dimensional antenna pattern of the 7.6mm-bow-tie in free space is shown in figure 82a. In figure 82b, the gain performance of the 7.6mm-bow-tie in free space is shown. The best gain performance over input-match frequency band is better than 4 dB. The maximum return loss of the bow-tie is obtained at 8.5 GHz and the radiation pattern of the 7.6 bow-tie in free space is shown in figure 82c. Figure 82c is plotted at 8.5 GHz and the radiation pattern had better than 4 dB gain.

The multi-scale triangular-patch HIGP/7.6mm-bow-tie combination was analyzed as shown in figure 83 and figure 84. The return loss measurement results are shown in figure 83. The multi-scale HIGP/7.6-bow-tie combination had a better return loss at 5.5 GHz, and 8.5 GHz. The three dimensional antenna pattern of the combination is shown in figure 84a. Figure 84b shows the gain performance of the combination. Figure 84c is plotted at 8.5 GHz and the gain performance of the HIGP/7.6mm-bow-tie combination is approximately 8 dB, whereas the gain performance of the 7.6mm-bow-tie in free space is less than 5 dB, and the gain performance of the 7.6mm-bow-tie on a PEC surface is 4 dB. The gain performance of the 7.6mm-bow-tie is enhanced at least 3 dB via multi-scale HIGP.

a) 16 mm-Bow-tie Antenna in Free Space

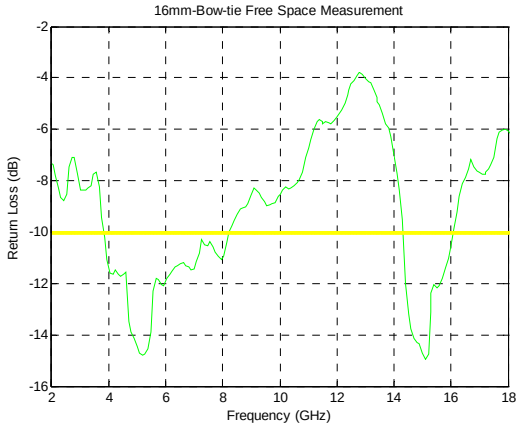

Figure 77. 16 mm-Bow-tie Return Loss Result

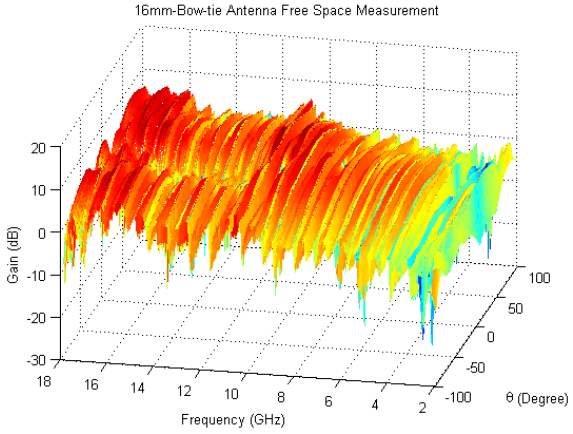

a) Bow-tie Antenna Horizontal Pattern

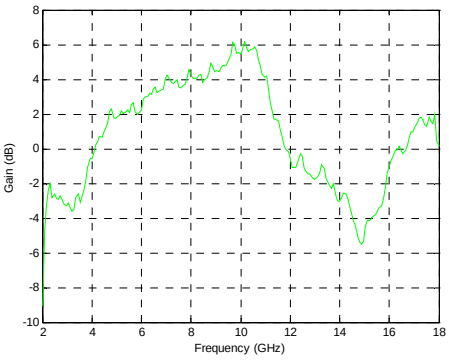

b) Gain Performance

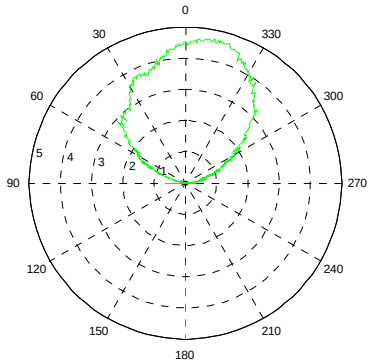

c) Radiation Pattern at 7 GHz

Figure 78. 16 mm-Bow-tie Antenna Measurement

b) Triangular Patch HIGP with 16 mm-Bow-tie Antenna

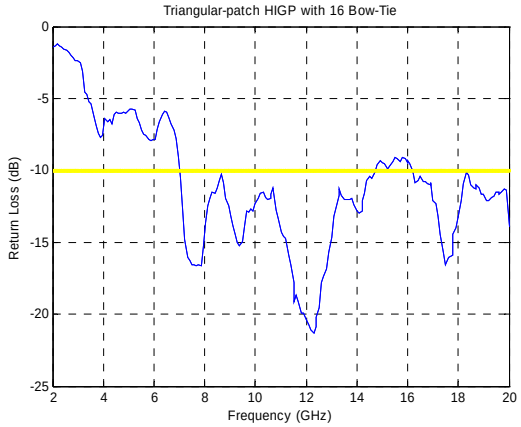

Figure 79. Triangular -patch HIGP/16 mm-Bow-tie Return Loss Result

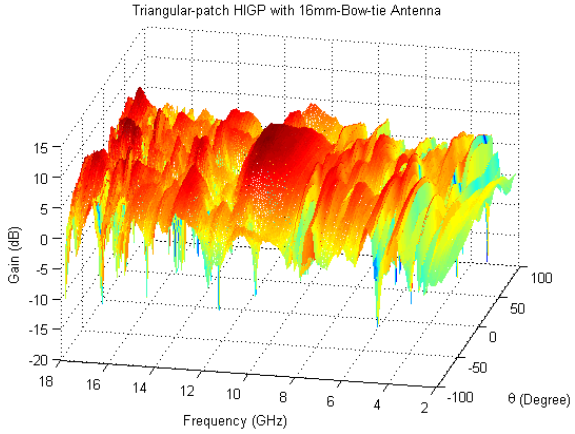

a) Triangular Patch HIGP/16mm-Bow-tie Antenna Horizontal Pattern

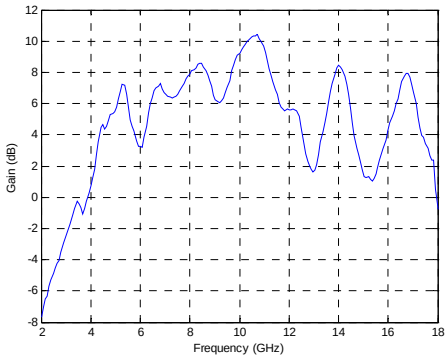

b) Gain Performance

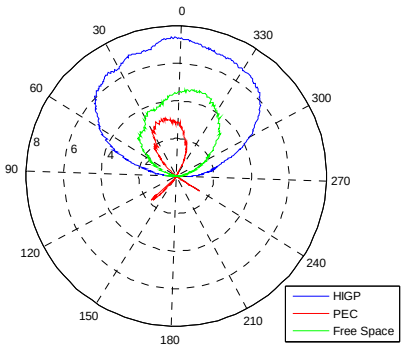

c) Radiation Pattern at 7 GHz

Figure 80. Triangular Patch HIGP/16 mm-Bow-tie Antenna Measurement

c) 7.6 mm-Bow-tie Antenna in Free Space

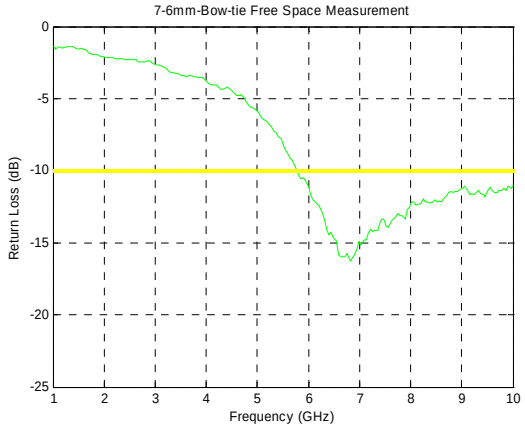

Figure 81. 7.6 mm-Bow-tie Return Loss Result

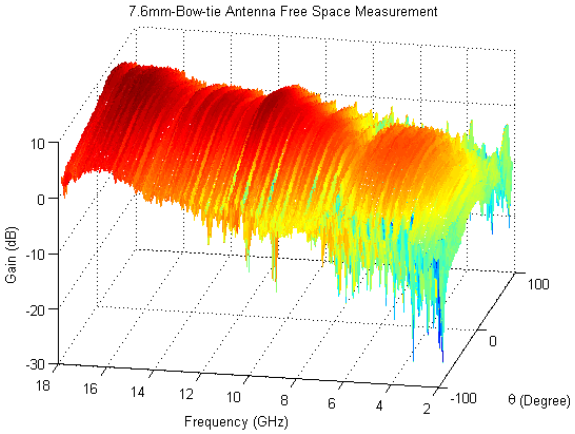

a) 7.6 mm-Bow-tie Antenna Pattern

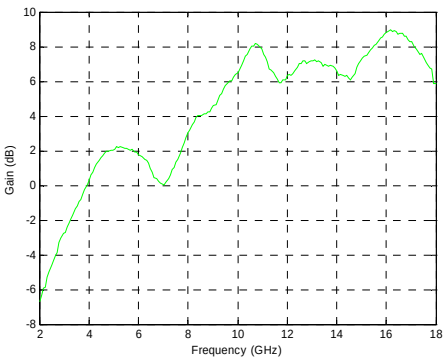

b) Gain Performance

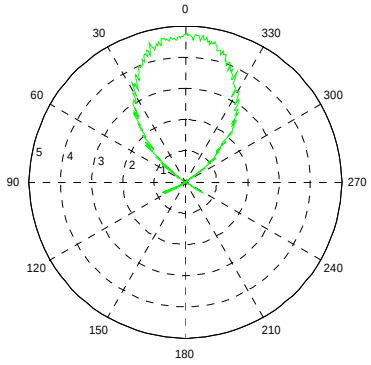

c) Radiation Pattern at 8.5GHz

Figure 82. 7.6mm-Bow-Tie Antenna Measurement

d) Triangular Patch HIGP with 7.6 mm-Bow-tie Antenna

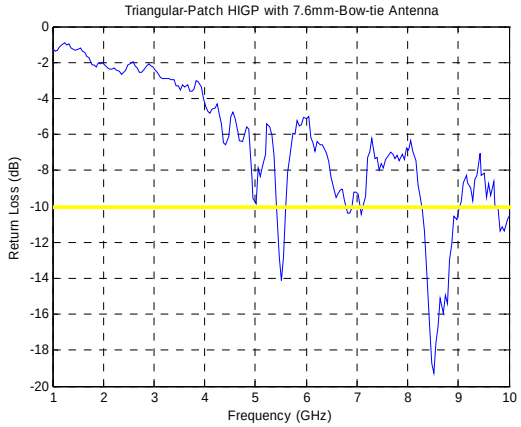

Figure 83. Triangular Patch HIGP/7.6 mm-Bow-tie Return Loss Result

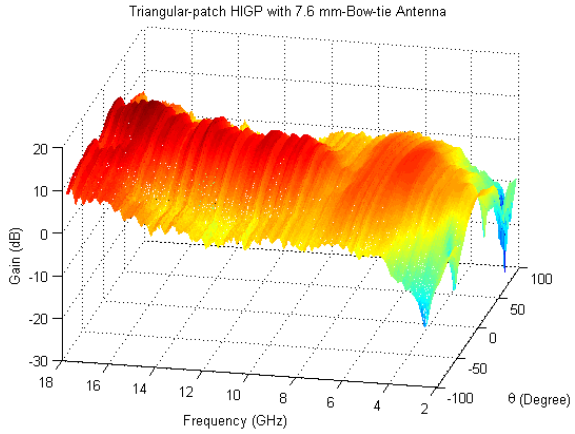

a) Triangular Patch HIGP/7.6 mm-Bow-tie Antenna Pattern

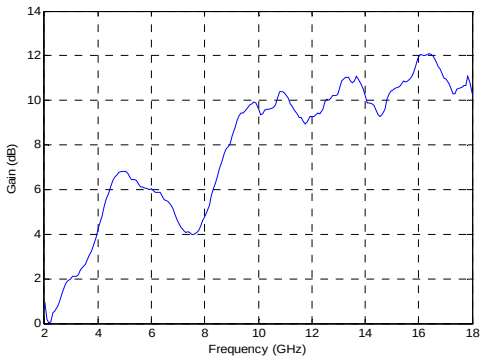

b) Gain Performance

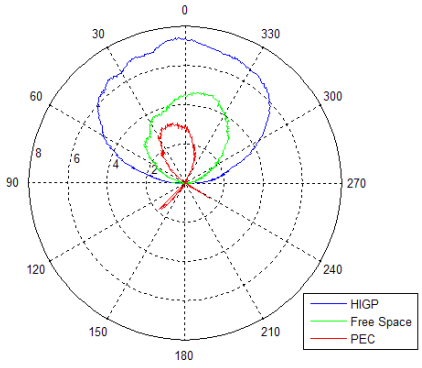

c) Radiation Pattern at 8.5 GHz

Figure 84. Triangular -patch HIGP/7.6 mm-Bow-tie Antenna Measurement

Chapter 5 Conclusion and Recommendations

5.1 Chapter Overview

This chapter presents the conclusions and the contributions of this research. The chapter concludes with recommendations for further high impedance ground plane studies and other antenna applications.

5.2 Conclusion of Research

The anticipated goal of this research was to develop a conformal printed broadband antenna directly on a conformal high impedance ground plane, and to enhance the conformal antenna performance using novel electromagnetic features of high impedance ground planes, without the detrimental effects of absorber losses. We also proposed to mitigate the negative effects of a conducting ground-plane using a HIGP.

The benefits provided by HIGPs for such resonant, narrowband antennas motivated us to investigate the possible application of wide-band-gap HIGPs, and to develop a conformal broadband antenna. To achieve this goal, the operational frequency band gap of the desired broadband antenna should be the overlap of its surface wave frequency band gap and its input-match frequency band gap. An appropriate high impedance ground plane can be designed to overlap the surface wave frequency band and input-match frequency band gap.

In this research, the goal was to understand the affects of HIGP design parameters, such as patch width, gap width, substrate thickness and substrate permittivity,

on surface wave measurements, and narrowband antenna measurements. Similar square patch HIGPs were built and tested as in (Yang and Rahmat-Samii, 2003a:2691-2703) in order to obtain similar results. Similar HIGP structures verified surface wave and narrow band antenna measurement techniques, and motivated us to develop better high impedance ground planes. The results are also verified by Ansoft's commercial full-wave solver (HFSS v.10). In light of these measurements, optimized parameters are found to be patch width=0.5mm, and gap with=0.4 mm.

A log-periodic and a bow-tie antenna were chosen to develop better HIGPs. Optimized design parameters were used to develop an appropriate HIGP for these antennas. The sizes and periodicities of the ground planes were chosen such that samples have band-gaps that appear successively in frequency and cover the operational frequency band.

Since the log-periodic antenna has a circular geometry, it seems that a circular patch HIGP would be more appropriate for the log-periodic antenna, However, the 11by11 square patch HIGP provided better return loss and antenna gain. Subsequently, both square patch and circular patch HIGPs provided better return loss and gain performance.

Finally, a bow-tie antenna was chosen for an integrated HIGP/antenna structure. HIGP elements were chosen to be triangular to form a natural, commensurate blending of the bow-tie into the structure. Two novel multi-scale triangular patch HIGP/bow-tie antenna combinations also provided better return loss and gain performance. The gain performance of HIGP/bow-tie combinations were 3 dB higher than the gain performance of the bow-ties in free space.

The return loss and the gain results of the HIGP-antenna combinations show that the HIGP provides a suitable platform for the bow-tie with removing the undesired effects of a PEC ground plane. The measurements indicate that the HIGP-antenna combination has better gain than the bow-tie in free space, and the bow-tie over a PEC surface.

5.3 Recommendations and Advices for Future Research

Since high impedance ground planes (HIGP), or electromagnetic band gap (EBG) mushroom-like structures exhibit novel electromagnetic features, they lead to a wide range of electromagnetic applications. The following are a few recommendations for the research in building and testing of high impedance ground planes.

Compactness, wider bandwidth, higher efficiency, and ease of fabrication and integration are always sought for electromagnetic applications. Since planar antennas have features above, they can be reasonably improved in different size and shapes with an appropriate HIGP design.

Substrate thickness and substrate permittivity are two of the main design parameters. But these parameters have production constraints, since they are ordered off the shelf. Thus, another material, Rohacell^{TM} 31, can be used due to the parameter constraints of RT/Duroid 5880 (Linton and Scanlon, 2006). Even if a Rohacell^{TM} 31 had been available due to the time constraints we had no chance to use it. In Appendix A and B, the features of materials are shown.

Moreover, three-dimensional high impedance ground planes can be designed and built. Tunable impedance surfaces can be also developed using HIGPs. Reflective beam-steering can be another future work. Tunable surfaces can be used as an electronic beam-steering reflector by programming the high impedance surface (Engheta and Ziolkowski, 2006:304).

Designing, patterning, plating, and testing of HIGP samples may take time. Equipment may fail, ordered parts may be out of stock, or the delivery time of the materials may be extended. Make a plan of attack, prepare a time schedule for yourself and stick to it. Review your designs with your colleagues and advisors to maximize your success. More importantly always be positive, never give up, and success will come with hard work and patience.

Appendix A: Electromagnetic Features of the RT/duroid 5880 HF Laminate

PROPERTY	TYPICAL VALUE				DIRECTION	UNITS	CONDITION	TEST METHOD
	RT/duroid® 5870		RT/duroid 5880					
Dielectric Constant, ε_r	2.33 2.33 ± 0.02 spec.		2.20 2.20 ± 0.02 spec.		Z Z		C24/23/50 C24/23/50	1 MHz IPC-TM-650, 2.5.5.3 10 GHz IPC-TM-2.5.5.5
Dissipation Factor, tan δ	0.0005 0.0012		0.0004 0.0009		Z Z		C24/23/50 C24/23/50	1 MHz IPC-TM-650, 2.5.5.3 10 GHz IPC-TM-2.5.5.5
Thermal Coefficient of ε_r	-115		-125			ppm/°C	-50 - 150°C	IPC-TM-650, 2.5.5.5
Volume Resistivity	2 X 10^7		2 X 10^7		Z	Mohm cm	C96/35/90	ASTM D257
Surface Resistivity	2 X 10^8		3 X 10^7		Z	Mohm	C/96/35/90	ASTM D257
Tensile Modulus	Test at 23°C	Test at 100°C	Test at 23°C	Test at 100°C				
	1300 (189)	490 (71)	1070 (156)	450 (65)	X	MPa (kpsi)	A	ASTM D638
	1280 (185	430 (63)	860 (125)	380 (55)	Y			
ultimate stress	50 (7.3)	34 (4.8)	29 (4.2)	20 (2.9)	X			
	42 (6.1)	34 (4.8)	27 (3.9)	18 (2.6)	Y			
ultimate strain	9.8	8.7	6.0	7.2	X	%		
	9.8	8.6	4.9	5.8	Y			
Compressive Modulus	1210 (176)	680 (99)	710 (103)	500 (73)	X	MPa (kpsi)	A	ASTM D695
	1360 (198)	860 (125)	710 (103)	500 (73)	Y			
	803 (120)	520 (76)	940 (136)	670 (97)	Z			
ultimate stress	30 (4.4)	23 (3.4)	27 (3.9)	22 (3.2)	X			
	37 (5.3)	25 (3.7)	29 (5.3)	21 (3.1)	Y			
	54 (7.8)	37 (5.3)	52 (7.5)	43 (6.3)	Z			
ultimate strain	4.0	4.3	8.5	8.4	X	%		
	3.3	3.3	7.7	7.8	Y			
	8.7	8.5	12.5	17.6	Z			
Deformation Under Load, Test at 150°C			1.0		Z	%	24hr/14 MPa (2 Kpsi)	ASTM D621
Heat Distortion Temperature	>260 (>500)		>260 (>500)		X,Y	°C (°F)	1.82 MPa (264 psi)	ASTM D648
Specific Heat	0.96 (0.23)		0.96 (0.23			J/g/K		Calculated
Moisture Absorption — Thickness 0.31" (0.8mm)	0.9 (0.02)		0.9 (0.02)			mg (%)	D24/23	ASTM D570
Moisture Absorption — 0.62" (1.6mm)	13 (0.015)		13 (0.015					
Thermal Conductivity	0.22		0.20		Z	W/m/K		ASTM C518
Thermal Expansion	X	Y	Z	X	Y	Z			
	-5.0	-5.5	-11.6	-6.1	-8.7	-18.7		-100°C
	-0.6	-0.9	-4.0	-0.9	-1.8	-6.9		15
	-0.3	-0.4	-2.6	-0.5	-0.9	-4.5	mm/m	25
	0.7	0.9	7.5	1.1	1.5	8.7		75
	1.8	2.2	22.0	2.3	3.2	28.3		150
	3.4	4.0	58.9	3.8	5.5	69.5		250
								ASTM D3386 (10K/min) (Values given are total change from a base temperature of 35°C)
Td	500		500			°C TGA		ASTM D3850
Density	2.2		2.2					ASTM D792
Copper Peel	20.8 (3.7)		22.8 (4.0)			pli (N/mm)	after solder float	IPC-TM-650 2.4.8
Flammability	94V-0		94V-0					UL
Lead-Free Process Compatible	Yes		Yes					

[1] SI unit given first with other frequently used units in parentheses.
[2] References: Internal TR's 1430, 2224, 2854. Test were at 23°C unless otherwise noted.
Typical values should not be used for specification limits.

STANDARD THICKNESS:		STANDARD PANEL SIZE:	STANDARD COPPER CLADDING:
0.005" (0.127mm),	0.031" (0.787mm)	18" X 12" (457 X 305mm)	¼ oz. (8 µm) electrodeposited copper foil.
0.010" (0.254mm),	0.062" (1.575mm)	18" X 24" (457 X 610mm)	½ oz. (17µm), 1 oz. (35µm), 2 oz. (70µm) electrodeposited and rolled copper foil.
0.015" (0.381mm),	0.125" (3.175mm)	18" X 36" (457 X 915mm)	
0.020" (0.508mm),		18" X 48" (457 X 1.224m)	

Revised 11/06 0696-1106-0.5CC **Publication #92-101**

Appendix B: Electromagnetic Features of the Rohacell™ HF

Dielectric Properties of ROHACELL® HF

Properties	Unit	ROHACELL® 31 HF	ROHACELL® 51 HF	ROHACELL® 71 HF	Survey
ε' (f= 2,5 GHz)	[-]	1,05	1,06	1,07	Seavey Engineering Ass., Report 9335-700
tan δ (f= 2,5 GHz)	[-]	<0,0002	<0,0002	<0,0002	
ε' (f= 5 GHz)	[-]	1,04	1,06	1,106	
tan δ (f= 5 GHz)	[-]	0,0016	0,0008	0,0016	
ε' (f= 10 GHz)	[-]	1,04	1,07	1,09	
tan δ (f= 10 GHz)	[-]	0,0017	0,0041	0,0038	
ε' (f= 26,5 GHz)	[-]	1,04	1,05	1,09	
tan δ (f= 26,5 GHz)	[-]	0,0106	0,0135	0,0155	

The values above are based on limited batches only and are not calculated on statistical evaluation
Our technical advice on the applications of our products is given without obligation. The buyer is responsible for their use and processing, and is also liable for observing any third-party rights. Technical data concerning our products are typical values. Subject to alteration. ROHACELL■ is a registered trademark of Röhm GmbH & Co. KG, D-Darmstadt.

2001-01-09

Bibliography

Alu A., N. Engheta, A. Erentok, and R.W. Ziolkowski. "Single-Negative, Double-Negative, and Low-Index Metamaterials and Their Electromagnetic Applications," *IEEE Antenna and Propagation Magazine*, 49: 23-36 (February 2007).

Balanis, Constantine A. *Antenna Theory: Analysis and Design,3rd Edition.* New York:John Wiley&Sons, 2005.

Barnes, W.L., T.W. Priest, S. Kitson, and J. Sambles, "Physical Origin of Photonic Energy Gaps in the Propagation of Surface Plasmons on Gratings," *Physical Review B*, 54:6277-6244 (September 1996).

Bell, Jodie and M. Iskander, "A Low-Profile Archimedean Spiral Antenna Using an EBG Ground Plane," *IEEE Antennas and Wireless Propagation Letters*, 3:223-226 (2004).

Broas, R. Jimenez, D. Sievenpiper, and E. Yablonovitch. "An Application of High-Impadance Ground Planes to Phased Array Antennas," *IEEE Transanctions on Antennas and Probagation*, 53:1377-1381 (April 2005).

Brown, E., C. Parker, and E. Yablonovitch, "Radiation Properties of a Planar Antenna on a Photonic-Crystal Substrate," *Journal of the Optical Society of America B*, 10:404-407 (February 1993).

Caloz Christophe and Tatsuo Itoh. *Electromagnetic Metamaterials Transmission Line Theory and Microwave Applications*. Hoboken, NJ : John Wiley and Sons Inc., 2006.

Colburn J., and Y. Rahmat-Samii, "Patch Antennas on Externally Perforated High Dielectric Constant Substrates," *IEEE Trans. Antenna and Propagation Magazine*, 38: 1537-1544 (October 1990).

Compton, R., R. McPhedran, Z. Popovic, G. Rebeiz, P. Tong, and D. Rutledge. "Bow-Tie Antennas on a Dialectric Half-Space: Theory and Experiments," *IEEE Antenna and Propagation Magazine*, AP35: 622-631 (June 1987).

Dogrul, Murat. *Design and Optimization of Broadband High Impedance Ground Planes for Surface mount Antennas.* MS thesis, AFIT/GE/ENG/08M-08. School of Engineering, Air Force Institute of Technology, Wright-Patterson AFB OH, March 2008.

Duhamel, R. H. And F. R. Ore, "Logaritmically Periodic Antenna Designs," *IRE National Convention Record, Part I*, 6:139-151 (March 1958).

Engheta, Nader and Richard W. Ziolkowski. *Matemarials Physics and Engineering Explorations*. Piscataway, NJ: IEEE Press, 2006.

Golla, Kevin J. *Broadband Application of High Impedance Ground Planes.* MS thesis, AFIT/GE/ENG/01M-11. School of Engineering, Air Force Institute of Technology, Wright-Patterson AFB OH, March 2001 (ADA392025).

Gonzalo, Ramon, P. de Maagt, M. Sorolla. "Enhanced Patch-Antenna Performance by Suppressing Surface Waves Using Photonic-Bandgap Substrates," *IEEE Transanctions on Microwave Theory and Techniques*, 47:2131-2138 (November 1999).

Joannopoulos, John, R. Meade, and J. Winn. *Photonic Crystals: Modeling the Flow of Light.* Princeton University Press, Princeton, NJ, 1995.

Kiminami, Katsuki, A. Hirata, and Toshiyuki Shiozawa. "Double-Sided Printed Bow-Tie Antenna for UWB Communications," *IEEE Antennas and Wireless Propagation Letters*, 3:152-153 (2004).

Kominami, Masanobu, D. M. Pozar, and D. Schaubert. "Dipole and slot elements and arrays on semi-infinite substrates," *IEEE Transanctions on Antennas and Propagation*, 33:600-607 (June 1985).

Kshetrimayum, S. Rakhesh. "A Brief Intro to Metamaterials," *IEEE Potentials*, 04:44-46 (December 2004).

Linton, David and William Scanlon. *Continiously Conformable Antenna Element for Advanced Wearable Communications Under Hostile Channel Conditions: USAF EOARD First Report.* Grant #FA8655-05-1-3058. School of Electronics, Electrical Engineering and Computer Science Queen's University Belfast, 21 March 2006 (RFT-053058).

Loi, K., S. Uysal, and M. Leong, "Design of a Wideband Microstrip Bow-tie Patch Antenna," *IEE Proceedings Microwave Antennas Propagation*, 145:137-140 (April 1998).

Mosallaei, Hossein and Kamal Sarabandi, "Antenna Miniaturization and Bandwidth Enhancement Using a Reactive Impedance Substrate," *IEEE Transanctions on Antennas and Propagation*, 52:2403-2414 (September 2004).

Munk, Benedikt A. *Frequency Selective Surfaces, Theory and Design.* New York:John Wiley&Sons, 2000.

Rahmat-Samii, Yahya and H. Mosallaei, "Electromagnetic Band-Gap Structures: Classification, Characterization and Applications," *Proc. 11th International Conferance Antennas and Propagation, Manchester, U.K.*, 560-564 (17-20 April 2001).

Rogers Corporation, *RT/duroid®5870 /5880 High Frequency Laminates.* Data Sheet. Revised 11/06 0696-1106-0.5CC Publication #92-101 USA. 2006 http://www.rogerscorporation.com/mwu/pdf/5000data.pdf

Rohacell, *Dielectric Properties of Rohacell™ HF* . Seavey Engineering Ass. Report 9335-700 Germany. 2004. http://www.rohacell.com/en/performanceplastics8344.html

Rutledge, David, P. Katehi, and N. Alexopoulos, "Substrate Optimization for Integrated Circuit Antennas," *IEEE Transanctions on Microwave Theory and Techniques, 83*:550-557 (June 1983).

Saville, Micheal A. *Investigation of Conformal High-Impedance Ground Planes.* MS thesis, AFIT/GE/ENG/00M-17. School of Engineering, Air Force Institute of Technology, Wright-Patterson AFB OH, March 1200 (ADA380617).

Schloer, K. *Antenna Gain Enhancement Using a Photonic Band Gap Reflector*. MS thesis, AFIT/GE/ENG/99M-26. School of Engineering, Air Force Institute of Technology, Wright-Patterson AFB OH, March 1999 (ADA361779).

Sievenpiper Dan. *High-Impedance Electromagnetic Surfaces*. Ph.D. dissertation. Department of Electrical Engineering, University of California at Los Angles, Los Angles, CA, 1999.

Sievenpiper, Dan F., L. Zhang, R.F. J. Broas, N. G. Alexopolus, and E. Yablonovitch, "High-Impedance Electromagnetic Surfaces with a Forbidden Frequency Band," *IEEE Transanctions on Microwave Theory and Techniques,* 47:2059-2074 (November 1999).

Sievenpiper, Dan F., R. Broas, and E. Yablonovitch, "Antennas on High-Impedance Ground Planes" *IEEE Transanctions on Microwave Theory and Techniques,* 47:1245-1248 (November 1999).

Veselago, V. "The electrodynamics of substances with simultaneously negative values of ε and μ," Soviet Physics Uspekhi, 10:509-514 (February 1968).

Yablonovitch E, "Inhibited Sponteneous Emission in Solid-State Physics and Electronics," *Physical Review Letters*, 58:2059-2062 (May 1987).

Yablonovitch E, "Photonic Crystals," *Journal of Modern Optics.*, 41:173-194 (February 1994).

Yang, Fan and Y. Rahmat-Samii, "Reflection Phase Characterizations of the EBG Ground Plane for Low Profile Wire Antenna Applications," *IEEE Transanctions on Antenna and Propagation*, 51: 2691-2703 (October 2003).

Yang, Fan and Y. Rahmat-Samii, "Microstrip Antennas Integrated with Electromagnetic Band-Gap (EBG) Structures: A Low Mutual Coupling design for Array Applications," *IEEE Transanctions on Antenna and Propagation*, 51: 2936-2946 (October 2003).

Vita

Lieutenant Bora Cakiroglu was born in Kastamonu, Turkey in 1979. He graduated from Kuleli Military High School in Istanbul, in 1998. He entered the Turkish Air Force Academy, where he graduated with a Bachelor of Science degree in Industrial Engineering in August 2002. His first assignment was at Canakkale Air Radar Base as an interceptor controller.

In August 2006, he was selected for the Air Force Institute of Technology, Wright-Patterson AFB, Ohio. He entered the Department of Electrical Engineering, Air Force Institute of Technology to begin a Master of Science program in Electromagnetics.

REPORT DOCUMENTATION PAGE

Form Approved
OMB No. 074-0188

1. REPORT DATE *(DD-MM-YYYY)*	**2. REPORT TYPE**	**3. DATES COVERED** *(From – To)*
27-03-2008	Master's Thesis	September2006 –March2008

4. TITLE AND SUBTITLE

CONSTRUCTION AND TESTING OF BROADBAND HIGH IMPEDANCE GROUND PLANES (HIGPS) FOR SURFACE MOUNT ANTENNAS

5a. CONTRACT NUMBER

5b. GRANT NUMBER

5c. PROGRAM ELEMENT NUMBER

6. AUTHOR(S)

Bora Cakiroglu, First Lieutenant, TUAF

5d. PROJECT NUMBER

5e. TASK NUMBER

5f. WORK UNIT NUMBER

7. PERFORMING ORGANIZATION NAMES(S) AND ADDRESS(S)
Air Force Institute of Technology
Graduate School of Engineering and Management (AFIT/EN)
2950 Hobson Way, Building 640
WPAFB OH 45433-8865

8. PERFORMING ORGANIZATION REPORT NUMBER

AFIT/GE/ENG/08-02

9. SPONSORING/MONITORING AGENCY NAME(S) AND ADDRESS(ES)

George W. York, EOARD, Deputy CC and RF Sensors
223/231 Old Marylebone Road London NW1 5TH United Kingdom
DSN: From Europe: 235-4354; From US: 314-235-4354
Email: george.york@london.af.mil

10. SPONSOR/MONITOR'S ACRONYM(S)

11. SPONSOR/MONITOR'S REPORT NUMBER(S)

12. DISTRIBUTION/AVAILABILITY STATEMENT

APPROVED FOR PUBLIC RELEASE; DISTRIBUTION UNLIMITED.

13. SUPPLEMENTARY NOTES

14. ABSTRACT

The purpose of this research was to design and build appropriate broadband high impedance ground planes for surface mount antennas. Broadband, low-profile antennas, such as spirals, log-periodics, and bow-ties, suffer substantially in gain and bandwidth performance when they are brought close to a conducting surface. Thus, when standard broadband antenna designs are conformally placed on vehicle bodies, they can no longer achieve the high data rates required by modern communication. A simple remedy for this has been to place an absorber lined cavity behind the antenna to preserve some bandwidth, at the expense of reduced gain. However, recently introduced high impedance ground planes have novel electromagnetic features that have been shown to improve conformal antenna performance without the detrimental effects of absorber losses.

In this research, first, square patch ground planes for narrowband antennas were built and analyzed. Second, a log-periodic broadband antenna was analyzed with square and circular patch ground planes. Finally, two novel triangular-patch high impedance ground plane designs as a meta-substrate for a broadband bow-tie antenna were presented. Consequently, the high impedance ground plane provided a suitable platform for the bow-tie with removing the undesired effects of a regular metallic ground plane. Results indicated that the novel designs have better gain than the bow-tie in free space, and the bow-tie over a metallic surface.

15. SUBJECT TERMS
High impedance ground-plane, triangular-patch mushroom structure, bow-tie antenna.

16. SECURITY CLASSIFICATION OF:			**17. LIMITATION OF ABSTRACT**	**18. NUMBER OF PAGES**	**19a. NAME OF RESPONSIBLE PERSON**
a. REPORT	**b. ABSTRACT**	**c. THIS PAGE**			Andrew J. Terzuoli, USAF (ENG)
U	**U**	**U**	**UU**	116	**19b. TELEPHONE NUMBER** *(Include area code)* (937) 785-3636, ext 4717 Email: Andrew.Terzuoli@afit.edu

Standard Form 298 (Rev. 8-98)
Prescribed by ANSI Std. Z39-18